Dissertation

submitted to the

Combined Faculties for the Natural Sciences and Mathematics

of the Ruperto-Carola University of Heidelberg, Germany

for the degree of

Doctor of Natural Science (Dr. sc. nat.)

Characterization of the protein-protein interaction network within the central domain of the *S. cerevisiae* kinetochore

Ana Stelkić

2011

Dissertation

submitted to the

Combined Faculties for the Natural Sciences and Mathematics

of the Ruperto-Carola University of Heidelberg, Germany

for the degree of

Doctor of Natural Science (Dr. sc. nat.)

Dissertation Referees:

Prof. Dr. Michael Brunner

PD Dr. Johannes Lechner

Written and presented by,

Dipl. molecular biologist and physiologist Ana Stelkić

born in Zrenjanin, Serbia

Oral examination: 26.01.2012

TABLE OF CONTENTS

LIST OF ABBREVATIONS

aa	amino acid
AEBSF	4-(2-Aminoethyl) Benzenesulfonyl Fluoride
Amp	Ampicillin
AP-MS	Affinity Purifications followed by Mass Spectrometry
ATP	Adenosine Tri-Phosphate
bp	base pair
°C	degree Celsius
Cam	Chloramphenicol
CBP	Calmoduline Binding Peptide
CEN	Centromere
Chr	Chromosome
CIAP	Calf Intestinal Alkaline Phosphatase
DDT	Dithiothreitol
DMSO	Dimethyl Sulfoxide
DNA	Deoxyribonucleic Acid
dNTP	deoxynucleosid 5`-Triphosphate
DOC	Deoxycholate
E.coli	*Escherichia coli*
EDTA	Ethylenediaminetetraacetic Acid
EM	Electron microscopy
EtBr	Ethidium Bromide
EtOH	Ethanol
FOA	5`-fluoroorotic Acid
g	gram
h	hour
His	Histidine
HRP	Horseradish Peroxidase
IgG	Immunoglobulin G

IMAC	Immobilized Metal Affinity Chromatography
IP	Immunoprecipitation
IPTG	Isopropyl-beta-D-Thiogalactopyranoside
KanMX6	Kanamycin/G418-resistance cassette
kb	kilo base
kDa	kilo Dalton
KT	kinetochore
lac	Lactose
LB	Luria-Bertani media
MALDI	Matrix Assisted Laser Desorption/Ionisation
mg	milligram
min	minute
ml	milliliter
µg	microgram
µl	microliter
MDa	Mega Dalton
MS	Mass Spectrometry
MT	microtubule
Ni-NTA	Nickel Nitrilotriacetic Acid
OD	Optical Density
o/n	over night
ORF	Open Reading Frame
p	plasmid
PAGE	Polyacrilamid Gel Electrophoresis
PBS	Phosphate Buffered Saline
PCR	Polymerase Chain Reaction
PEG	Polyethylene Glycol
ProA	Protein A
PVDF	Polyvinylidendifluoride
^{R}	Resistance (e.g. Amp^{R})
rbs	ribosomal binding site
rpm	rotations per minute
RT	room temperature

S.cerevisiae	*Saccharomyces cerevisiae*
SEC	Size Exclusion Chromatography
SDS	Sodium Dodecyl Sulfate
TAP	Tandem Affinity Purification
TBS	Tris Buffered Saline
TEV	Tobacco Etch Virus protease
Tm	melting Temperature
U	Unit
UV	Ultraviolet
WB	Western Blot
WT	Wild Type
Y	Yeast strain

AO-complex	Ame1 and His_6-Okp1 in pETDuet-1
MC-complex	Mcm21-TAP and Ctf19 in pCOLADuet-1
	His_{10}-Mcm21 and Ctf19 in pCOLADuet-1
CM-complex	His_6-Ctf19 and Mcm21 in pST39
CMO-complex	His_6-Ctf19, Mcm21 and Okp1 in pST39
COMA-complex	His_6-Ctf19, Mcm21, Okp1 and Ame1 in pST39
COMANN-complex	His_6-Ctf19, Mcm21, Okp1 and Ame1 in pST39 together with Nkp2, Nkp1 in pCOLADuet-1

ACKNOWLEDGEMENTS

The work described in this PhD thesis has been accomplished in the group of Dr. Johannes Lechner, at the Heidelberg University Biochemistry Center.

I am thankful to Hans for giving me the opportunity to work on this interesting project and accepting me as a part of his team. I am grateful for his constant support, close supervision and unquestionable availability.

I would like to express my gratitude to Professor Michael Brunner for being my firs referee, for his time, interest and helpful comments.

Many thanks to all the members of the Lechner lab for their help and support. For the friendly atmosphere and constructive discussions I am very thankful to my lab mates Stefan Kemmler and later Manuel Stach. I would like to thank Maria Knapp, Jürgen Reichert, Petra Ihrig and Susanne Eisel I would like to thank for excellent technical support and experimental advices. I would also like to thank Jennifer Ortiz, Verena Schmeiser and Caroline Funk for always being ready to answer the many questions I had during my initial experiments and for all I have learned from them.

Thanks to all the colleagues at the institute, especially to members of Sinning, Liakopoulos and Söllner groups.

During this work I made some true friends whose encouragement and support I will always remember. Special thanks to Yara Reis, Goran Stjepanovic, Johanna Roostalu, Daniela Richter, Hannah Schmidt-Glenewinkel, Mirjam Dubbert, Aleksandra Novakovic, Ana and Igor Kitanovic, and Chris Thorpe.

Lastly, I would like to thank my family. Without their constant encouragement and support this dissertation would never have been completed. Thanks to my parents for being there whenever I needed them. And finally, I would like to dedicate this work to my husband Saša and our daughter Katarina, the two brightest stars in my life.

SUMMARY

The kinetochore is a specialized structure composed of centromeric DNA and a large number of proteins. The primary function of the kinetochore is to connect chromosomes with the mitotic spindle throughout the cell cycle and to monitor the fidelity of these attachments in order to ensure proper chromosome segregation. Despite the fact that chromosome segregation is directed by the kinetochore, the architecture and assembly of such an intricate structure remains elusive. We use budding yeast as a model system to characterize direct interactions among the central domain of the kinetochore proteins, specifically the COMA-complex. The COMA-complex consists of four proteins; two nonessential proteins Ctf19 and Mcm21 and two essential proteins Ame1 and Okp1. Although the chromosome segregation is a highly conserved process, the human orthologues of the two essential Ame1 and Okp1 proteins have not been identified. The tetrameric complex is the core of the COMA-network which is composed of seven additional nonessential proteins: Ctf3, Mcm16, Mcm22, Chl4, Iml3, Nkp1 and Nkp2, more loosely associated. According to the central localization within the kinetochore, the COMA-complex represents one of the linker complexes (together with the Mtw1-, Ndc80- and Spc105-complexes) bridging the centromere-associate inner proteins with microtubule-bounded outer kinetochore proteins.

Here we present a biochemical approach to reconstitute and to characterize the budding yeast COMA-network. Our first aim was to reconstitute the COMA-complex *in vitro* and *in vivo*. A stabile heterodimer consisting of Ctf19 and Mcm21 proteins could be reconstituted as a tetrameric complex in solution. The Ame1 and Okp1 heterodimer showed noticeable instability and we were not able to reconstitute it. Surprisingly, the trimeric Ctf19, Mcm21 and Okp1-complex could be assembled *in vivo* independently of the Ame1 essential protein. Moreover, we demonstrated that the Okp1 coiled-coil region per se is sufficient to form a complex with Ctf19 and Mcm21 proteins *in vitro*. The tetrameric COMA-complex could have also been reconstituted *in vitro*, but the amount and the stoichiometry of the components were not satisfactory. In solution, the COMA-complex showed oligomerization behavior. Through the protein purification

experiments, we also found that the Ctf19, Mcm21 and Okp1-complex as well as the Ame1 protein separately may bind to unspecific, *E.coli* RNA.

To determine other kinetochore subunits that can directly or indirectly associate with the COMA-components, we performed co-immunoprecipitation from yeast cells with either Okp1-TAP or Ame1-TAP tagged proteins. Among many known interacting partners, the Dsn1 component of the Mtw1-central kinetochore complex was identified. To support this finding and to test if the binding between the Dsn1 and the COMA-proteins is direct or indirect, we performed *in vitro* reticulocyte lysate binding assay. The interaction between the Mtw1- and the COMA-complexes via the Dsn1 protein was confirmed.

Additional information has been gained from the co-immunoprecipitation experiments using budding yeast cells. We identified two proteins from the COMA-network, Nkp1 and Nkp2 proteins, as highly enriched. Since this may reflect the close proximity of these two proteins to the core of the COMA-network, we purified separately Nkp1 and Nkp2 dimer (which revealed the stabile heterodimer formation between these two Nkp proteins), combined it with the recombinant COMA-complex and reconstituted the hexameric protein complex at a 1:1:1:1:1:1 stoichiometry. Taken together, this study led to proposal of a new model for the spatial organization of the COMA-network.

In summary, we used affinity based protein isolation to identify new direct binding partners within the central domain of the budding yeast kinetochore. Our findings improve the current understanding of the overall kinetochore architecture. The complete characterization of the kinetochore structure and organization has to be fully known, ultimately leading to three-dimensional vision and biochemical features of the kinetochore complexes, in order to unravel the mechanisms of chromosome segregation and maintenance of genome stability. Our work is therefore one step further in answering relevant biological and medical questions concerning faithful chromosome segregation during mitosis.

ZUSAMMENFASSUNG

Das Kinetochor stellt eine Struktur dar, die aus centromerer DNA und einer großen Zahl an Proteinen besteht. Während der Zellteilung ist die primäre Aufgabe des Kinetochores, die Chromosomen mit der Mitosespindel zu verbinden und die Korrektheit dieser Verbindung zu überprüfen. Auf diese Weise kommt dem Kinetochore eine zentrale Bedeutung bei der korrekten Verteilung der Chromosomen während der Mitose zu. Dennoch ist bisher wenig über dessen Architektur und Zusammensetzung bekannt. Zur Analyse der Interaktionen zwischen den einzelnen Komponenten des Kinetochores untereinander und insbesondere zur genaueren Charakterisierung des COMA Komplexes wurde der Modelorganismus *S. cerevisiae* verwendet. Der COMA Komplex besteht aus zwei nicht-essentiellen (Ctf19 und Mcm21) und zwei essentiellen (Ame1 und Okp1) Proteinen. Obwohl die Chromosomensegregation ein hochkonservierter Vorgang ist, wurden die orthologen Proteine von Ame1 und Okp1 im Menschen bisher nicht identifiziert. Der tetramere Komplex ist der Kern des COMA-Netzwerkes, das aus sieben weiteren nicht-essentiellen Proteinen besteht: Ctf3, Mcm16, Mcm22, Chl4, Iml3, Nkp1 und Nkp2, die weniger stark assoziiert sind. Aufgrund der zentralen Anordnung im Kinetochor stellt der COMA-Komplex (zusammen mit dem Mtw1-Komplex und dem Spc105-Komplex) einen der Linker-Komplexe dar, der die Proteine des Inneren und des äußeren Kinetochores verbindet.
Mit Hilfe von biochemischen und zellbiologischen Methoden haben wir das Hefe COMA-Netzwerk rekonstituiert und charakterisiert.

- ***In vitro* und *in vivo* Rekonstitution des COMA-Komplexes.**

Ein stabiles Heterodimer bestehend aus den Proteinen Ctf19 und Mcm21 konnte als dimerer/tetramerer Komplex *in vitro* rekonstituiert werden. Das Heterodimer aus Ame1 und Okp1 zeigte beachtliche Instabilität, die eine Rekonstitution unmöglich machte. Dennoch konnte der trimere Komplex bestehend aus Ctf19, Mcm21 und Okp1 *in vivo,* unabhängig von dem essentiellen Protein Ame1, zusammengesetzt werden. Darüber hinaus konnten wir *in vitro* zeigen, dass die coiled coil Domäne von Okp1 alleine ausreichend für die Bildung eines Komplexes mit Ctf19 und Mcm21 ist. Der tetramere COMA-Komplex konnte ebenfalls *in vitro* rekonstituiert werden, allerdings waren

sowohl die Menge als auch die Stöchiometrie der einzelnen Komponenten nicht zufriedenstellend. In Lösung neigte der COMA-Komplex zur Bildung von Oligomeren. Zudem zeigte die Proteinaufreinigung, dass sowohl Ctf19, Mcm21 und Okp1 als auch Ame1 alleine unspezifisch mit RNA zu interagieren scheinen.

- **Die zentrale coiled-coil Domäne von Okp1 ist notwendig für die Bildung des COMA-Komplexes und ist essentiell für das Überleben der Zelle.**

Durch verschiedene Deletionskonstrukte des Okp1 Proteins konnten wir die zentrale coiled-coil Domäne des Proteins als die essentielle Region für die Okp1 Funktion und damit für die Lebensfähigkeit der Zelle bestimmen. *In vitro* Untersuchungen mit diesen Okp1 Deletionskonstrukten identifizierte die coiled-coil Region als Interaktionsdomäne, die zur Bildung des trimeren Komplexes mit Mcm21 und Ctf19 wechselwirkt.

- **Mtw1- und dem COMA-Komplex interagieren vorwiegend über das Protein Dsn1.**

Um andere Kinetochor Untereinheiten zu bestimmen, die direkt oder indirekt mit dem COMA-Komplex assoziieren können, wurde mit Hilfe des Okp1-TAP Konstrukts eine Co-Immunopräzipitation aus Hefezellextrakt durchgeführt. Neben vielen bekannten Interaktionspartnern wurde Dsn1, eine Komponente des zentralen Kinetochor-Komplexes Mtw1, identifiziert. Um dieses Ergebnis zu unterstreichen und zu analysieren, ob Dsn1 direkt oder indirekt an die COMA Proteinen bindet, haben wir einen *in vitro* Reticulozyten Lysat-Assay durchgeführt. Dadurch konnte die Interaktion zwischen dem Mtw1- und des COMA-Komplexes über Dsn1 bestätigt werden.

- **Der COMA-Komplex scheint über die Proteine Mif2 und Cse4 mit centromerem Chromatin zu interagieren.**

Vorläufige Daten von *in vitro* Bindungsstudien legten nahe, dass Cse4 sowohl mit Ame1 als auch mit dem CMO-Komplex interagiert, wohingegen Mif2 nur mit dem CMO-Komplex und nicht mit Ame1 allein wechselwirkt. Dieses Ergebnis weist auf folgende räumliche Organisation der zentralen Kinetochorschicht hin: Mif2 und CMO sind sich näher als Mif2 und Ame1.

- **Die Proteine Nkp1 und Nkp2 stabilisieren direkt den COMA-Komplex. Ein hexamerer Komplex konnte mit einer Stöchiometrie von 1:1:1:1:1:1 rekonstituiert werden.**

Durch Co-Immunopräzipitationsexperimente mit Hefezellen wurden zwei Proteine – Nkp1 und Nkp2- des COMA-Netzwerkes identifiziert, die stark angereichert waren. Dies spiegelt möglicherweise die Nähe dieser beiden Proteine zum Kern des COMA-Netzwerkes wider. Nkp1 und Nkp2 wurden daraufhin getrennt als Dimere aufgereinigt (dies zeigt die Bildung eines stabilen Heterodimers der beiden Nkp- Proteine) und mit dem rekombinierten COMA-Komplex gemischt. Dabei konnte ein hexamerer Komplex mit einer Stöchiometrie von 1:1:1:1:1:1 rekonstituiert werden. *In vitro* Untersuchungen zeigten, dass der Nkp-Dimer vorwiegend über die Proteine Ame1 und Okp1 mit dem COMA-Komplex interagiert. Zusammenfassend kann man sagen, dass diese Erkenntnisse das derzeitige Verständnis des COMA-Netzwerkes und der allgemeinen Hefe Kinetochor Architektur verbessern.

1. INTRODUCTION

A new cell can only be borne by duplicating and dividing an already existing cell. One of the most important points during the process of cell replication is the transmission of genetic information into a pair of daughter cells. Before the separation of the two copies of a chromosome (sister chromatids), each chromosome has to be properly connected with microtubules of the mitotic spindle. To ensure faithful chromosome segregation over many generations, the series of events leading to cell reproduction are tightly regulated during the cell cycle. The spindle assembly checkpoint (SAC) monitors connections between microtubules and chromosomes as well as tension applied across the centromere. Microtubules connect to a chromosome via kinetochores, which are proteinaceous structures assembled onto the centromeric region of the sister chromatids. Improper kinetochore-microtubule attachments activate the SAC and block chromosome segregation until errors are corrected and all chromosomes are connected to the mitotic spindle in a bipolar manner. Although these control mechanisms work very efficient and accurately, error in less than one in 10^5 events still persists and may result in either a cell death or cancer. Detailed understanding of the structures and principles of cell division can help us to learn the pathways by which cancers appear and develop. Observations about the molecular mechanisms of cell division made on unicellular organisms like the budding yeast could further knowledge of the mammalian cells mitosis and diseases associated with its aberrations.

1.1 *Saccharomyces cerevisiae* as a model organism

In this study, *Saccharomyces cerevisiae* (budding yeast, baker`s yeast) was employed as a model organism to analyze structural organization of the kinetochore. The *S. cerevisiae* has been widely used as an important model system to unravel biological processes in higher eukaryotes for the investigation of basic cellular processes which are usually highly conserved. As a single cell organism, it has a short generation time and it can easily be cultured and genetically manipulated. The complete budding yeast genome has been known for 15 years and comprises about 6000 genes arranged on 16 chromosomes. Present knowledge about the degree of conservation between budding yeast and vertebrates in respect to gene and protein sequences as well as signaling pathways, makes *S. cerevisiae* an attractive model for human diseases and cancer research (Menacho-Marquez and Murguia 2007), (Kitagawa and Hieter 2001).

Within the scope of the kinetochore field of the research, budding yeast is especially beneficial model organism. Its point centromeres are only about 125 bp in size while its proteinaceus kinetochores contain approximately 60 subunits and homologues for most of these proteins have been identified in vertebrates. This structure is estimated to be at least 5 MDa in size in contrast to vertebrates with much more complex kinetochores, in terms of size and function, yet without drastic alternation in overall kinetochore architecture (Chan, Liu et al. 2005).

1.2 The budding yeast cell cycle

The cell cycle is a series of events that leads to growth, duplication and finally division of the cell. In eukaryotic cells, the cell cycle can be divided into two major stages. The first, interphase, during which cells growth and prepare for their division, is the phase before cells can enter cell division. Interphase proceeds in stages G1, S and G2. The second major phase during the cell cycle is mitosis (M-phase, cell division phase), during which the replicated genetic information gets precisely separated into two distinct cells (Fig. 1.1).

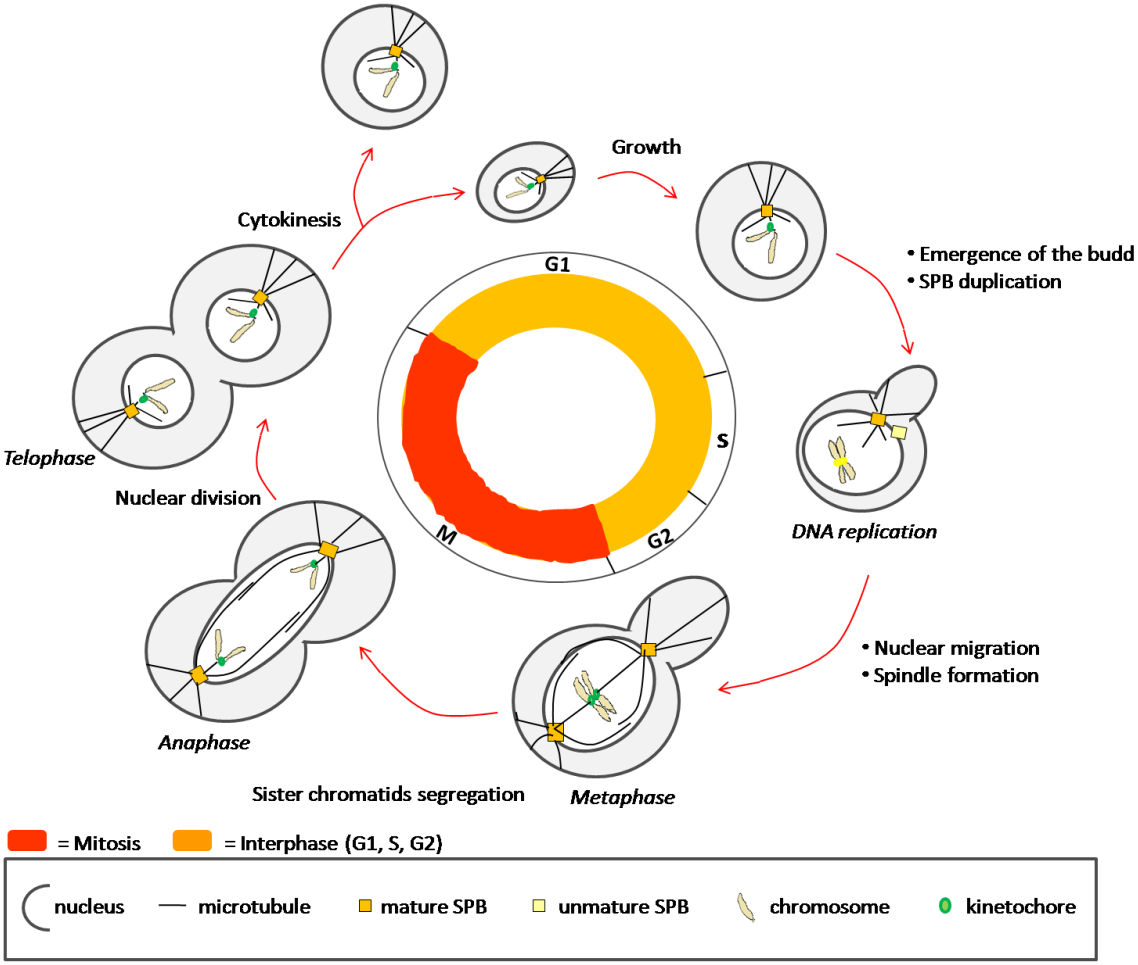

Fig. 1.1 Events during the *S. cerevisiae* cell cycle.

Two gap phases, G1 and G2, postpone the cell cycle to allow cell growth. During these phases, the cell inspects the environmental conditions and makes a decision about cell cycle progression. In the G1 phase budding yeast cells do not bud, they contain a haploid set of chromosomes and a single spindle pole body (SPB), which is the yeast equivalent of the mammalian microtubule organizing centre. Cells can be arrested in this phase by lack of nutrients or by the presence of mating hormones (alpha-factor). Some cell types continue to divide throughout the life of an organism. Certain cell types remain in a so called non-dividing phase (G0) until they get an environmental signal to cycle again. If the cell is devoted to division, DNA replication and SPB duplication are initiated at the G1/S-transition. Later in S phase, when the new SPB becomes mature, two SPBs separate in order to build up a mitotic spindle but both remain embedded in the nuclear envelope. Three types of microtubules nucleating from the SPBs expand to perform different functions. 2-4 astral (cytoplasmic) microtubules project towards the cell membrane where they perform an important function by generating forces that direct

the spindle positioning. Intranuclear microtubules give rise to the mitotic spindle, which consists of 32 kinetochore microtubules and 8 overlapping interpolar microtubules (Tanaka, Mukae et al. 2005); (Morgan 2007); (Hoyt and Geiser 1996). During S phase a small bud emergences, which is a morphological characterization of this stage of the budding yeast cell cycle. Budding yeast undergo closed mitosis, which means that the nuclear envelope remains intact during the whole cell cycle, while in other eukaryotes nuclear-envelope break down in late S phase. Further differences among higher eukaryotes and budding yeast concern the timing of kinetochore-microtubule interactions. In mammalian cells interactions between kinetochore and spindle microtubules occur only during mitosis, while in budding yeast the kinetochores detach transiently from the microtubules only in early S phase when the centromeric DNA is replicated (Kitagawa and Hieter 2001). During the second gap, G2 phase, the cell will continue to grow and a new SPB will finally become mature. This phase is very short in budding yeast but it is an integral step in which cell prepares for the upcoming division (mitosis).

Mitosis is a fundamental process in which faithful segregation of sister chromatids occur, and which ensures that daughter cells inherit the same genetic information possessed by their parental cell. The central function of mitosis is carried out by a complex macromolecular structure called the mitotic spindle. The mitotic spindle apparatus is a dynamic array of microtubules, spindle pole bodies and microtubule associated motor proteins, beside the chromatin and kinetochores (Hoyt and Geiser 1996). Mitosis is highly conserved from yeast to higher eukaryotes and it can be divided into five stages: prophase, prometaphase, metaphase, anaphase and telophase. In **prophase** of higher eukaryotes chromatin condenses to form chromosomes, while in budding yeast chromatin compacts much less, thus making it impossible for visualization by light microscopy. During **prometaphase** kinetochore microtubules (K-fibers) from the mitotic spindle attach to chromosomes via the kinetochores resulting in movement of the chromosomes. In budding yeast each kinetochore is connected to a single K-fiber (Peterson and Ris 1976; Winey, Mamay et al. 1995), in contrast to higher eukaryotes in which kinetochore interacts simultaneously with several microtubule filaments (McEwen, Heagle et al. 1997). In **metaphase** two SPBs are embedded in opposite poles of the nuclear envelope, therefore contributing to a short metaphase mitotic spindle formation. At that cell cycle stage chromosomes are distributed along the

metaphase spindle. Correct bipolar attachment of chromosomes and microtubules emerging from opposing sites of the cell creates tension, leading to the splitting of two sister chromatids at their centromeric region while their chromatid arms remain together. This dynamic process could be nicely visualized as a "chromosome breathing" by fluorescent microscopy (He, Asthana et al. 2000). **Anaphase** starts with sister chromatids` separation and their movement toward the opposite poles of the dividing cell. Correct segregation of the sister chromatids to each daughter cell can only occur if the bipolar (amphitelic) kinetochore-microtubule attachment under tension is achieved. According to the current concept of mitosis, the anaphase starts by the silencing of the spindle assembly checkpoint (SAC) mechanism, thus promoting the activation of the anaphase promoting complex (APC) (Musacchio and Salmon 2007); (Khmelinskii and Schiebel 2008). The large APC/C is a multimeric E3 ubiquitin ligase which is activated by its co-factor Cdc20. One of its ubiquitination targets is the 26S proteasome dependent proteolysis of various key regulators like Pds1/securin. Degradation of Pds1 leads to release of active protease Esp1/separase which is involved in cleavage of the cohesion subunit Scc1 (Sister chromatid cohesion 1). The overall outcome of cohesion removal is rapid movement of sister chromatids toward the opposite spindle poles in early anaphase, referred to as anaphase A (Peters, Tedeschi et al. 2008). Anaphase B is characterized by the further separation of sister chromatids and elongation of the mitotic spindle. In budding yeast two anaphase events occur almost simultaneously with the major contribution to the separation coming from anaphase B (Kitagawa and Hieter 2001). In the final stage of mitosis, **telophase**, the spindle reaches its maximum length and finally gets disassembled. Around the same time the cytokinesis starts and consequently the formation of two separated cells terminate one cell cycle round.
Taken together, the cell-cycle machinery of all eukaryotes comprises a robust and reliable control system which regulates the timing and order of cell cycle events.

1.3 The kinetochore

Kinetochores are large structures that consist of centromeric DNA (CEN) and associated proteins, built on centromeric part of chromosomes. They are essential for the accurate segregation of chromosomes during mitosis. They perform many crucial functions.

- The inner kinetochore participates in building an interface with centromeric chromatin.
- The outer kinetochore forms a microtubule-binding interface.
- Kinetochores generate the spindle assembly checkpoint signals, as a control mechanism that monitors cell cycle progression and the completion of kinetochore-microtubule attachment (Meraldi, McAinsh et al. 2006).

Electron microscopy studies have revealed that the higher eukaryotic kinetochore consists of three layers with differential electron density properties (Tomkiel, Cooke et al. 1994). Microscopic visualization of unicellular eukaryotes` kinetochores, such as budding yeast, could not been done directly (Kitagawa and Hieter 2001). Nevertheless, *S. cerevisiae* is an excellent model system to study kinetochore structure and function, since the critical features of kinetochores have been well conserved from yeast to humans (Meraldi, McAinsh et al. 2006). Thus, kinetochores are generally described as composed of three distinct regions; inner, middle and outer layers (Fig. 1.2).

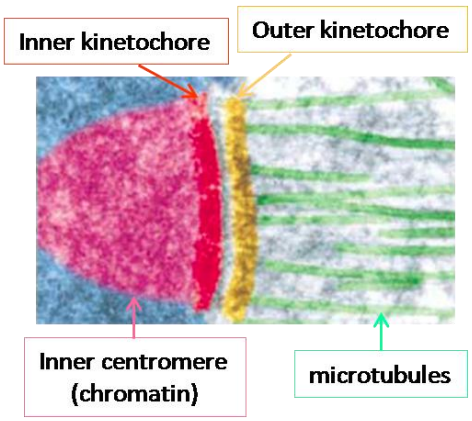

Fig. 1.2 Overall organization of the kinetochore (adapted from Cleveland et. al. 2003)**.**

1.3.1 Inner kinetochore components

Kinetochore assembly is restricted to centromeres (Lampert and Westermann 2011). The inner kinetochore components provide a platform for other components to assembly and they involve centromeric DNA (CEN) sequence and proteins which are able to directly interact with it.

Often studied human or budding yeast chromosomes are monocentric (the centromere is only present as a single primary constriction and not present all along the chromosomes as it is for holocentric chromosomes e.g. *C. elegans*). Monocentric chromosomes can be divided into two types. One is a point centromere and the other one is a regional centromere. Point centromeres have only been discovered in budding yeast, including *Saccharomyces cerevisiae*. The centromeric DNA (CEN-DNA) of the *S. cerevisiae* is approximately 125 bp long (Fig. 1.3). The centromeres of fission yeast *Schizosaccharomyces pombe*, for example, are regional and 30-110 Kb long. The other example of regional centromere is human CEN which spans around 2-4 Mbp of highly repetitive DNA.

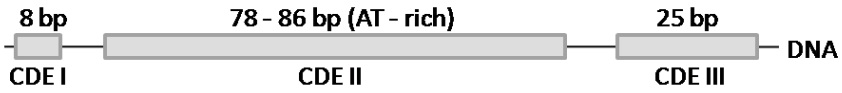

Fig. 1.3 The centromeric DNA sequence of *S. cerevisiae*

The centromeric region (CEN-DNA) of *S. cerevisiae* contains tree conserved DNA elements CDEI, II and III (Fitzgerald-Hayes, Clarke et al. 1982), (Hieter, Pridmore et al. 1985). The 8 bp long CDEI is a partially conserved DNA region and the 26 bp long CDEIII is a highly conserved element, and both represent imperfect palindromes. Between them is located the AT-rich (>90%) CDEII element of 78-86 bp length (Clarke and Carbon 1980), (Hegemann and Fleig 1993). Only CDEIII and part of CDEII are essential and just a point mutation within CDEIII can abolish kinetochore function (McGrew, Diehl et al. 1986), (Ng and Carbon 1987). It was suggested that chromosome missegregation associated with mutations within CDE-elements were due to the failure of kinetochore proteins to assemble properly at the centromeric DNA. Together these three DNA sequences form the platform necessary for the assembly of the protein complexes that build the kinetochore.

Regardless of centromeres composition or length, one common feature of all eukaryotic centromeres is the assembly of modified nucleosomes. An evolutionary conserved isoform of histone H3 variant, Cse4 (*Chromosome segregation 4*) in *S. cerevisiae* (CENP-A in humans), establishes identity of centromeres. It is essential for the assembly of all central and outer kinetochore proteins (Collins, Castillo et al. 2005). Cse4 is an epigenetic mark that interacts with CDEI and CDEII elements (Meluh, Yang et al.

1998). A Cse4-containing centromeric nucleosome could be an [H2A:H2B] $_2$-[Cse4:H4]$_2$ octamer. On the other hand, in budding yeast it has been postulated that the Scm3 (*Suppressor of Chromosome Missegregation 3*) protein is required for recruitment of Cse4 to the kinetochore, participating in an atypical hexameric nucleosome [Cse4:Scm3:H4]$_2$ formation (Mizuguchi, Xiao et al. 2007), (Camahort, Li et al. 2007). However, the most recent studies revealed that the Scm3 protein plays a major role as a key chaperone in loading the Cse4 protein to the specialized nucleosome core, rather than altering the overall nucleosome structural organization (Cho, Corbett et al. 2011).

DNA-affinity purifications discovered more centromere-associated proteins. Cbf1 (*Centromere binding factor 1*) binds to CDEI as a homodimer (Baker, Fitzgerald-Hayes et al. 1989) through its helix-loop-helix protein domain. Cbf1 is a transcription factor as well as a kinetochore component. Albeit it is a non-essential gene, its deletion increases the probability of chromosome loss and results in hypersensitivity to spindle drugs like benomyl (Cai and Davis 1989).

The CBF3-complex (*Centromere-Binding Factors*) is the kinetochore-initiating complex which is comprised of four essential components: Cbf3a (Ndc10), Cbf3b (Cep3), Cbf3c (Ctf13) and Cbf3d (Skp1) which bind to CDEIII (Connelly and Hieter 1996), (Doheny, Sorger et al. 1993), (Espelin, Kaplan et al. 1997), (Goh and Kilmartin 1993), (Lechner and Carbon 1991), (Stemmann and Lechner 1996), (Strunnikov, Kingsbury et al. 1995). Skp1, which is a part of the ubiquitous SCF ubiquitin ligase complex, interacts with the Ctf13 by their F-box-containing components. A Cep3p dimer, the partial crystal structure of which was recently solved, recruits a Skp1-Ctf13 heterodimer. Next, the formed complex finally associates with Ndc10 and binds to two sites on CDEIII (Bellizzi, Sorger et al. 2007). In addition to its inner kinetochore localization, Ndc10 has been also shown locate to the mitotic spindle (Bouck and Bloom 2005). CBF3-complex dependency has been shown for all known kinetochore proteins, including Cse4 (Ortiz, Stemmann et al. 1999).

While the Cbf1 protein and the protein complex CBF3, which bind in a sequence-specific manner to CDEI and CDEIII respectively, no kinetochore protein has been identified so far that binds to CDEII.

Another essential inner kinetochore protein is Mif2 (*Mitotic Fidelity of chromosome transmition*), a budding yeast orthologue of vertebrate CENP-C protein. It was initially identified as a gene that caused aberrant chromosome segregation when

expressed at high levels (Brown, Goetsch et al. 1993). The AT-hook of Mif2 binds to the minor groove of CDEIII in a dimeric form (Reeves and Nissen 1990). Although CBF3-complex is required for the recruitment of all kinetochore proteins, including Cse4 as well as Mif2, it seems that the Mif2 dimer itself recruits middle kinetochore proteins (e.g. COMA and MIND) for kinetochore localization but not Cse4 (Cohen, Espelin et al. 2008), (Measday, Hailey et al. 2002).

1.3.2 Complexes forming the kinetochore middle

The budding yeast middle kinetochore components represent diverse complexes that include the COMA-network, MIND or Mtw1-complex and KNL1 or Spc105-complex.

A subset of at least eleven different proteins, which form a linker layer between the proteins that are in contact with centromeric DNA and the subunits bound to microtubules during kinetochore assembly, will be referred as the COMA-network in this study. Identification of these proteins has been made through the yeast tandem affinity purification (De Wulf, McAinsh et al. 2003). According to their sedimentation properties, the budding yeast COMA-network consists of the discrete core of the network and additional auxiliary protein subunits. The core protein complex, also termed the COMA-complex, is composed of Ctf19 (*Chromosome Transmission Fidelity*), Okp1 (*Outer Kinetochore Protein*), Mcm21 (*MiniChromosome Maintenance*) and Ame1 (*Associated with Microtubules and Essential*) proteins (De Wulf, McAinsh et al. 2003). Only two of them, Okp1 and Ame1, are essential. All the other proteins from the COMA-network are dispensible for cell growth (Measday, Hailey et al. 2002), (Ortiz, Stemmann et al. 1999). Quantitative measurements of fluorescently labeled Ctf19 molecules by super-resolution microscopy revealed that there are approximately 2-3 COMA-complexes per kinetochore in budding yeast (Joglekar, Bouck et al. 2006). The current founding members of the COMA-network and their homologues in different species are listed in Table 1.1.

Human	Mouse	Chicken	*D. melanogaster*	*C. elegans*	*S. pombe*	*S. cerevisiae*
-	-	-	-	-	-	Okp1
-	-	-	-	-	-	Ame1
CENP-P	-	CENP-P	-	-	Fta2	Ctf19
CENP-O	-	CENP-O	-	-	Mal2	Mcm21
CENP-I	Cenpi	CENP-I	-	-	Mis6	Ctf3
CENP-N	-	CENP-N	-	-	Mis15	Chl4
CENP-M	-	CENP-M	-	-	Mis17	Iml3
CENP-H	Cenph	CENP-H	-	-	Fta3	Mcm16
-	-	-	-	-	-	Mcm22
-	-	-	-	-	-	Nkp1
-	-	-	-	-	-	Nkp2

Table 1.1 Protein composition of the kinetochore COMA-network among different species.

Surprisingly, only some components of the COMA-network in *S. cerevisiae* are conserved among fungi and human kinetochores. Moreover, the two essential Okp1 and Ame1 protein components do not have identified human homologues. This asserts the COMA protein network as kinetochore components with a high degree of sequence divergence through evolution, in contrast to most of the other kinetochore multiprotein complexes (e.g. Mtw1-, Spc105- or Ndc80-complex) (Meraldi, McAinsh et al. 2006).

The current, albeit limited, understanding of how this central network of proteins interact within the network as well as with other components of the kinetochore, is based on variety of genetic and biochemical approaches. It has been demonstrated that protein complex composed of Okp1, Ctf19 and Mcm21 interacts with the CBF3-complex as well as with Cse4, Mif2 and Cbf1 proteins (Ortiz, Stemmann et al. 1999). Genetic synthetic dosage lethality screening demonstrated that Ctf3 protein interacts with Mcm16 and Mcm22, as well as with Ctf19 proteins (Measday, Hailey et al. 2002). Revealed by co-immunoprecipitation, ChIP and fluorescent imaging techniques, it has been reported that Chl4p and Iml3p are interacting proteins that localize to centromeres in a Ctf19-dependent manner (Pot, Measday et al. 2003). In addition, Chl4 and Iml3 are important for preventing non-disjunction of sister chromatids during meiosis and they promote cohesin and Sgo1 association with the pericentromere (in budding yeast, an approximately 50 kb region around the centromere) (Fernius and Marston 2009), (Kiburz, Reynolds et al. 2005). A synthetic genetic array using a spindle checkpoint

mutant (*mad2Δ*) strain of yeast has identified the YBP2 gene, and proposed a model in which Ybp2 transiently interacts with proteins in COMA- and Ndc80-complexes pushing them away from each other rather than holding them together (Ohkuni, Abdulle et al. 2008). It has been observed that the yeast Ipl1-Sli15 kinase complex plays a crucial role in correcting chromosome orientation by promoting reorientation of mitotic spindle in a tension dependent manner (Tanaka 2005). The COMA-complex, in particular the Ame1 protein, has been proposed to be required for Sli15-mediated correction of defective kinetochore attachments (Knockleby and Vogel 2009), (Pot, Knockleby et al. 2005).
Over the past decade, most of the *S. cerevisiae* kinetochore components have been characterized and assigned to discrete functional subcomplexes. However, the COMA-network remains functionally and structurally relatively uncharacterized, suggesting the complicated pattern of interactions and diverse functions of this inner kinetochore division.

The Mtw1-complex of four essential proteins (in higher eukaryotes also called MIND or Mis12-complex) is a conserved central kinetochore complex. It has been identified in budding yeast and it contains Mtw1 (*Mis TWelve-like*), Nnf1 (*Necessary for Nuclear Function*), Nsl1 (*Nnf1 Synthetic Lethal*) and Dsn1 (*Dosage Suppressor of NNF1*) proteins (Euskirchen 2002). The complex can be assembled from two stable heterodimers: Mtw1-Nnf1 and Dsn1-Nsl1 (Hornung, Maier et al. 2010). Correct recruitment of the complex depends on the presence of inner constitutive kinetochore components, such as Cse4 and CBF3-complex proteins (Goshima, Saitoh et al. 1999), (Scharfenberger, Ortiz et al. 2003) on one hand, and on the other hand it is involved (itself) in the recruitment of outer kinetochore subunits that bind to microtubules, in particular the Ndc80- and DDD-complexes (Hornung, Maier et al. 2010), (Petrovic, Pasqualato et al. 2010), (Scharfenberger, Ortiz et al. 2003). Using a combination of biochemistry and functional genomics in *C. elegans*, recent studies have implicated that in multiple organisms the counterpart of the Mtw1-complex, the Mis12-complex, forms the network together with KNL-1 (Spc105p in budding yeast) and the Ndc80-complex. These three complexes constitute the KMN network which is the core microtubule attachment site of the kinetochore (Cheeseman, Chappie et al. 2006).

The Spc105-complex consists of the two essential Spc105 protein (*Spindle Pole Component*) and Kre28 protein and it is poorly described in budding yeast (Nekrasov, Smith et al. 2003). Homologues in different eukaryotes are known as Spc7, KNL-1 or

Blinkin. It was shown that this complex tightly interacts with two other complexes (Mis12/Mtw1 and Ndc80) and with components of the spindle assembly checkpoint (SAC). Studies of the *D. melanogaster* Spc105 protein suggest a role in providing a platform within the outer kinetochore upon which various other kinetochore proteins can assemble (Schittenhelm, Chaleckis et al. 2009).

1.3.3 Proteins building the kinetochore-microtubule interface

One primary function of the kinetochore is to stably attach chromosomes to the mitotic spindle and to either generate or transduce the forces that are required for chromosome segregation (Cheeseman and Desai 2008). Various microtubule-binding proteins are involved in creating a stable and yet dynamic attachment site, including the Ndc80-complex, DDD-complex (also referred as to Dam1- or DASH-complex only known in *S. cerevisiae*), chromosome passenger complex, several motor proteins and plus-end tracking proteins (+TIP).

A fundamental kinetochore outer complex that contributes to the kinetochore-microtubule interface is the Ndc80-complex. Its overall spatial organization has been documented using electron microscopy combined with limited proteolysis and antibody labeling, and it appears as a long rod-like structure with two globular domains at either end and an α-helical coiled-coil domain in between (Wei, Sorger et al. 2005). The Ndc80 (Hec1 in human) and Nuf2 proteins form a heterodimer which point toward the plus-ends of spindle microtubules and physically contacts with them. The other end of the complex is composed of Spc24 and Spc25 dimer and it localizes proximal to the middle/inner kinetochore (DeLuca, Dong et al. 2005). It has been observed that *in vitro* Ndc80-Nuf2 and Spc24-Spc25 form stable subcomplexes that can self-assemble into the integral Ndc80-complex (Ciferri, De Luca et al. 2005). All four proteins are essential for cell viability and well conserved from yeast to human (Janke, Ortiz et al. 2001), (Wigge and Kilmartin 2001). Recent structural approaches that include the use of a human engineered “bonsai” Ndc80-complex (containing truncated rod-like structure) revealed an interface of predominantly electrostatic interactions between kinetochore and microtubules (Ciferri, Pasqualato et al. 2008).

Beside the Ndc80-complex, the DDD-complex is a kinetochore component also necessary for microtubule attachment in budding yeast but not conserved outside fungi. The current explanation for the specific requirement of this protein complex in *S. cerevisiae* is that this exhibits specific adaptation to the yeast-specific point centromere and a single microtubule attachment per kinetochore (Lampert and Westermann 2011). Its localization onto budding yeast kinetochores depends on the presence of Ndc10-, Ndc80-complex and kinetochore-microtubules (Cheeseman, Enquist-Newman et al. 2001), (Janke, Ortiz et al. 2002), (Li, Bachant et al. 2002). The DDD-complex consists of ten essential proteins (Dam1, Duo1, Ask1, Dad1, Dad2, Dad3, Dad4, Spc19, Spc34 and Hsk1) that can *in vitro* self-assemble in the form of a ring around the microtubules (Westermann, Drubin et al. 2007). It has been shown by electron microscopy that the DDD-ring can slide laterally along the lattice of a microtubule *in vitro* and it can perform as a force transducer for a chromosome movement (Asbury, Gestaut et al. 2006). The reality of the DDD-ring could not be proven *in vivo* so far. Up to now, a metazoan DDD-complex has not been discovered. However, the three components Ska1-complex have been recently suggested to play a corresponding role at the vertebrate kinetochore (Welburn, Grishchuk et al. 2009).

There are different regulatory processes and mechanisms that can differentiate between correct and incorrect kinetochore-microtubule attachments. The spindle assembly checkpoint (SAC) can arrest cell cycle progression until all chromosome pairs are properly attach to the mitotic spindle. The Chromosomal Passenger Complex (CPC) plays an essential role in the regulation of bi-orientation by correcting aberrant kinetochore-microtubule attachments and lack of tension (Kotwaliwale and Biggins 2006), (Ruchaud, Carmena et al. 2007). The CPC comprises of one enzymatic component, Aurora B kinase (Ipl1 in budding yeast), and three more non-enzymatic parts: INCENP (Sli15 in yeast), Survivin (Bir1 in yeast) and Borealin (Nbl1 in yeast). According to the current understanding, the physical distance between the kinase and its kinatochore substrates can explain the relationship between the CPC and SAC. In an amphitelic orientation of chromosome where sister chromatids are under tension, intra-kinetochore stretching results in increased vicinity between the kinase and its substrates. As opposed to kinetochores which are not under tension, the Ipl1 kinase is not able to phosphorylate its kinetochore substrates that contribute to the microtubule binding; the SAC is active and kinetochore-microtube attachment is labile (Liu, Vader et

al. 2009), (Santaguida and Musacchio 2009). It has been shown that Ndc80- and DDD-complexes are substrates of Ipl1 in yeast and (Aurora B) in mammals thereby participating in establishment of a bipolarly attached kinetochore (Cheeseman, Anderson et al. 2002), (DeLuca, Gall et al. 2006), (Shang, Hazbun et al. 2003).

The interface between kinetochore and microtubules further involves motor proteins and a number of microtubule + TIPs (plus-end *t*rack*i*ng *p*roteins). These +TIPs of budding yeast include Stu1, Stu2, Bim1 and Bik1 proteins. Their localization at the kinetochore and the roles that they are play are different and still not fully investigated. Stu1 localizes to kinetochores early in the cell cycle and regulates kinetochore capture and spindle stability (Ma, McQueen et al. 2007), (Ortiz, Funk et al. 2009). Stu2 associates with kinetochore independent on microtubules and it is important for stabilization and increased frequency rescue of microtubules that have attached kinetochores (Kitamura, Tanaka et al. 2010), (Tanaka, Mukae et al. 2005). Unlike Stu2, Bik1 localizes exclusively to attached kinetochores (Kitamura, Tanaka et al. 2010). It has been shown that Bik1 and Bim1 proteins have redundant roles in the regulation of kinetochore-microtubule dynamics, but further investigation of whether these proteins have more specific roles on kinetochore biorientation or force-generation is still needed (Lin, de Carvalho et al. 2001), (Westermann, Drubin et al. 2007). Motor proteins play a very important role in chromosome segregation. Plus-end directed motor proteins Kip1 and Cin8 or minus-end directed Kar3 protein, regulate kinetochore microtubule assembly dynamics and influence organization and synchronization of chromosome movements (Gardner, Bouck et al. 2008), (Westermann, Drubin et al. 2007).

Figure 1.4 illustrates a scheme of the general kinetochore organization as well as the *S. cerevisiae* kinetochore subunits arrangement. All listed proteins that make up each kinetochore complex were assigned in the previous chapter.

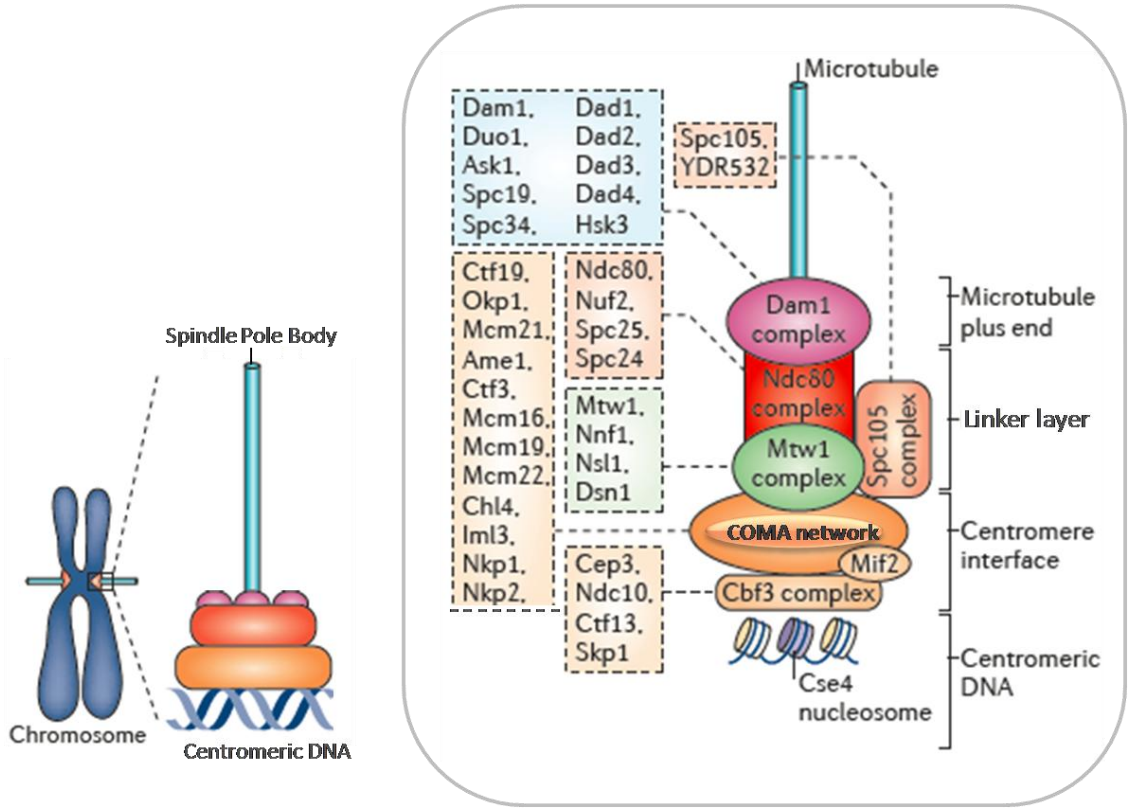

Fig. 1.4 A model of budding yeast kinetochore organization (adapted from Lampert and Westermann, 2011).

Schematic of the general organization of the budding yeast kinetochore and its constitutive subunits that clusters in distinguishable protein complexes.

1.4 Yeast kinetochore architecture and organization

Since the first kinetochore proteins were discovered and characterized during the 1990s, more than 65 structural components of the *S. cerevisiae* kinetochore have been identified so far. The question is still if this is the final number. Most of these proteins have been identified using the affinity-based protein purifications followed by mass spectrometry analysis. This biophysical approach revealed the main protein complexes that are involved in the kinetochore structure (De Wulf, McAinsh et al. 2003), (Nekrasov, Smith et al. 2003), (Westermann, Cheeseman et al. 2003). Next, it has been shown that most kinetochore components form discrete subcomplexes containing more than one subunit (De Wulf, McAinsh et al. 2003). The average weight of a typical budding yeast kinetochore complex is about 200 kDa. The reason for kinetochore assembly from subcomplexes and not monomeric proteins might lie in the increased kinetochchore

stability and efficiency of new kinetochore formation after DNA replication. Analysis of discrete recombinant protein subcomplexes revealed the important information that kinetochore assembly occurs in a hierarchical manner (De Wulf, McAinsh et al. 2003). Using ChIP or electron microscopy techniques it has been proposed the overall kinetochore organization and the alternative approach ascertained details of kinetochore configuration by reconstituting complexes *in vitro*. For instance, although the COMA-, Mtw1- or Ndc80-complex assembly apart from each other, it is known that the COMA-complex interacts directly with Mtw1-complex but not with Ndc80-complex or that the Mtw1-complex can further physically interact with Ndc80- and Spc105-complexes (Hornung, Maier et al. 2010), (Maskell, Hu et al. 2010). These and other studies using *in vitro* interactions between many protein subcomplexes revealed important physical relationships between different protein subcomplexes and one is beginning to understand the procedure of kinetochore assembly and the overall kinetochore molecular architecture.

Entirely different approaches to obtain *in vivo* insight into protein arrangement within the kinetochore and even count accurate protein numbers of constitutive kinetochore proteins provided new ideas about kinetochore organization. Quantitative measurements of fluorescently labeled structural kinetochore proteins revealed the number of major kinetochore subcomplexes with molecular accuracy (Alushin and Nogales 2011), (Joglekar, Bouck et al. 2006). Since the hallmark of the kinetochore represents a nucleosome containing a centromere-specific histone H3 variant (named CENP-A in vertebrates and Cse4 in *S. cerevisiae*) in two copies per budding yeast kinetochore, the copy number counted for each structural protein complex was relative to the Cse4 molecules. The authors determined that copy number varies from one or two for Mif2 protein up to sixteen to twenty for DDD-complex. This study ascertained, by using the labeled Ctf19-GFP molecules that three copies of the COMA-complex localize per each budding yeast kinetochore.

The two approaches, biochemical approach and quantitative florescence microscopy, in synergy provides the ground for understanding the organization and architecture of this sophisticated and complex structure that is the kinetochore. It has proposed two alternative models for kinetochore organization that are in agreement with both biochemical experiments and microscopic data (Santaguida and Musacchio 2009). The vertical kinetochore implies that the specialized histone alone provides the physical

nucleus for the sequential assembly of other inner and then outer kinetochore components along straight kinetochore verticals. In this model all structural kinetochore proteins have to be strongly connected because the forces exercised by bond microtubules converge directly. On the other hand, the horizontal model proposes horizontal distribution of the kinetochore components, specifically the linker layer kinetochore components. In this model generated kinetochore-microtubule pulling forces can be divided between several contact points, rather than the single one proposed in the vertical model, since both the surrounding and central nucleosome can participate in it.

Despite much work on kinetochore structure and organization, complete understanding of the kinetochore architecture remains unclear. To unravel whether the vertical, horizontal or a new model of the kinetochore architecture represents the objective and true act, persist to be the goal of the researcher.

2. OBJECTIVES

The kinetochore is a large and complex proteinacous structure assembled on the centromere which has many different functions. One of the most important functions is that the kinetochore forms the interface between centromeric DNA and the spindle microtubules and thus supports sister chromatid segregation in mitosis. The kinetochore consists of three protein layers (inner, central and outer) that hierarchically assemble onto the centromeric DNA. The inner kinetochore structures, which are in direct contact with the centromeric DNA, and the outer layer, that associates with microtubules, are best characterized in various species, from the budding yeast to vertebrates. The structure and function of the COMA-network, which is located in the middle of the kinetochore, however, remains least characterized.

The COMA-network is a group of proteins that consists of eleven subunits (Ctf19, Okpl, Mcm21, Ame1, Ctf3, Mcm16, Mcm22, Chl4, Iml3/Mcm19, Nkp1 and Nkp2) that are found to consistently co-purify from yeast extracts when one of their members is affinity purified (Cheeseman, Anderson et al. 2002), (De Wulf, McAinsh et al. 2003). Four subunits of the multiprotein network are the core of the network: the two essential Ame1 and Okp1 proteins, as well as the two nonessential Ctf19 and Mcm21 proteins, together building the COMA-complex.

Therefore, the main goal of this thesis is to establish the overexpression and purification of the tetrameric COMA-complex that would serve as a starting point for further structural studies among the COMA proteins, and also with other biochemically distinct kinetochore complexes.

While all current structural information on the COMA-network is mainly derived from the yeast cell extracts for the distinct complexes, there are no studies that include individual protein-protein interactions. Therefore, an additional aim of this thesis was to establish a binding assay that would reveal the direct physical interaction between particular proteins of the central and inner kinetochore defining the interaction surfaces between the individual components.

Thus, a combination of biochemical reconstitutions and structural characterization of the COMA-proteins may help to refine our understanding of the overall structural organization of the yeast kinetochore. Moreover, this could lead to a better understanding of the chromosome segregation machinery for the simple kinetochore of *S. cerevisiae*, but also that of the very complex human one. Hence, the ultimate goal of current and future research in the field of kinetochore and centromere biology is to

better perceive the mechanisms of accurate chromosome segregation, and errors in them, which can lead to a wide range of diseases, including cancer and aneuploidy-related disorders.

3. RESULTS

3.1 *In vitro* reconstitution of the COMA-complex

We tried to reconstitute the budding yeast COMA-complex and its sub-complexes from *E. coli*. The four-protein complex was described earlier based on genetic (Meraldi, McAinsh et al. 2006) and biophysical (De Wulf, McAinsh et al. 2003) studies done in budding yeast (refer to chapter 1.3.2). Our analysis gained more detailed insight into the organization of this central kinetochore complex and a protein network around it.

3.1.1 The expression system

Novagen offers the Duet line of co-expression vectors that we used in the *in vitro* reconstitution of the COMA tetrameric protein complex.
The Duet vectors contain two T7*lac* promoters followed by a ribosomal binding site (rbs) and multiple cloning site regions. After the second multiple cloning site, there is a T7 terminator.
For the purpose of reconstitution and biochemical characterization of the four COMA proteins, we used three compatible vectors (Fig. 3.1.1):

- pETDuet-1, which carries the ColE1 replicon and *bla* gene (ampicillin resistance), was used for co-expression of Ame1 and His_6-Okp1 proteins
- pCOLADuet-1, which carries the ColA replicon and it is kanamycin resistant, was used for co-expression of Mcm21-TAP and Ctf19 proteins
- pCOLADuet-1 was also used for co-expression of His_{10}-Mcm21 and Ctf19 proteins.

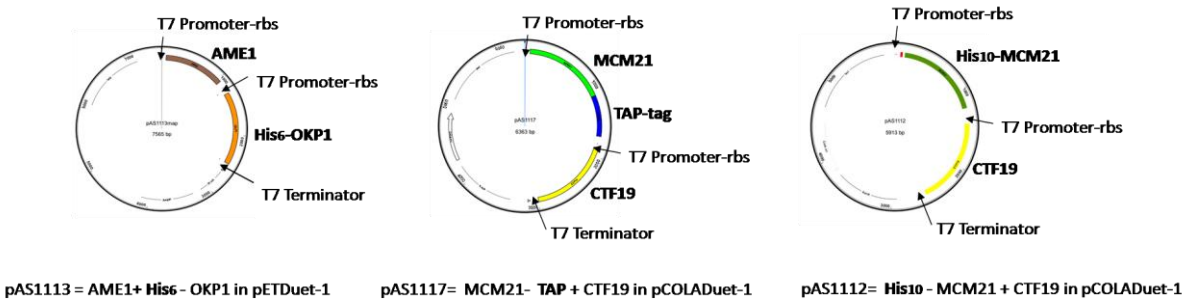

Fig. 3.1.1 Components of the COMA-complex cloned into the pET expression vectors.

Schematic presentation of the expression vectors, highlighting transcription start (promoter) and stop (terminator) sequences as well as position and order of cloned genes. pETDuet-1 vector was used to clone AME1 and His_6-OKP1 dimer while pCOLADuet-1 plasmid was used for His_{10}-MCM21 and CTF19 as well as MCM21-TAP and CTF19 genes.

Protein expressions were performed in Rosetta (DE3)pLysS cells (Novagen) that had been designed for the expression of eukaryotic proteins that contain codons rarely used in bacteria, supplying tRNA for the AUA, AGG, AGA, CUA, CCC and GGA on a chloramphenicol-resistant plasmid.

To reconstitute the fully assembled COMA-complex we developed two strategies. First, we planned to express two plasmids separately and to reconstitute the COMA-complex; from the pET- plasmid (which was Amp^R) two essential genes AME1 and OKP1, and from the pCOLADuet- plasmid (which was KanMX6 resistant) two nonessential genes, MCM21 and CTF19. The second strategy was to express all four COMA proteins together and to purify the tetrameric COMA-complex.

3.1.2 Protein purification strategy

To evaluate direct protein-protein interactions and to biochemically characterize protein complexes we used affinity purifications followed by mass spectrometry. In the standard protein purification procedure, after cell lyses, two purification steps are commonly used. The first step is immobilized metal affinity chromatography (IMAC) followed by size exclusion chromatography (SEC).

IMAC is a separation technique that is based on the coordination between imidazole groups and metal ions. Recombinant proteins fused with a histidine tag (His_6- or His_{10}-tag) bind to immobilized divalent ions like Ni^{2+}, Co^{2+}, Fe^{2+} and Zn^{2+}. In this way the target

protein can be retained on a Me^{2+} chelating matrix and purified from the mixture of proteins in the cell lysate (Fig. 3.1.2).

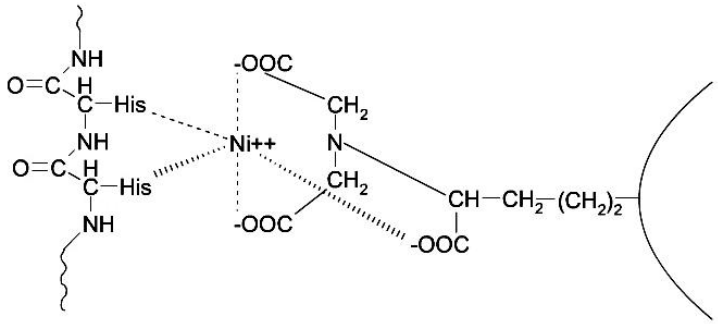

Fig. 3.1.2 Interaction between two neighboring histidine residues and Ni- NTA matrix.

Size exclusion chromatography (SEC) separates proteins based on their size and shape. It serves as a very good method for estimating the molecular weight of measured proteins and also enables separation from impurities with very different molecular weight from the target protein. Additionally and more importantly, SEC serves as one of the most useful tools for separating high molecular aggregates and monitoring the monodispersity, stability and oligomeric state of a target protein. A monodisperse and folded protein generally gives a single symmetrical peak, while a polydisperse, unstable or unfolded protein typically gives multiple asymmetric peaks (Barth, Boyes et al. 1994). A monodisperse size exclusion profile is a good indicator of a protein that is of suitable quality for further biochemical studies.

3.1.3 Reconstitution of the Ctf19 and Mcm21 heterodimer

To reconstitute the Mcm21 and Ctf19 protein complex two expression constructs were made: one with a His-tagged and one with a TAP-tagged construct.

One pCOLADuet-1 expression vector contained the C-terminally TAP-tagged MCM21 gene while the CTF19 had no tag. This vector was actually constructed to allow the purification of a fully assembled COMA-complex via two different tags if coexpressed together with the Ame1 and His_6-Okp1 dimer. In this case usage of both tags allows two subsequent purification steps and production of the highly pure protein complex albeit a

small amount (refer to Fig. 3.1.5). Here, the IgG-sepharose purified protein dimer was eluted by TEV-cleavage and analyzed by SDS-PAGE (Fig. 3.1.3 A).

The second expression vector also derived from the pCOLADuet-1, but instead of the TAP-tag MCM21 bore the N-terminally His_{10}-tag while CTF19 had no tag. The His_{10}-tag vector was made to reconstitute the Mcm21-Ctf19 heterodimer and to produce amounts of the recombinant proteins highly enough for further biochemical characterizations. For protein purification the HisTrap column (GE Healthcare) was used since it has been observed to be more efficient than batch purification with Ni-NTA Agarose beads (Qiagen). After elution with a high imidazole concentration samples were analyzed by SDS-PAGE (Fig. 3.1.3 B).

Proteins were further subjected to size exclusion chromatography (SEC) on a Superdex 200 column (GE Healthcare). SEC was used as an additional purification step in both His- and TAP-purification strategies and to investigate the homogeneity and stability of the dimer. The protein complex behaved similarly throughout both SEC purifications (Fig. 3.1.3).

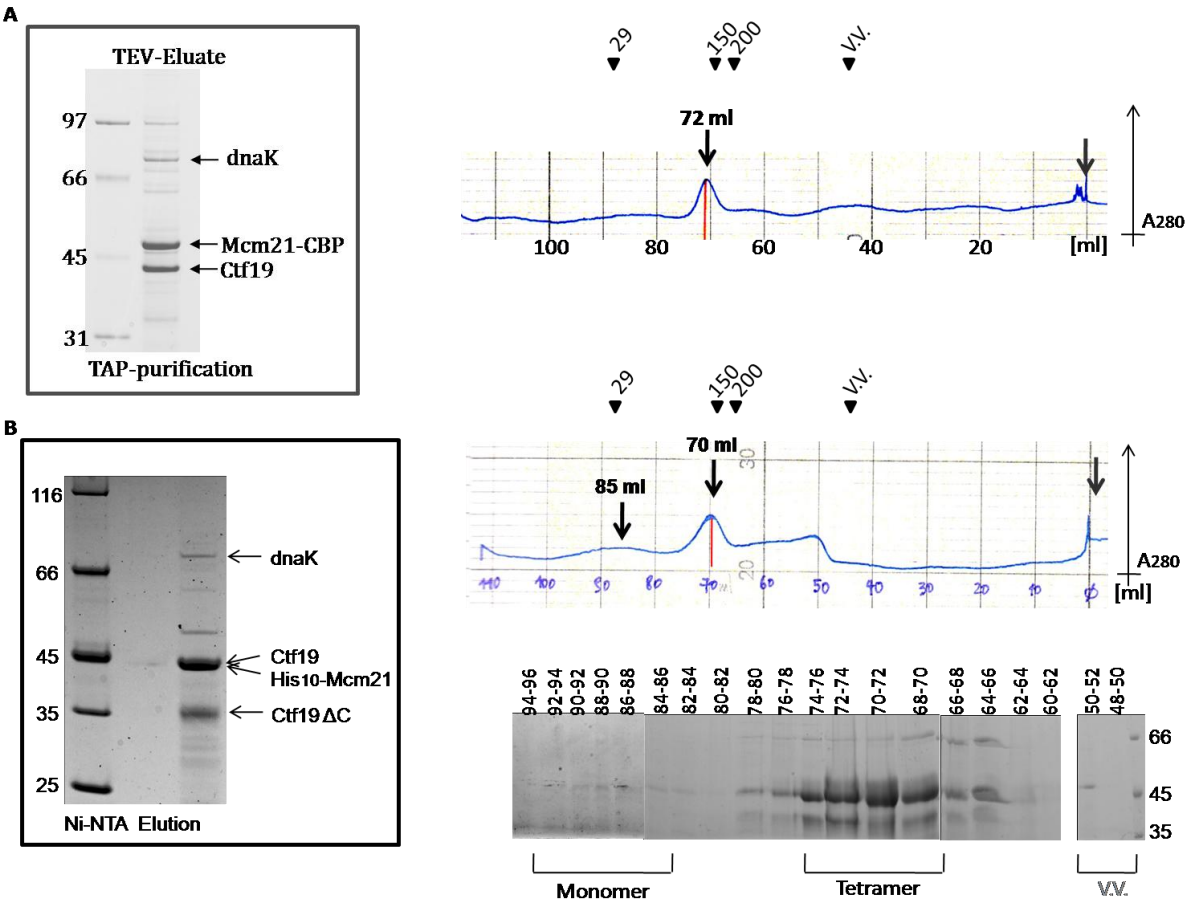

Fig. 3.1.3 Purification of Mcm21 and Ctf19 dimer.

Purified TAP- and His_{10}-fusion Mcm21 protein and Ctf19 protein were analyzed on SDS-PAGE and then further by SEC on S200 column. Injection time was indicated by an arrow.

(A) Mcm21-TAP and Ctf19 proteins were eluted by TEV-cleavage, 1% of elution was shown on the gel. Proteins were further analyzed on the S200 column. 75% collected fractions were TCA precipitated, analyzed on the gel by coll. coomassie staining and proteins were identified by the mass spec.

(B) His_{10}-Mcm21 and Ctf19 proteins were eluted with high imidazole concentration and 10% of elution was analyzed on the gel. Proteins were further analyzed by SEC on the S200. 75% collected fractions were TCA precipitated and analyzed on the gel by coll. coomassie staining. Proteins were identified by the mass spec.

Both variants of the Mcm21 Ctf19-dimer show a peak with an elution volume of approximately 70 ml, which corresponds to the molecular weight of the tetrameric complex. Mcm21 and Ctf19 proteins were also present in small amounts in eluted fractions around 85 ml, which corresponds to the monomeric sizes of these two proteins. Based on the absorbance at 280nm and SDS-PAGE analyzes, there is no significant amount of aggregated proteins that elute at the void volume of the column.

3.1.4 Reconstitution of the essential Ame1 and Okp1 heterodimer

For recombinant Ame1 and His_6-Okp1 dimer, purification was performed as described in the material and methods chapter. Briefly, proteins were first purified by IMAC. After elution with high imidazole concentration, the sample was analyzed by SDS-PAGE and more than two bands were observed. The most prominent bands originated from the Okp1 and chaperone protein dnaK, while the Ame1 protein was found as a weaker band together with the Okp1 and Ame1 degradation bands (Fig. 3.1.4 A).

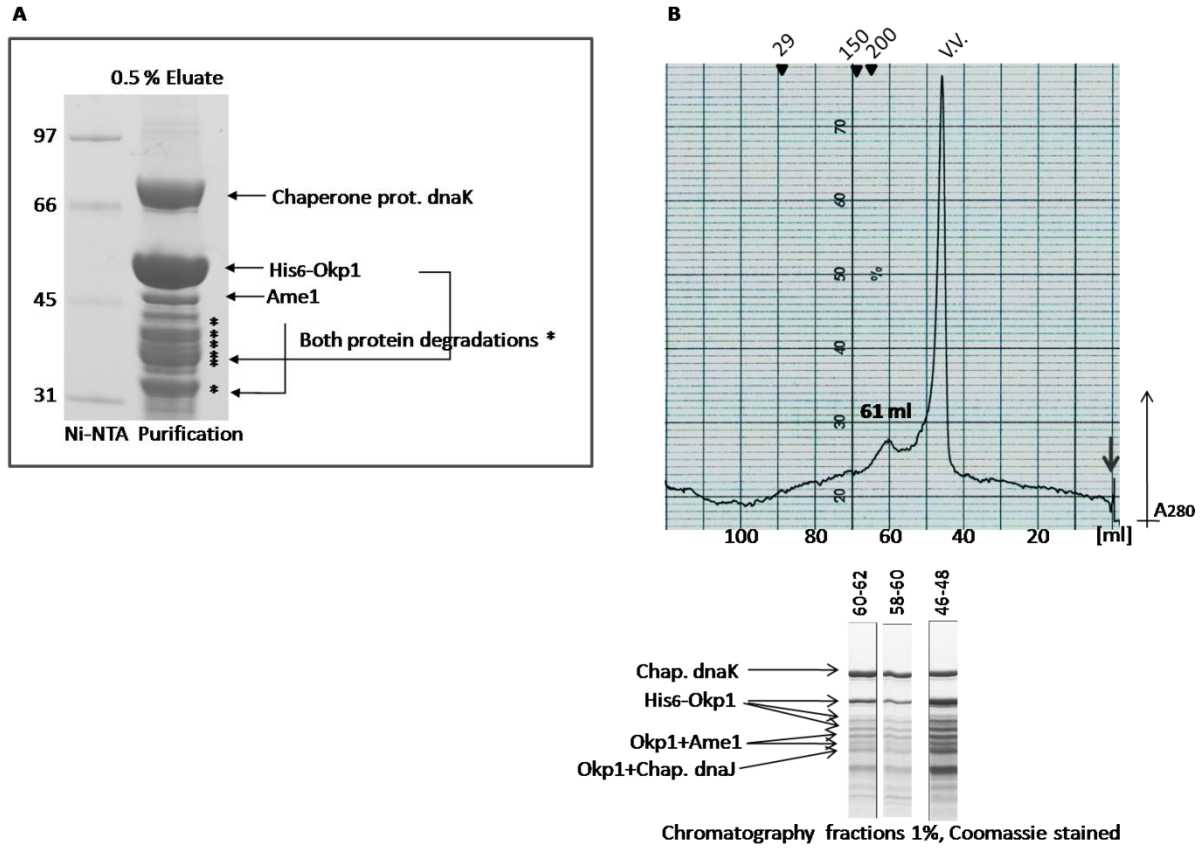

Fig. 3.1.4 Purification of the Ame1 and Okp1 dimer.

Induction was performed in medium containing 0,5 mM IPTG at 25°C for 6 hours. The purification buffer contained 20 mM HEPES pH 8, 250 mM NaCl, 10 mM $MgCl_2$, 40 mM Imidazole, 5% Glycerol and 0,1% Triton X-100.

(A) His_6-Okp1 and Ame1 proteins were purified by a HisTrap column, eluted with 400 mM imidazole, analyzed on SDS-PAGE by Coomassie staining and identified by mass spec analysis.

(B) Proteins were further purified by the SEC on a S200 column. The chromatogram shows absorbance at 280 nm during the run. The arrow indicates injection of the sample. Most proteins were in the aggregated state and elute in the void volume peak.

After the IMAC purification, the His_6-fusion proteins were subjected to size exclusion chromatography on a Superdex 200 column (Fig. 3.1.4 B). Since the purity of the IMAC-eluted sample was not very good, the SEC was used as an additional purification step. The calculated molecular weight of the Ame1 His_6-Okp1 dimer is 85kDa which, according to the known protein standards run on the same chromatography column, should elute around 75ml. However, the majority of the protein complex was found in a heavily aggregated form in the void volume peak (V.V. ~ 43 ml). Besides the void volume

peak, there is a small amount of protein that elutes at 61 ml which also correspond to a higher oligomeric state of the complex.

Additional expression optimization and the choice of a different binding buffer composition did not improve the biochemical behavior of the Ame1 and His_6-Okp1-dimer (Tables 3.1.1 and 3.1.2).

Component	Temperature [°C]	Time [h]
50 mM Lactose	18	14-16 (overnight)
	25	14-16 (overnight)
	30	14-16 (overnight)
1 mM IPTG	20	6
	20	14-16 (overnight)
	25	3
	25	6
	30	6
	37	3
0,75 mM IPTG	20	6
	25	6
0,5 mM IPTG	20	6
	25	6
	25	14-16 (overnight)
0,1 mM IPTG	20	6
	20	14-16 (overnight)

Table 3.1.1 Induction conditions tested during the optimization procedure for Ame1 and His_6-Okp1 dimer expression.

20 mM HEPES	20-50 mM Tris	NaCl	$MgCl_2$	Imidazole	Glycerol	B-ME	Triton X-100
pH 7,5	pH 7,5	100 mM	0	5 mM	0	0	0
pH 8,0	pH 8,0	150 mM	10 mM	20 mM	5%	5 mM	0,1%
	pH 8,5	200 mM		40 mM	10%	10 mM	0,2%
		250 mM				20 mM	0,5%
		300 mM					1%
		500 mM					
		1 M					

Table 3.1.2 Tested binding buffer compositions for the Ame1 and His_6-Okp1 dimer purification optimization.

3.1.5 It is possible to assemble the COMA complex by co-expressing two heterodimers

Seeing that separate expression and purification of the Ame1 His_6-Okp1 heterodimer did not give protein complex to work with, we tried to test whether the recombinant COMA-complex could be reconstituted by the co-transformation of both MCM21-TAP CTF19 (pAS1117) and AME1 His_6-OKP1 (pAS1113) expression vectors into *E.coli*. The purification strategy considered a usage of both tags in two sequential affinity purification steps. Firstly, IMAC exploiting the His_6-tag on the Okp1 protein. Secondly, the elution with high imidazole concentration the COMA-complex by chromatography with a human IgG agarose resin, using the TAP-tag on Mcm21. From the colloidal coomassie-stained SDS-PAGE it is clear that all four subunits of the COMA-complex could be in principal reconstituted *in vitro* by this method (Fig. 3.1.5).

However, all four subunits of the COMA-complex were not present at the 1:1:1:1 stoichiometric ratios. Tagged proteins, His_6-Okp1 and Mcm21-TAP proteins were present more abundantly than the Ame1 and Ctf19 components. Furthermore, the Ame1 protein persisted degrading through the purification procedure. However, analysis of the putatively formed tetrameric complex on coomassie-stained gel revealed a possible physical interaction between the Okp1 and Mcm21 proteins. According to the results it appears that the Okp1 protein, even in the absence of the Ame1, can directly interact with the Mcm21 protein, with or without being in the complex with Ctf19. This conclusion is supported by the synergy of two facts: noticeably smaller amounts of Ame1 and Ctf19 proteins compare to the Okp1 and Mcm21 and, more importantly, there is no background binding for any of the four proteins and the two tags. The latter was examined background binding in the described double purification experiment. We expressed the two plasmids separately. Mcm21-TAP and Ctf19 dimer was then applied onto the HisTrap column and the Ame1 and His_6-Okp1 dimer was used for the TAP-purification. Neither of the complex components showed unspecific binding.

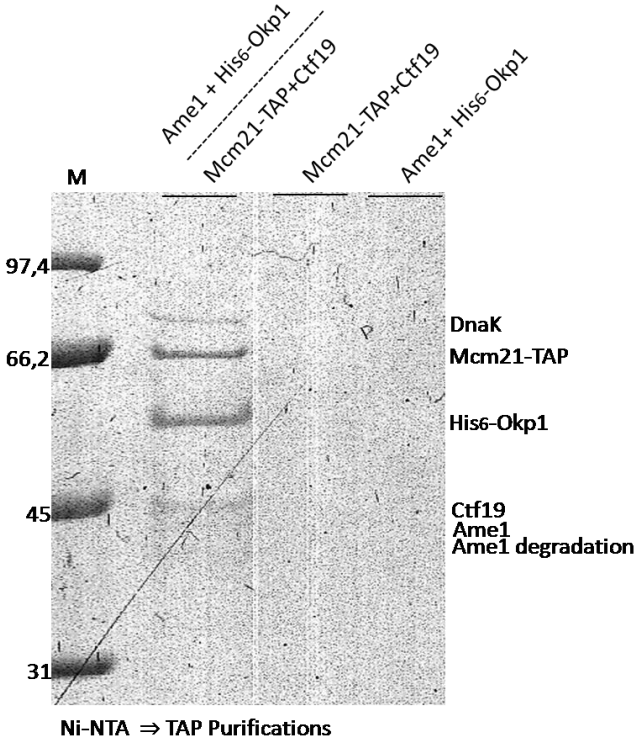

Fig. 3.1.5 Reconstitution of the COMA complex by two affinity purification steps.

Coll. coomassie-stained gel showing reconstituted tetrameric COMA-complex and two control purifications. In the first line after the protein marker, 25% of the acid eluted COMA-complex was shown. In the second line it is shown that there is no background binding of the Mcm21-TAP and Ctf19 proteins if only the IMAC was performed. In the third line no Ame1 and His_6-Okp1 proteins could be detected if only the TAP- purification was performed.

In summary, to reconstitute the budding yeast COMA-complex, we employed two compatible pET-vector expression strategies. Based on expression level and purity, only the Mcm21-TAP Ctf19 dimer showed satisfying behavior and could be identified as highly expressed and stable. The Ame1 His_6-Okp1 dimer showed noticeable instability right from the early stage of IMAC purification. Further purification by SEC showed severe protein aggregation, which made the Ame1 His_6-Okp1 dimer unsuitable for detailed biochemical studies. Despite all the effort to optimize expression and purification conditions, we were never able to reconstitute the Ame1 His_6-Okp1 dimer. When all four components of the COMA-complex had been co-expressed, it might have caused the stabilization effect on the complex. Also, it was indirectly apparent that Okp1 and Mcm21 (with or without being in a complex with Ctf19) proteins can directly interact, but that still remain to be tested directly. Nevertheless, Ame1 protein remained unstable and easy degradable in all expression and purification procedures applied. After two subsequent affinity purification steps, all four components from the COMA-

complex could be identified, but in very small amounts. The stoichiometry between the complex components and a presence of degradation products was also unacceptable. Thus a new expression strategy to reconstitute the budding yeast COMA-complex had to be employed.

3.2 *In vivo* reconstitution of the COMA-complex

To reconstitute the budding yeast COMA tetrameric complex, we adapted a polycistronic expression strategy. The system utilizes the concept of a translation cassette, comprised of the coding region with necessary start and stop codons and of the translational initiation signal (Shine-Dalgarno sequence) and the enhancer (Ɛ) (Tan 2001). A helper expression plasmid, pET3aTr, was used as the source of the translation cassette which could be easily subcloned using particular restriction enzyme pairs into the polycistronic pST39 vector (Fig. 3.2.1).

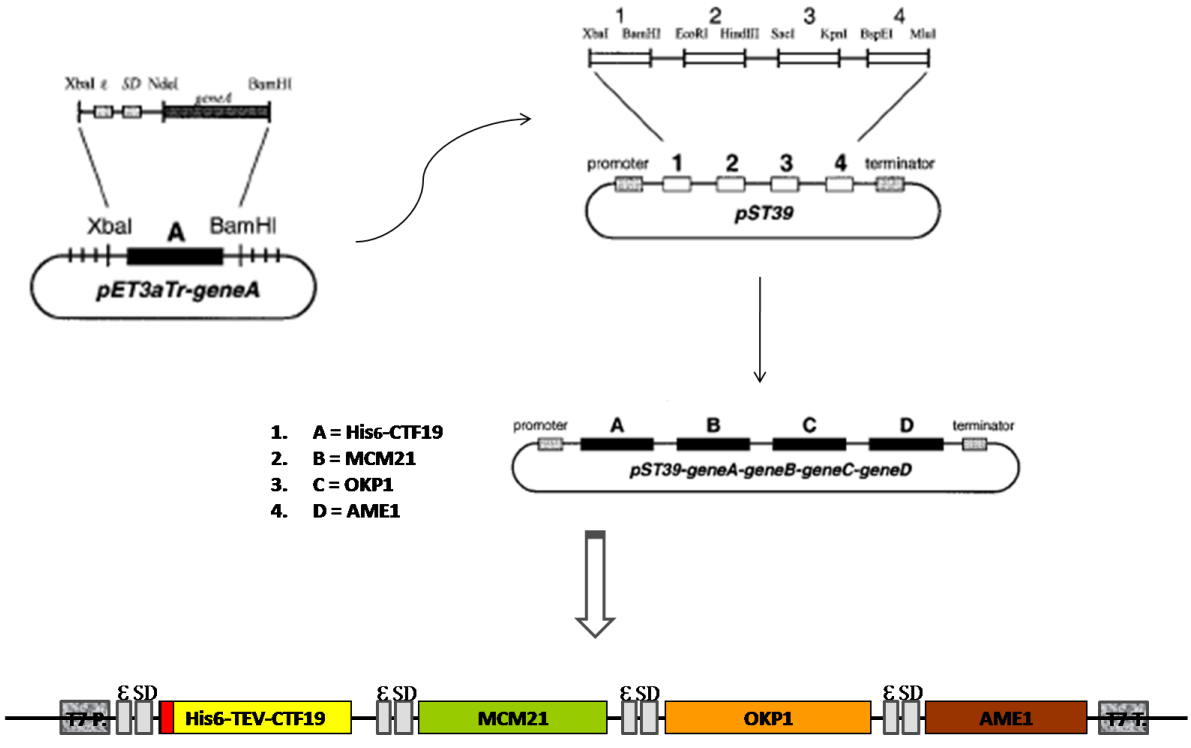

Fig. 3.2.1 Scheme of creation of a polycistronic expression vector from a monocistronic pET3aTr transfer expression vector (adapted from Tan, S., 2001).

Final expressions construct containing T7 promoter, T7 terminator and between them the four COMA genes with enhancers and Shine-Dalgarno sequences for each of them. The IMAC will be performed using the His_6-TEV-tag on the N-terminus of the first gene, CTF19 (schematized in red).

A common approach to produce recombinant protein complexes relies on the *in vitro* reconstitution method, which includes individual expression and purification of complex subunits before combining to form a complex. In contrast, polycistronic expression

vector is suitable for *in vivo* complex reconstitution. This method represents a fast, one-step purification method for up to four proteins. But more importantly, complex components may already be folded together in a cellular environment preventing aggregation of nascent unfolded polypeptides. Thus the order of the genes cloned into polycistronic expression vector might be a critical parameter. Therefore, the selected order of the genes for *in vivo* reconstitution of the COMA-complex was based on conclusions from the previous *in vitro* reconstitution assays. Since the two nonessential genes, Mcm21 and Ctf19, had been expressed and purified from the pET-vectors as stable components, these two genes were cloned close to the promoter. The N-terminally His_6-tagged CTF19 subunit was positioned on the first and the MCM21 subunit on the second place from the promoter. Further, the Ame1 protein has been shown to be the most difficult COMA-complex component to purify. Thus the AME1 was positioned on the last, fourth position from the promoter in the pST39. The remaining OKP1 gene was cloned into the third cassette of the polycistronic expression vector. Taken together, the COMA-expression plasmid comprised of the His_6-CTF19, MCM21, OKP1 and AME1 genes, respectively. In an attempt to gain as much information as possible about the COMA-complex reconstitution, we aimed to reconstitute dimeric, trimeric and tetrameric subcomplexes.

3.2.1 Start to assemble the COMA complex- Ctf19 and Mcm21 stable heterodimer

To confirm the stable subcomplex formation between the Ctf19 and Mcm21 components of the COMA-complex, we expressed these two genes from the polycistronic pST39 expression vector. The initial purification after the IMAC is shown in the Fig. 3.2.2.

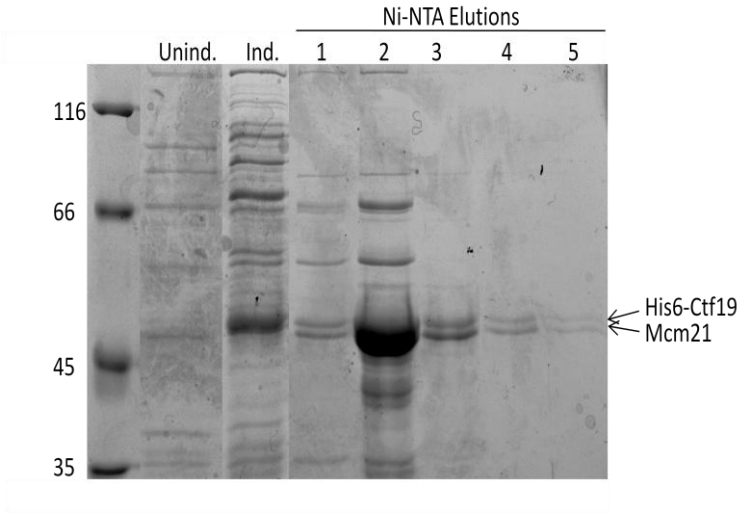

Fig. 3.2.2 Expression and purification of the Ctf19 and Mcm21 dimer.

The Coomassie-stained gel shows different steps during purification: control extract (0,02%), extract after induction with IPTG (0,05%) and five sequential elutions from the HisTrap column (1%).

The purification strategy used a His_6-tag on the N-terminus of the Ctf19 subunit and a HisTrap column. Subsequently, the complex was purified by size exclusion chromatography (SEC). For this purpose, two different chromatography columns were used: Superdex 200 16/60 (data not shown; similar behavior as shown in Fig. 3.1.3 B for the pET-vector expression) and the Superose 6 10/300. Since the S200 column has an optimal separation range for proteins up to 200 kDa MW (suitable for the His_6-Ctf19 Mcm21 dimer with calculated MW=86 kDa but also for the fully assembled COMA-complex with calculated MW=170 kDa) this column would be the most adequate choice. However, to compare different chromatography profiles from various COMA-subcomplexes (in particularly the trimeric CMO-complex; Fig. 3.2.8) that were analyzed on the Superose 6 10/300 column, also the His_6-Ctf19 Mcm21 dimer was analyzed on the Superose 6 column (Fig. 3.2.3).

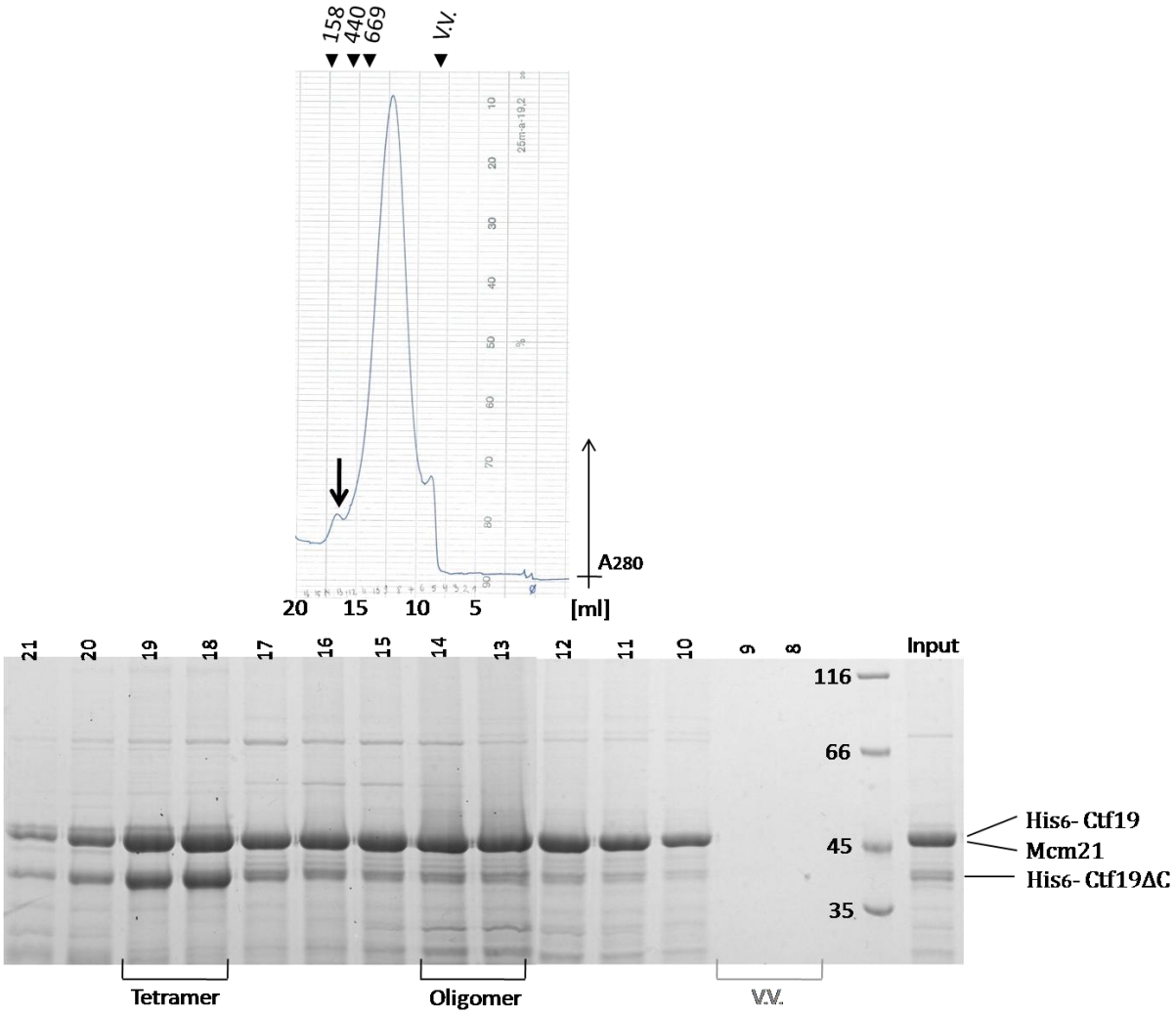

Fig. 3.2.3 The size exclusion chromatography (SEC) of the CM-dimer.

Purified His_6-Ctf19 and Mcm21 were analyzed by the SEC on the Superose 6 column. 50% of collected fractions were TCA-precipitated and separated on the coomassie-stained SDS-PAGE.

The chromatogram presents absorbance at 280 nm during the His_6-Ctf19 Mcm21-dimer separation on the Superose 6 column. To analyze the correspondences between the protein bands and absorption, protein samples were checked on colloidal coomassie-stained gels. Beside the void volume peak at 8ml, two other absorption peaks could be observed on the chromatogram. The major peak around 12,5-13ml corresponds to either a high oligomeric state of the analyzed proteins or it was highly elongated. The minor peak around 17-18ml corresponds to a putative tetrameric form of the His_6-Ctf19 Mcm21-complex (calculated MW=170 kDa), also determined when the protein dimer was expressed from the pCOLADuet-plasmid and analyzed on the S200 column (refer to Fig.3.1.3B). This analysis demonstrated that the largest peak on the chromatogram at

280 nm does not correspond to the highest amount of protein. Particularly, the putative tetrameric form of the complex, represented in a small peak around 17-18ml, contains more proteins then the peak at 13 ml. Taken together, this indicates that something else beside proteins can absorb in the range of the large peak, possibly bound nucleic acids.

An additional band around 40 kDa sizes was found predominantly in fractions that contains the putative tetrameric complex (Fig. 3.2.3). Mass spectrometry analysis identified it as an N-terminal part of the Ctf19 protein (Fig. 3.2.4). Theoretical (calculated) MW for the His_6-CTF19ΔC is 36 kDa which could corresponds to the experimentally obtained MW of around 40 kDa. Since the lack of sites for trypsin digestion and since the Ctf19ΔC was affinity purified via the His_6-tag on the N-terminus, we assumed that the N-terminus of the protein was preserved from the proteolytic degradation.

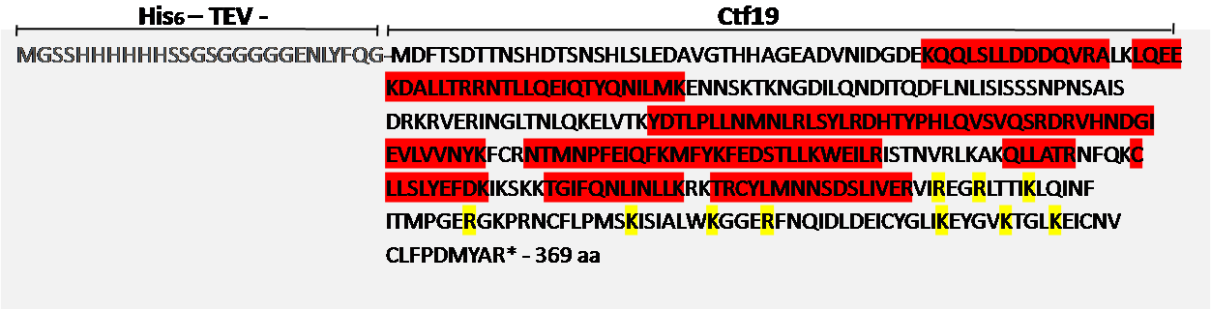

Fig. 3.2.4 Sequence of the His_6-Ctf19ΔC protein after the SEC, analyzed by MS.

The protein band around 40 kDa in size, located in the putative tetramer region, was extracted from the gel and analyzed by the MALDI-TOF-MS. Marked by red color=matched peptides found by mass spec. Marked by yellow color=predicted trypsin cleavable sites that were not recognized in the His_6-Ctf19ΔC protein.

The MALDI-TOF-MS analysis indicates that the truncated Ctf19 protein can also stably interact with the Mcm21 protein *in vitro*. Thus, the N-terminal 280 amino acids of the Ctf19 protein appear sufficient to interact with Mcm21 on SEC, excluding the C-terminal region as an interaction interface between these two proteins.

Also, analyzed SEC elution volumes contained dnaK *E.coli* chaperone, implying that some additional factors may be necessary for the complex stability and maintenance.

3.2.2 Assembly of the Ctf19, Mcm21 and Okp1 heterotrimer

As mentioned before, the OKP1 gene was cloned into the third cassette of the polycistronic expression vector. The expression and purification of the trimeric His_6-Ctf19 Mcm21 and Okp1 (CMO-) complex were carried as described before for the CM-dimer (Fig. 3.2.5).

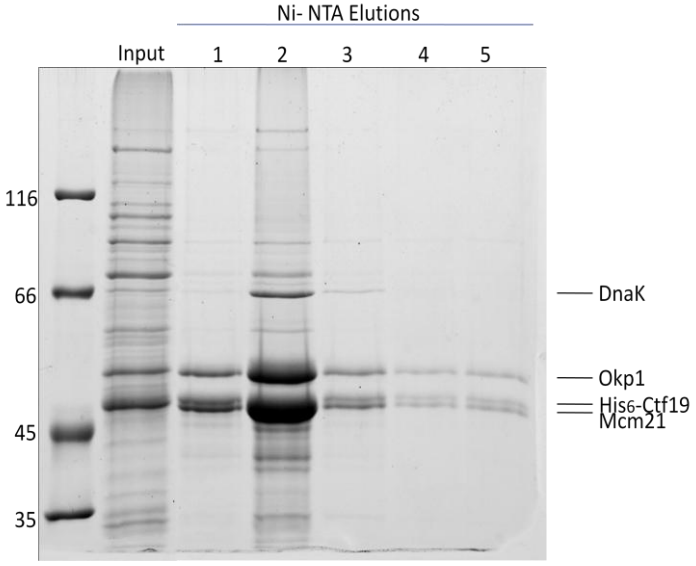

Fig. 3.2.5 IMAC purification of the Ctf19, Mcm21 and Okp1 (CMO-) complex.

The Coomassie-stained gel shows cell lysate after induction with IPTG (Input =0.01 %) and five fractions eluted with high imidazole concentration from the HisTrap column (1-5 = 1%).

The coomassie-stained gel revealed that the Okp1 protein coeluted with His_6-Ctf19 Mcm21 after the IMAC. In fact, the appearance of coomassie-stained bands indicated a 1:1:1 stoichiometry of the trimeric complex (refer to lane 3 Fig. 3.2.5). An important implication of this finding is that the budding yeast His_6-Ctf19 Mcm21 Okp1-complex forms a stable structure that does not depend on the presence of the Ame1 component.
In order to exclude unspecific protein binding to the matrix of the IMAC and to confirm that the Okp1 protein has not been purified as a contaminant, an expression plasmid without the His_6-tag was constructed and used for protein expression and purification. Cell lysates and protein elutions from the IMAC were compared by coomassie-stained gels as well as by the Western analysis (for each protein separately). This revealed that

there was no background binding for any of the tested kinetochore proteins, Ctf19, Mcm21 or Okp1 and that the trimeric complex indeed formed a stabile complex (Fig. 3.2.6).

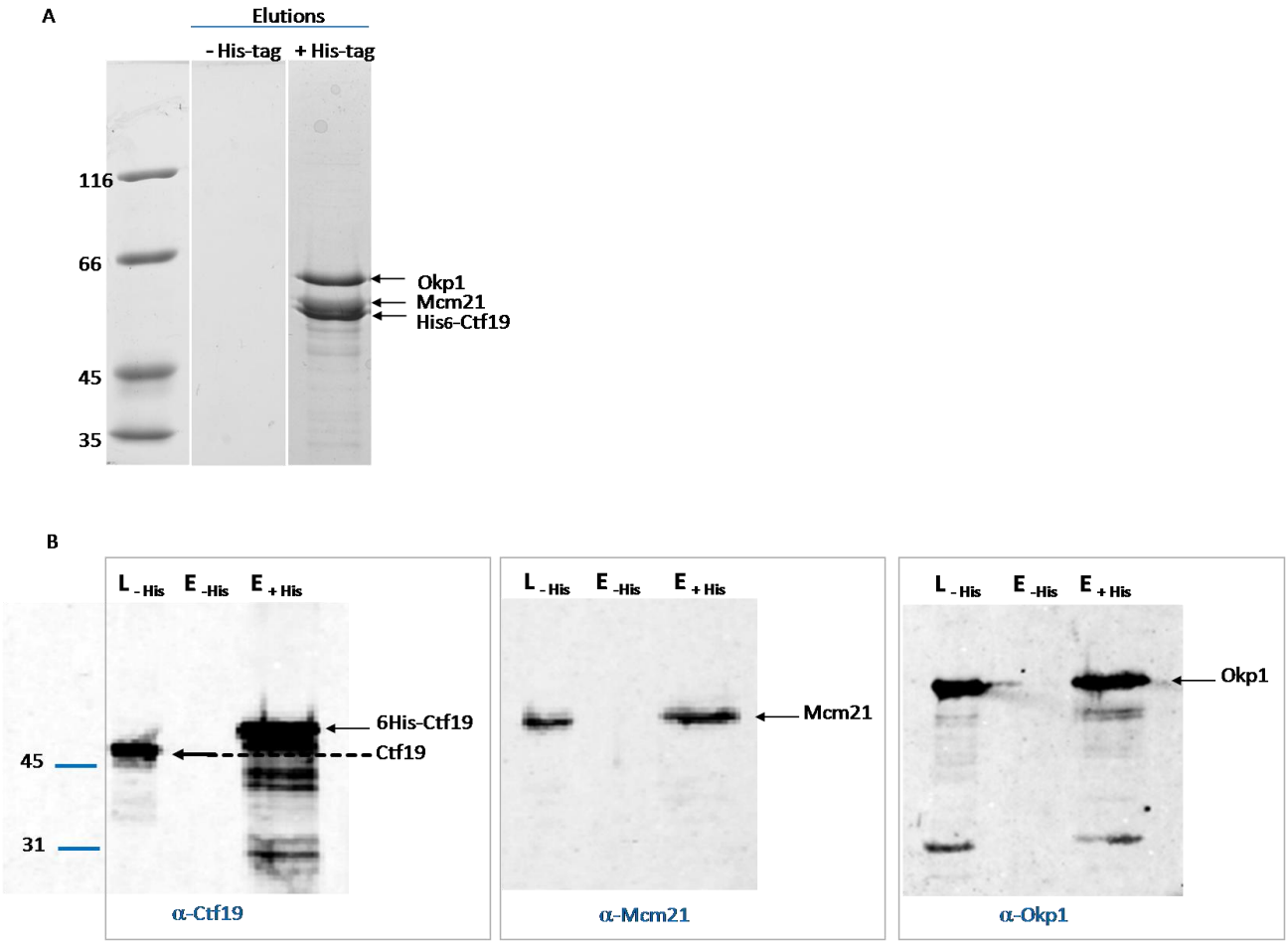

Fig. 3.2.6 Unspecific binding of the His_6-Ctf19 Mcm21 Okp1-complex was not detected.

(A) Comparing elution fractions (0,3%) from the constructs carrying His_6-tag and the one without the tag on the coomassie level, no background binding was detected.

(B) On the Western blot levels, Ctf19, Mcm21 and Okp1 proteins were examined from the same sample but using three different antibodies. Proteins were detected in the cell lysates (0,01%) but not in the elutions (1%) from the expression of the non-tagged plasmid, which was shown in the first two lines in each SDS-PAGE. Elution of the His_6-tagged plasmid was loaded as the third line in each SDS-PAGE as a control for Western blot analysis.

To characterize the size and oligomeric state of the His_6-Ctf19 Mcm21 Okp1-complex, the IMAC-purified complex was further analyzed by the SEC on the Superose 6 and Superdex 200 columns. The absorbance at 280nm was measured and collected fractions were analyzed on coomassie-stained gels (Fig. 3.2.7).

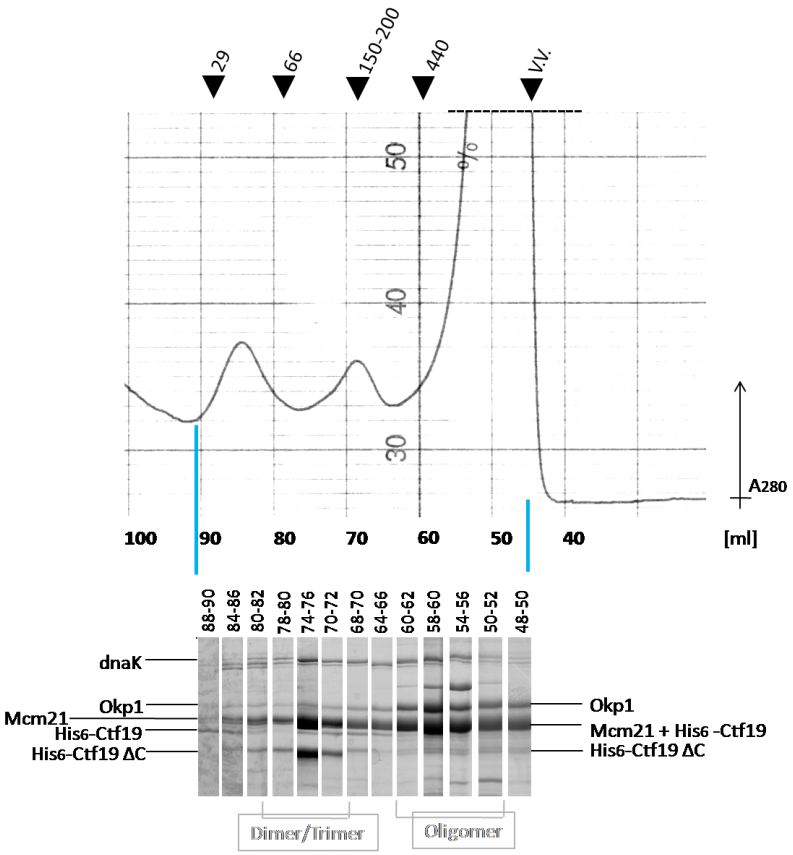

Fig. 3.2.7 The SEC run of the His_6-Ctf19 Mcm21 Okp1-complex onto the S200 column.

After the IMAC purification proteins were applied onto the PD-10 desalting column, concentrated and used for the SEC onto the S200 column. 20% of each eluted fraction was directly analyzed on SDS-PAGE stained by coll. coomassie.

The size exclusion profile of the His_6-Ctf19 Mcm21 Okp1-complex indicates that the solubilized proteins are present in different oligomeric states. While the largest peak of absorption at 280 nm presents the void volume of the column, there are two smaller additional peaks eluting at the higher volumes. The major problem in interpreting this experiment emanates from the fact that the absorption peaks at 280nm did not correlate with the peaks in protein amounts estimated by coomassie-stained gels (elaborated in the following section 3.2.3). Analysis of the fractionated protein on colloidal-coomassie stained gels revealed presence of a highly oligomerized state of the complex, but also the putative dimeric or trimeric form of the complex (around 74-76ml). The formerly observed tetrameric His_6-Ctf19 Mcm21 form that elutes around 70-72ml (Fig. 3.2.3) without the Okp1 protein might be present here too. By observing the protein densities it appears that the Okp1 protein mainly contributes to the higher oligomeric forms of

the CMO-complex, thus enabling the predominant presence of the His_6-Ctf19 Mcm21 putative tetramer around 74 ml.

Since the CMO-complex appeal to be larger than expected, we decided to test the same sample on the Superose 6 10/300 column, which has an optimal separation range (5-5000 kDa) for larger proteins compare to the S200 (separation range 5-250 kDa)(Fig. 3.2.8).

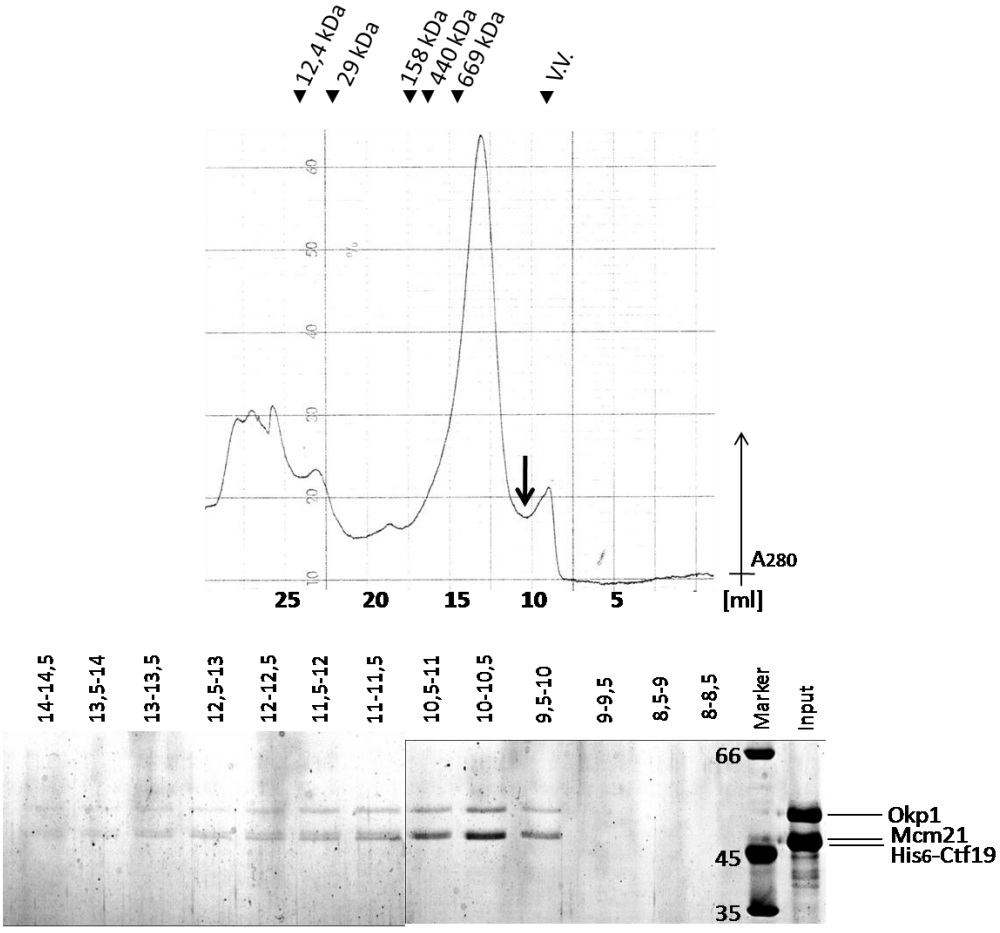

Fig. 3.2.8 The SEC run of His6-Ctf19 Mcm21 Okp1-complex onto Superose 6 column.

The sample was centrifuged and injected onto the Superose 6 10/300 column right after the IMAC (Input=5%). 4% of each eluted fraction was directly analyzed on SDS-PAGE stained by coll. coomassie.

The size exclusion profile, as detected by absorption measurement at 280 nm, of the trimeric-complex on Superose 6 consists of a small void volume peak and a large peak at 13ml (which corresponds to approximately 800 kDa molecular weight). Nevertheless, as for the SEC run onto the S200, the absorption peaks at 280 nm and the amount of proteins verified by the coomassie-staining on the SDS-PAGE after the run at Superose 6,

could not be correlated. Most proteins eluted within the 10.-11.ml and this corresponds to very high molecular weight proteins, higher than routine protein standards used for the column equilibration. Either the protein complex has a very elongated shape, or it is in the oligomeric form. From the biophysical studies performed on *S. cerevisiae* crude cell extracts, it is known that the whole COMA-complex as well as the two heterodimers, Ame1-Okp1 dimer and Ctf19-Mcm21 dimer, does not show a spherical but an elongated shape (De Wulf, McAinsh et al. 2003). Here, we used standard calibration curve for the Superose 6 10/300 to estimate the measured size of the CMO-complex (Fig. 3.2.9).

Component	Molecular Weight [Da]	Amount per Vial [mg]	Elution Volume [ml]
Thyroglobulin	669000	5	13,7
Ferritin	440000	0,4	15,6
Aldolase	158000	4	17
Carbonic anhydrase	29000	3	22
Cytochrome C	12400	2	23,5
CMO-complex	1348495	1	10,5

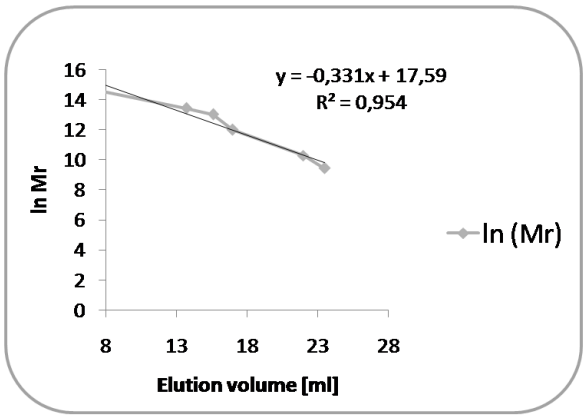

Fig. 3.2.9 Calibration of the Superose 6 10/300 GL

The standard curve for the Superose 6 was made using the 0,5ml of protein standards mixture (listed in table above) to the column. The curve is prepared by blotting the logarithm of the molecular weights of the calibration proteins against the elution volumes. The molecular weight of the CMO-complex was then extrapolated from the curve.

The extrapolated molecular weight of the oligomerized CMO-complex, which eluted at 10,5ml, is 1,34 MDa. Since the presence of nucleic acids can influence the

chromatography behavior of proteins, we next asked if the major peaks observed in the last experiments originate from nucleic acid contamination in the protein samples.

3.2.3 What causes the absorbance at 280 nm in the CMO-protein sample?

The protein amounts during the SEC were measured using a UV-detector registering absorbance at 280 nm. However, the protein amounts from the collected fractions analyzed on coomassie-stained gels could not be correlated with the chromatograms obtained. To explain this, we first asked if the SEC tested proteins could absorb enough to be seen on the chromatogram, and second, if any non-protein component from the solutions that absorbs UV-light at 280 nm might interfere with the measured signal strength.

Protein primary structures, in the concrete presence of aromatic amino acids (as well as two cysteine residues linked by a disulfide bond); will define protein absorption features at 280 nm. Compositional features of Ctf19, Mcm21 and Okp1 proteins were summarized in Table 3.2.1.

	Ctf19	Mcm21	Okp1
Number of amino acids	369	368	406
Molecular weight [kDa]	42,782	42,971	47,349
Theoretical pI	8,79	4,90	6,08
Charge	9,5	- 17	- 0,5
Number of Trp (W)	2	3	2
Number of Tyr (Y)	11	5	12
Number of Cys (C)	7	1	1
Extinction coefficient [M^{-1} cm^{-1}]	27390	23950	28880
Abs 0.1% (=1 g/l) at 280 nm	0,640	0,558	0,610

Table 3.2.1 Compositional features of CMO-complex proteins.

From the Ctf19, Mcm21 and Okp1 protein sequences it is clear that they all have sufficient number of tyrosines and tryptophans absorbing at 280 nm, and if analyzed in acceptable concentrations should be detectable.

Many other cellular components, in particularly nucleic acids, also absorb UV light. The ratio of A_{260}/A_{280} is often used as a criterion of the purity of protein or nucleic acid samples during their purification (Table 3.2.2).

% protein	% nucleic acid	260/280 ratio
100	0	0,57
95	5	1,06
90	10	1,32
70	30	1,73

% nucleic acid	% protein	260/280 ratio
100	0	2,00
95	5	1,99
90	10	1,98
70	30	1,94

Table 3.2.2 The ratio of absorptions at 260nm and 280nm used to asses nucleic acid contamination of protein solutions and vice versa (adapted from Sambrook and Russell, 2001).

The 260/280 ratio of collected chromatography fractions from the SEC peak on the Superose 6 shown in Fig. 3.2.8 was around 2. This is an indication of high nucleic acid content in the protein samples.

In order to remove nucleic acid contamination, we first wanted to determine which nucleic acids are present within the purified His_6-Ctf19 Mcm21 Okp1 proteins. To resolve this, Benzonase, DNaseI and RNase A were used to treat either crude or purified samples (Fig. 3.2.10).

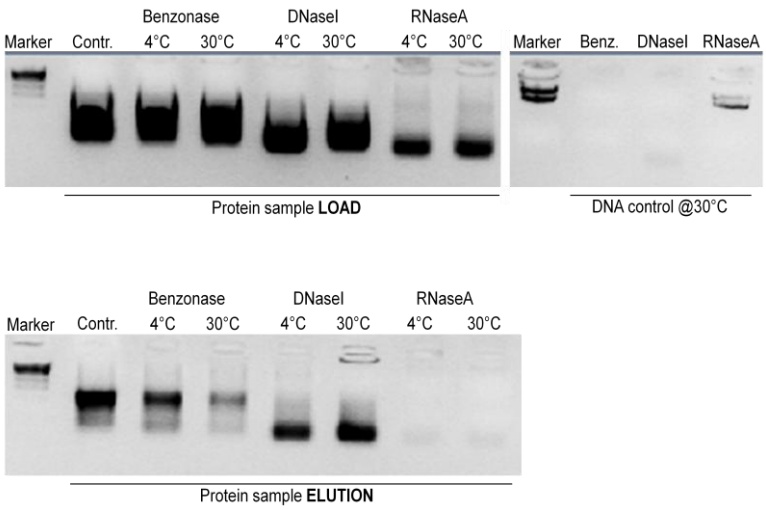

Fig. 3.2.10 RNA presence in purified protein sample identified by RNaseA treatment.

Two types of the protein samples, crude cell lysate and IMAC-elution, as well as the protein expression plasmid DNA as a control for nuclease treatment, were tested by gel electrophoresis and EtBr staining. Untreated samples were referred as controls (Contr.) for each of the tested sample type. 0,04% of cell lysate (load) and 1% of elution were treated with 0,005U of Benzonase, 50 µl/mg DNaseI and 50 µl/mg RNaseA at 4°C and 30°C for 1 hour. 1 µg of plasmid DNA was treated with the same amount of nucleases at 30°C for 1 hour. Samples were then analyzed on 1% agarose gel stained with EtBr.

Benzonase, recombinant endonuclease which was specifically developed to degrade all forms of DNA and RNA, did not efficiently remove nucleic acids for unknown reasons. Upon digestion at 4°C or at 30°C, either when crude cell lysate or purified proteins were used, benzonase treatment was inefficient. The DNaseI treatment weakly diminished the nucleic acid content, but only for the purified samples and not for the crude cell extracts. The functionality of both enzymes was tested by digestion of plasmid DNA under the same conditions. Incubation of the crude cell extracts with the RNase A did not completely remove RNA and it caused protein degradations (data not shown). However, after the purified protein sample was treated with RNase A no RNA could be observed on the EtBr-stained agarose gel. These results suggest that His_6-Ctf19 Mcm21 Okp1 protein complex may interact with RNA.

To test whether the central kinetochore CMO-complex interacts with nucleic acids we performed the band shift assay. Does the nucleic acid in the samples show altered mobility in gel after the protein is removed? We wanted to explore if there is a difference in mobility of the RNA in the presence and absence of the proteins. Under the experimental conditions described in the materials and methods chapter, the protein was removed by Proteinase K treatment followed by phenol/chloroform extraction. After the protein complex was removed, nucleic acids migrated faster through the agarose gel (Fig. 3.2.11 A lane 2). This effect is a consequence of either specific or unspecific interaction between nucleic acids or the purified proteins.

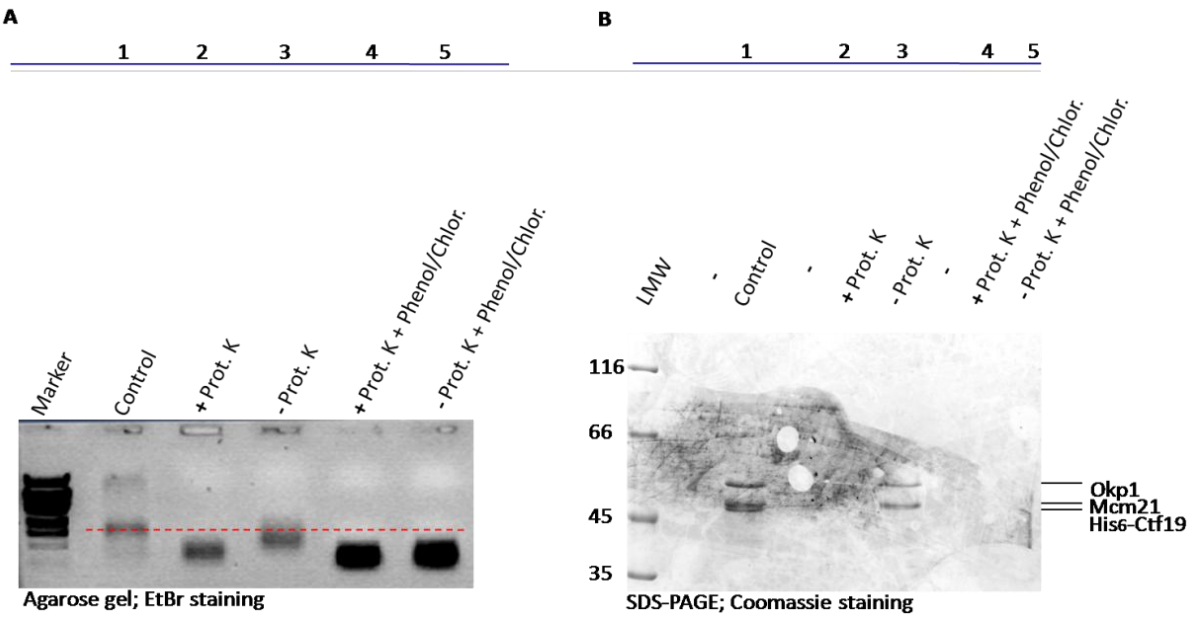

Fig. 3.2.11 Protein-RNA interaction tested by a gel shift assay.

Purified trimeric protein complex was first treated with 100µg/ml Proteinase K for 2 hours at 37°C and then RNA was extracted by phenol/chloroform/isoamyl alcohol. Samples were checked for both, nucleic acids (A) and protein content (B). Analyzed samples constituted 2% purified protein fractions.

In the protein sample where Proteinase K was omitted, a minimal band shift compared to the control was observed, possible due to a minor protein degradation (Fig. 3.2.11 A and B lanes 3). Following phenol/chloroform/isoamyl alcohol extraction in samples with or without Proteinase K, no proteins could be detected on the SDS-PAGE (Fig. 3.2.11 B lane 5). If the same sample was analyzed on the EtBr-stained agarose gel, significant band shift compared to the control was noticed (Fig. 3.2.11 A lane 5). These data indicate that the His_6-Ctf19 Mcm21 Okp1-complex may bind RNA. Since the RNA originated from the host cells, we conclude that the protein-RNA interaction we observed was an unspecific interaction. Nevertheless, this observation may indicate that the COMA-complex once localized to the CEN-DNA (via the CBF3-complex) could interact directly with the DNA.

3.2.4 Assembly of the Ctf19, Mcm21 and Okp1 complex pre-treated with RNaseA

We were wandering whether the RNA contamination affects the CMO-complex purification; particularly elution behavior in gel filtration of the complex. Thus, a new strategy for the His_6-Ctf19 Mcm21 Okp1-complex purification was applied. The expression of the protein complex was as previously described. After the first Ni-NTA purification, eluted proteins were collected, run through desalting PD-10 column, treated with RNase A at 4°C for 20-30 min and then used for the second Ni-NTA, the second PD-10 column and finally the SEC. We used the second IMAC in order to eliminate RNAse A from the sample before the SEC. Notably, the profile of absorption at 280 nm of the RNase A treated sample (Fig. 3.2.12) is very different from the one of the untreated sample shown before (Fig. 3.2.8).

Protein purification scheme:

Ni-NTA purification ⇒ PD10 desalting column ⇒ RNaseA treatment ⇒ second Ni-NTA purification ⇒ second PD10 column ⇒ SEC

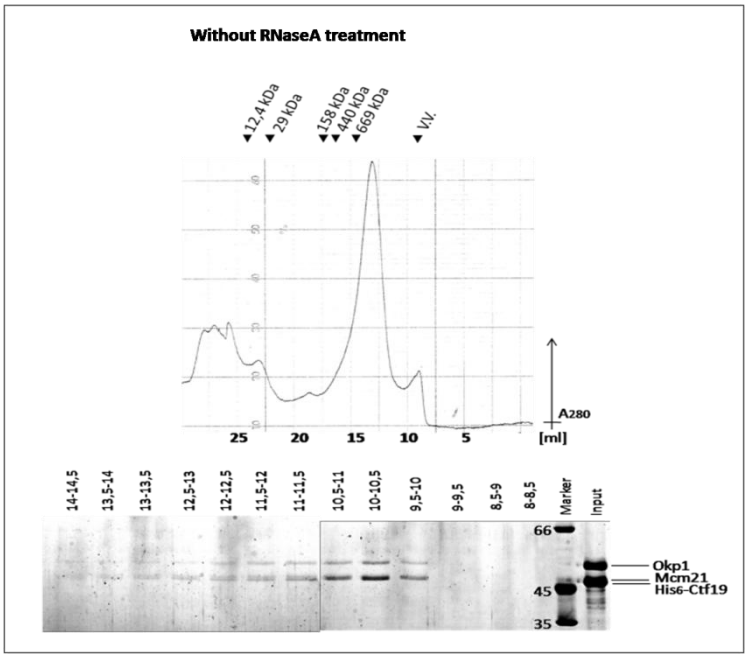

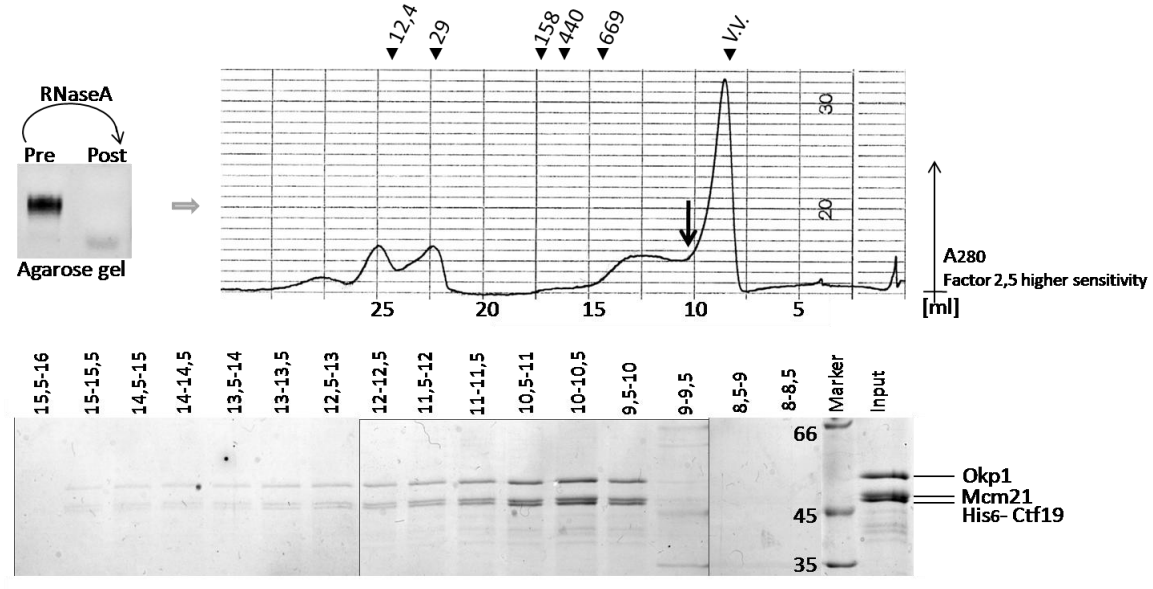

Fig. 3.2.12 The size exclusion chromatography (SEC) of the His_6-Ctf19 Mcm21 Okp1-complex pre-treated with RNaseA.

The trimeric CMO-complex was analyzed on the Superose 6 column after two sequential Ni-NTA purifications. The second purification was included because of the RNaseA treatment of the sample following the first affinity purification step. The chromatogram shows a strong void volume peak and a small peak at 12,5-13 ml. 4% of each collected fraction was directly analyzed on the coll. coomassie-stained SDS-PAGE. Top, left panel shows the chromatogram of the purified proteins without the RNaseA treatment. Here, the UV-meter was set to measure the absorbance at 280 nm with 2,5 lower sensitivity compared to the RNaseA treated sample.

A comparison of the SEC using the Superose 6 for the RNase A treated and the RNase A untreated samples, ascertained a similarity in the elution volume and stoichiometry of the His_6-Ctf19 Mcm21 Okp1-complex. The size exclusion profile at 280 nm of the sample pre-treated with the RNaseA on the Superose 6, consists of a big void volume peak at 8 ml and a smaller broad peak around 12,5-13 ml. When the protein sample was treated with the RNase A, the void volume peak on the Superose 6 became approximately 5 times higher compared to the peak at 12,5-13 ml (if the RNase A treatment is omitted, the void volume peak was about 5 times smaller than the 13ml-peak) while the elution profile remain the same (proteins eluted around 10,5 ml). We concluded from this experiment that the major peak at 12,5-13 ml originated from RNA, which does not interact with the purified CMO-complex. Also, the obtained purified CMO-complex is indeed in the oligomeric form, with molecular weight approximately 1,34 MDa.

3.2.5 Further biochemical analysis of the CMO- complex by limited proteolysis

Limited proteolysis by trypsin, was used to map proteolitically resistant segments of the His_6-Ctf19 Mcm21 Okp1-complex in order to get more information on the protein domains that are stable and/or involved in complex formation. Trypsin digestion, which cleaves at the C-terminus of lysine or arginine except when either is followed by proline, was used to probe the sites for enhanced flexibility or local unfolding of a polypeptide chains (Fontana, de Laureto et al. 2004). We used the recombinant CMO-trimeric complex purified first by the HisTrap column and then run through the PD-10 column. Treatments at 1:20, 1:100 and 1:500 (wt/wt) ratios of enzyme to substrate for time-dependent proteolysis were carried out with a similar outcome. Proteolytic fragments were separated on the SDS-PAGE and analyzed by MALDI-TOF-MS (Fig. 3.2.13).

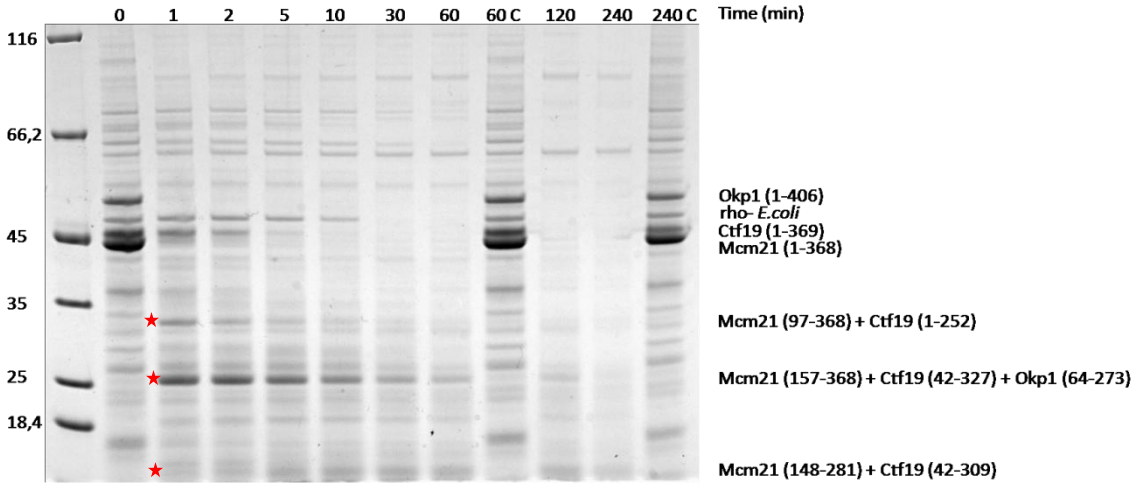

Fig. 3.2.13 Time-dependent limited proteolysis treatment of the CMO-complex with trypsin.

Purified CMO-complex was digested with Trypsin at 1/100 (wt/wt) of enzyme to proteins ratio at 37°C for 4 hours. Aliquots were collected after 1, 2, 5, 10, 30, 60, 120 and 240 minutes. As control samples, aliquot was taken at the beginning; time point zero, as well as after 1 and 2 hours from the sample where Trypsin was omitted. After running SDS-PAGE, newly appeared bands (★) were analyzed by MS.

Mapped proteolytically resistant segments of the proteins may suggest locations of coiled-coil regions in each protein. By comparing the predicted coiled-coil domains (Lupas, Van Dyke et al. 1991) and analyzed stabile peptides derived by trypsination, a certain analogy can be made (Fig. 3.2.14).

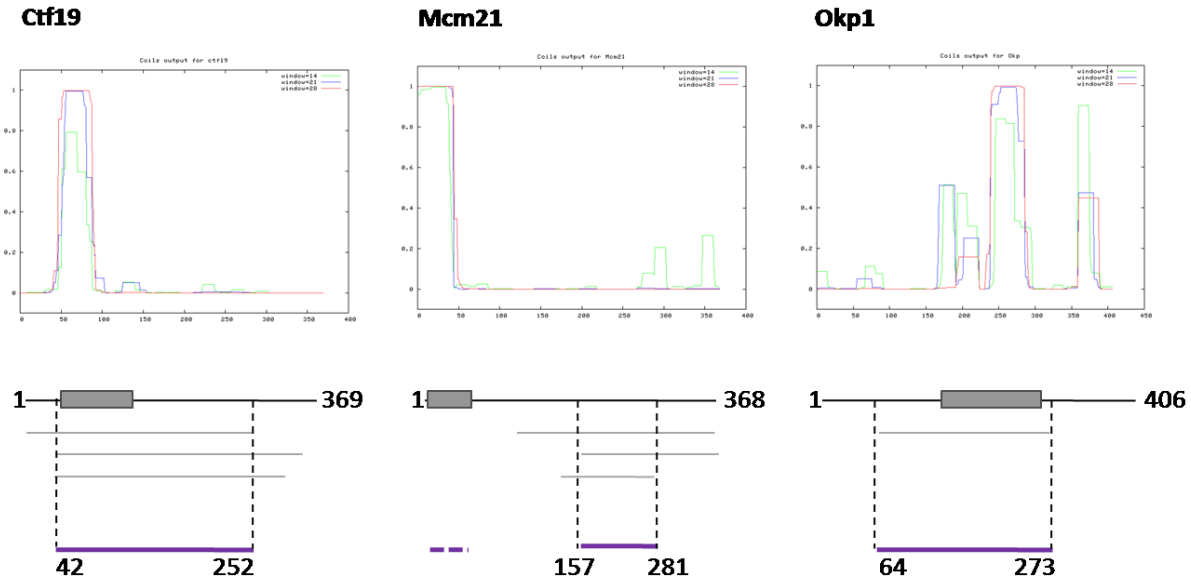

Fig. 3.2.14 Comparison of the obtained proteolytic peptides with the coiled-coil predicted algorithm output for the Ctf19, Mcm21 and Okp1 proteins.

The upper panel of the figure shows the plots that were predicted coiled-coil domains and their schemes (gray rectangle) for each of the three proteins. In the bottom of the figure experimentally obtained protease resistant fragments (in dark gray) and the deduced minimal protein segment resistant to the tripsination (in violet) were depicted for the same CMO-protein complex.

Experimentally obtained protease resistant fragments for each protein were compared and the minimal stabile protein region was then deduced. Derived domains clearly demonstrate that predicted coiled-coil domains of the Ctf19 and Okp1 proteins include the protease resistant fragments. The calculated coiled-coil region for the Mcm21 protein was not found on SDS-PAGE as an intact part of the obtained peptide. This can be explained if assume the presence of a flexible and unstructured region between the very N-terminal coiled-coil region (approximately 11 kDa, that was too small to be seen on the PAGE) and the more stable packed central region of the protein. In order to inspect whether this N-terminal fragment of Mcm21 protein interacts with the Ctf19 or Okp1 protein and thereby contributes in the complex formation, a gel filtration chromatography could be performed.

3.2.6 Further biochemical analysis of the CMO- complex by dynamic light scattering

Dynamic light scattering (DLS) was used as a powerful tool to measure the hydrodynamic radius (R), polydispersity and the presence of aggregates in the protein samples. The DLS method is based on the fact that molecules in solution undergo Brownian motion, causing fluctuations in the scattered light intensity. A detector, set at 90° angle according to the incident laser light, then measures the change in light intensity. The translational diffusion coefficient D_T is automatically calculated from this data, based on the certainty that the small particles diffuse faster than the large ones. From the D_T a hydrodynamic radius of the molecule in solution (R) can be calculated (in nm). Furthermore, the molecular weight (MW) of the particle can also be estimated if it is assumed that the shape of the particle can be represented as spherical or elongated (Borgstahl 2006).

A trimeric protein complex, purified by the IMAC, was verified on the SDS-PAGE, the amount of proteins were estimated and the sample was diluted to approximately 0,5 µg/µl in buffers containing different salt concentrations. The measurements were performed for the four different buffers, containing 150mM, 200mM, 300mM and 500mM NaCl, at 4°C and 20°C. The two extreme measurements, the one with the buffer containing the highest salt concentration (500mM NaCl) at the 20°C, and the other with the buffer containing the lower salt concentration (150mM NaCl) at 4°C, were compared in the Fig. 3.2.15.

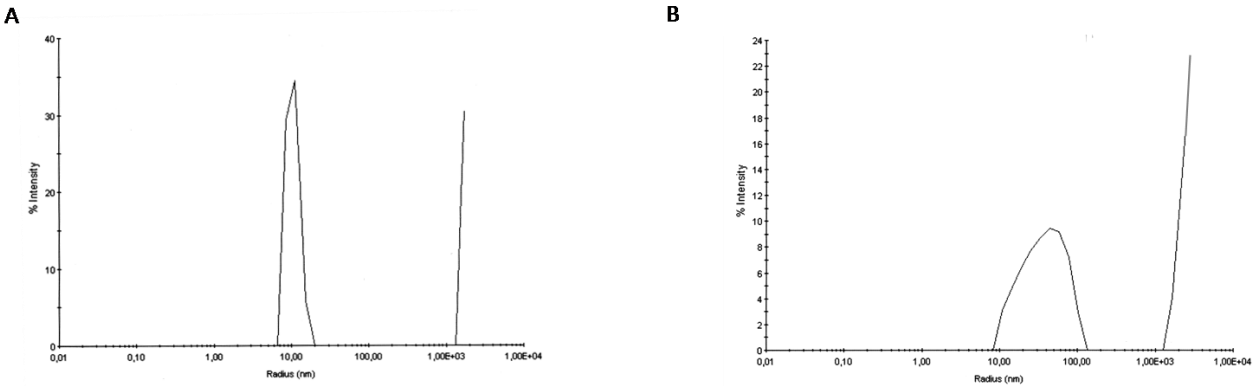

	Item	R (nm)	%Pd	MW-R (kDa)	%Int	%Mass
A	Peak 1	10.5	18.1	827	69.5	99.4
	Peak 2	1748.4	0.0	130115000	30.5	0.6
B	Peak 1	42.0	57.2	21146	59.5	86.2
	Peak 2	2544.4	17.2	313028000	40.5	13.8

Fig. 3.2.15 Two representative DLS measurements and the summarization of the obtained results.

The size distribution of the CMO-complex particles at the two extreme experimental conditions, measured by the dynamic light scattering (DynaPro, Protein Solutions) and the specific data grid of each measurement in the bottom of the figure.

(A) Measured at 4°C in buffer containing 150 mM NaCl, CMO-complex behaves as approximately 70% homogenous with particle sizes around 800 kDa.

(B) As the ionic strength of buffer increase, with the maximal tested 500 mM NaCl, especially if the temperature increase from 4°C to 20°C, the complex highly aggregates.

Before interpreting the data, we should mention that the measurements were evaluated as acceptable, according to the two parameters: baseline, which was regularly around 1, and low SOS errors. The SOS error (sum of squares) is the difference between the measured data and the calculated intensity correlation curves. The software determines the uniformity of particle sizes by comparing the single particle size with a Gaussian distribution and uses this value for the SOS error determination. Also, the polydispersity (Pd) or standard deviation is indicative of the peak distribution. %Pd, or normalized polydispersity, is calculated by dividing Pd by R and reported as a percent. The last two parameters in Fig. 3.2.15 were peak intensity and peak mass in percentages and the sum of these parameters for all the peaks within one measurement has to be 100%. The percentage mass calculation correlates the size of particles with the percentage of the peak intensity to assert the factual peak measure. All this information was adapted from the DynaPro Operator Manual.

The DLS measurements at various conditions revealed differing behavior and homogeneity of the protein sample. The best results were achieved if the lower strength buffer was used at 4°C. The sample was characterized as an oligomeric complex in a solution with an estimated molecular weight of 827 kDa, which is approximately six times bigger than the theoretical molecular weight for 1:1:1 stoichiometry of the CMO-complex. For the best result that we obtained, a normalized polydispersity (standard deviation, %Pd) was 18,1; which is between 15 and 30, thus presenting the complex as more likely to be able to crystallize. Unfortunately, we were not able to crystallize the trimeric His_6-Ctf19 Mcm21 Okp1-complex under various conditions using the primary, diverse reagent system crystallization screen for proteins (Index screen, Hampton Research).

As the ionic strength of the buffer and the temperature increased, with the maximal tested 500 mM NaCl and measured at 20°C, the complex highly aggregates.

The DLS measurements described above were done before we ascertained the presence of nucleic acids within the COMA-kinetochore protein samples. To perform the DLS measurements with the RNase A pre-treated sample remain to be done.

3.2.7 Attempts to reconstitute the COMA-tetrameric complex

To reconstitute the fully assembled COMA-complex, the AME1 gene was cloned into the forth cassette of the polycistronic expression vector. The expression and purification of the tetrameric His_6-Ctf19 Mcm21 Okp1 Ame1 (COMA-) complex were typically carried as described for the dimeric and trimeric complexes (Fig. 3.2.16).

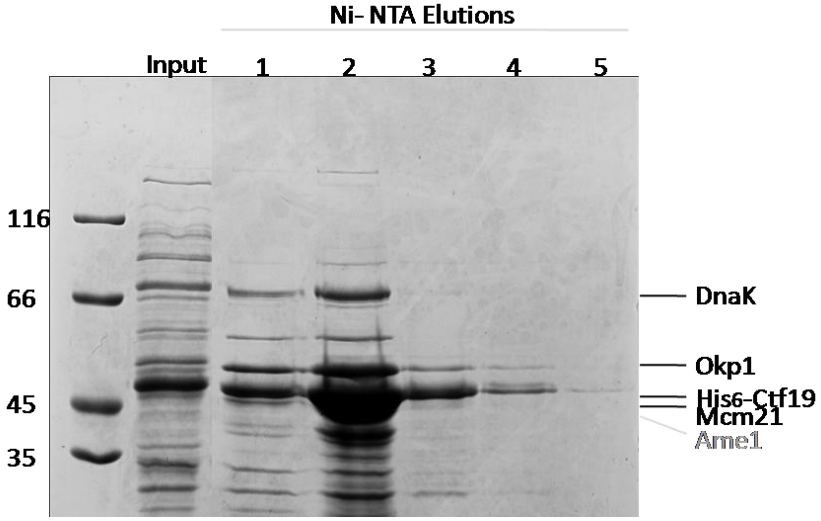

Fig. 3.2.16 IMAC purification of the COMA-complex.

The Coomassie-stained gel shows cell lysate after induction with IPTG (Input =0.01 %) and five fractions eluted with high imidazole concentration from the HisTrap column (1-5 = 1%). Ame1 protein was no found in elutions by the MALDI-TOF-MS analysis.

From unknown reasons, attempts to *in vivo* reconstitute the COMA-complex did not result in the detection of all four proteins by the MALDI-TOF-MS analysis. The missing subunit was the Ame1 complex component finally added. According to the Western blot analysis, only a small amount of the Ame1 protein was detected in the second eluted fraction (data not shown). In a recent publication (Hornung, Maier et al. 2010) it was shown that the COMA-complex could have been reconstituted *in vivo* from the polycistronic vector when the complex was purified through the Ame1-tagged protein.
Subsequently we wished to know if the quaternary COMA-complex could be reconstituted *in vitro*. For this, we expressed and purified the His_6-Ctf19 Mcm21 Okp1-complex and the His_{10}-Ame1 protein separately (Fig. 3.2.17).

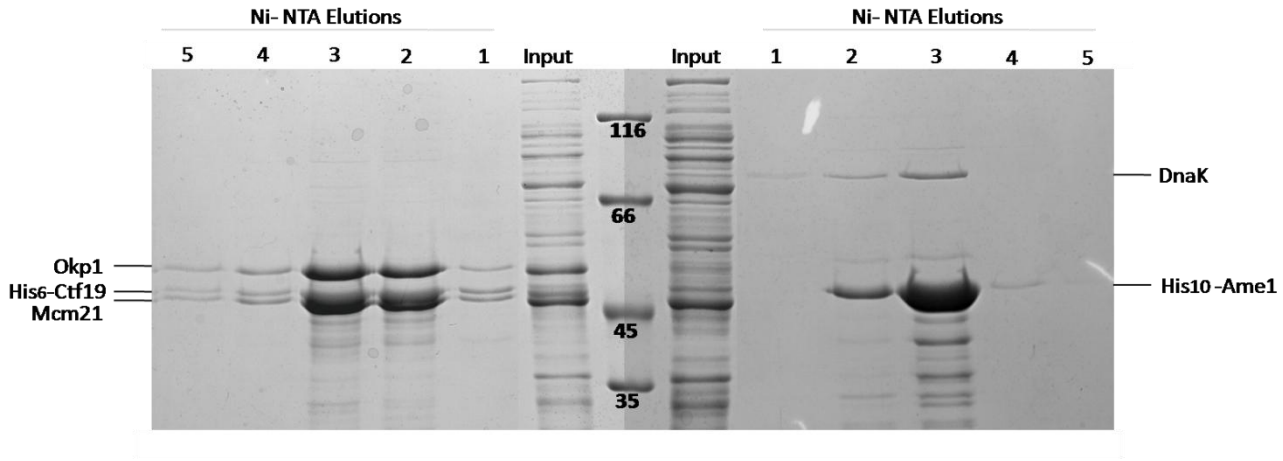

Fig. 3.2.17 IMAC purification of the CMO-complex and the Ame1 protein separately.

The Coomassie-stained gel shows cell lysates after induction with IPTG (Input =0.01 %) and five fractions eluted with high imidazole concentration from the HisTrap column (1-5 = 1%) for both purifications.

After elution from the IMAC columns, all the COMA-components were verified by the MALDI-TOF-MS. Purified proteins were mixed together in a 1:1:1:1 ratios and further purified by the size-exclusion chromatography (SEC). RNase A was added to the mixed COMA proteins before the SEC (Fig. 3.2.18).

Protein purification scheme:

Separate Ni-NTA purifications for the CMO- complex and Ame1 protein ⇒ Mix + RNaseA treatment ⇒ SEC

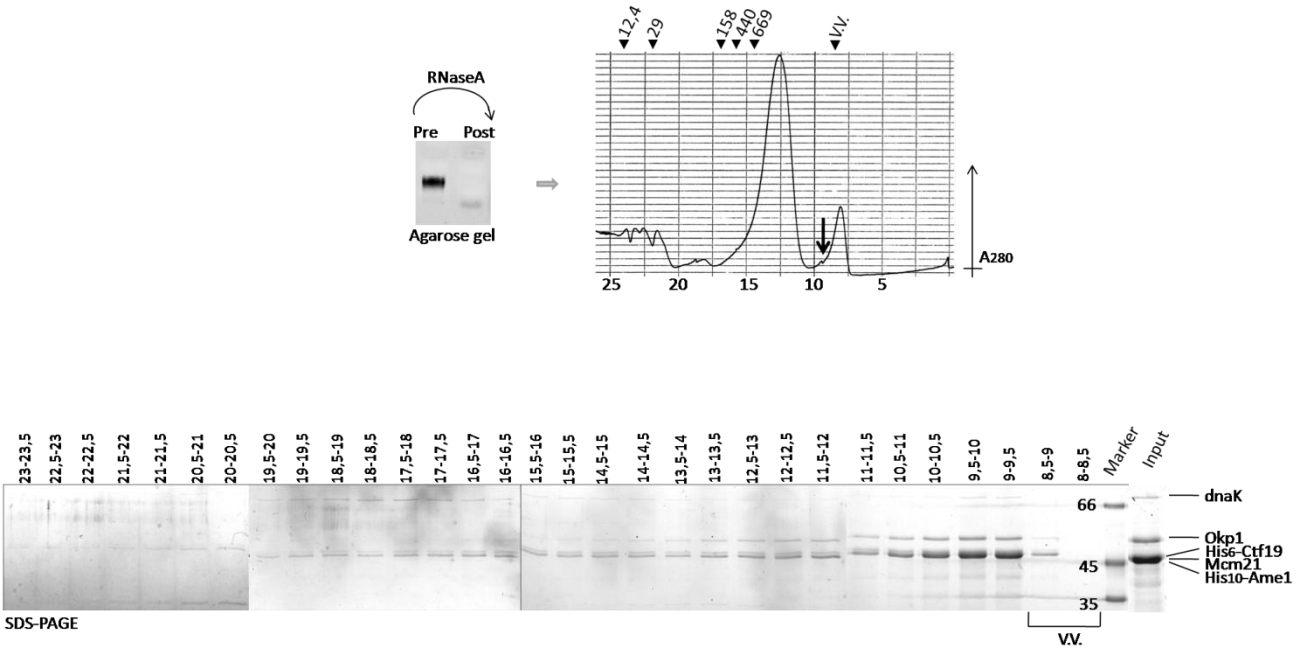

Fig. 3.2.18 The size exclusion chromatography (SEC) of the COMA-complex, pre-treated with RNaseA.

The COMA-complex was analyzed on the Superose 6 column after the IMAC and RNaseA treatment (Input = 2%). The chromatogram shows void volume peak around 8 ml and 12-12,5 ml peak. 4% of each collected fraction was directly analyzed on the coll. coomassie-stained SDS-PAGE where majority of the COMA-proteins were found around 9-10 ml fractions.

The chromatogram for the COMA-complex separation on the Superose 6 contains a void volume peak at 8 ml and a bigger broad peak around 12,5 ml. Analysis of the complex on coll. coomassie-stained gels showed that the protein complex co-eluted around 9-10 ml (which corresponds to the highly elongated or oligomeric state of the complex much higher than 669 kDa of the largest standard protein we used for the column calibration). In the SEC experiment the absorption peaks at 280 nm did not correlate to the higher amounts of proteins estimated by coomassie-stained gels, although RNase A was added. Even so, protein bands from the two absorption peaks 9-9,5ml and 12-12,5 ml were analyzed by the stained PAGE and MS, peptides from all four COMA proteins were identified. Besides this, if assume that the Mcm21 and Ame1 contribute equally to the third band, we can conclude that the COMA-complex was reconstituted with 1:1:1:1 stoichiometry (Fig. 3.2.19).

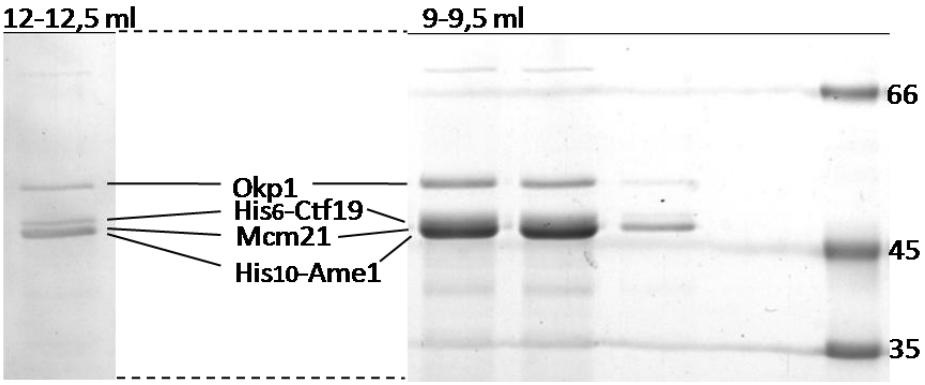

Fig. 3.2.19 Enlarged coll. coomassie-stained SDS-PAGE with analyzed chromatography fractions after the COMA-complex runs on the Superose 6.

The tetrameric COMA proteins were identified by MALDI-TOF-MS in both analyzed fractions. The complex stoichometry, according to the intensity of the stained protein bands, was estimated as 1:1:1:1.

In conclusion, comparing the elution profiles from the CMO-complex and the putatively formed COMA-complex, it is clear that the elution volume of the complex is altered in the presence of the Ame1 protein (from 10-10,5 ml for the trimeric CMO-complex to 9-9,5

ml for the putatively formed tetrameric COMA-complex). If extrapolated from the standard calibration curve, the corresponding molecular weight of the putative COMA-complex is 1,8 MDa (while for the CMO-complex was 1,34 MDa; Fig. 3.2.9) This is an evidence that *in vitro* all four components assembly in the complex.

In summary, attempts to reconstitute the tetrameric COMA-complex *in vivo* have failed but uncovered stable subcomplex formations of the CMO-complex, as well as a possible characteristic of the COMA proteins to interact with unspecific RNA. A stable subcomplex between the Ctf19 and Mcm21 was confirmed and revealed either as a tetrameric form or the dimeric form of the complex, possibly depending on the Okp1 protein co-expression. Further, we discovered that the trimeric CMO-complex could be assembled in the absence of the Ame1 protein. SEC analysis of the trimeric CMO-complex ascertained a highly elongated or oligomeric form of the complex in solution. Further analysis of the complex revealed unspecific RNA contamination in purified samples. After RNA was removed, the elution profile remained the same. The COMA-complex was *in vitro* assembled from the stable CMO-heterotrimer and the solely purified Ame1 protein. Coomassie-stained gels revealed that all four subunits of the complex were present at 1:1:1:1 stoichiometry when coeluted after the SEC.
Using the SEC we were able to determine an oligomeric behavior of the COMA proteins in solution. According to the used standard curve, we estimated that the CMO-complex is about 1,3 MDa and that the putatively formed COMA-complex forms even larger oligomers with approximately 1,8 MDa in size.

3.3 Okp1 domain analysis

From the hydrodynamic analysis of all known kinetochore components, it was suggested that the majority are typically organized in complexes (De Wulf, McAinsh et al. 2003). Most of the budding yeast kinetochore complexes have an average molecular weight of 200 kDa and they are comprises of four different subunits. In many kinetochore complexes that have been recently reconstituted, a full complex could be assembled from two stable heterodimers. Interestingly, we discovered that the trimeric CMO-complex could be assembled independently from the Ame1 essential protein (refer to chapter 3.2.2). Here we employed *in vivo* and *in vitro* approaches to further investigate the trimeric CMO-complex, with the emphasis on the essential Okp1 protein.

Ever since the three proteins, Ctf19, Mcm21 and Okp1, have been identified by one-hybrid screen, and confirmed by the ChIP analysis to be constituents of the budding yeast kinetochore, it was speculated that they form a complex. It was proposed that this protein complex most likely links CBF3 with further kinetochore components of the budding yeast centromere; Mif2, Cse4 and Cbf1 proteins (Ortiz, Stemmann et al. 1999). In order to assess the specificity of function of these three proteins, their known homologues were searched for. A very moderate homology between the Okp1 and mammalian CENP-F protein was observed. Four suggested regions (domains I-IV in Fig. 3.3.1) of possible homology between the Okp1 and CENP-F were not investigated further, but within this study we analyze the Okp1 protein domains taking this into the account for the Okp1 deletion constructs.

The OKP1-constructs which contain OKP1 that is truncated from the N- and C-terminus were generated (part of this constructs and analyses were made by diploma student in the Lechner group: Monika Lachner). The respective full length OKP1 was used as a control. In the first mutant, only the C-terminal part containing the last 124 amino acids was deleted (okp1Δ283-406). In the second mutant, the N-terminal region of the protein was deleted (okp1Δ1-115). The third mutant was truncated up to amino acid 116., thus eliminating the N- and C-terminals (okp1Δ1-115, Δ283-406). All these three deletion constructs were made to fully contain the central coiled-coil region of the Okp1 protein. The additional, fourth deletion construct was generated to contain only the first 230

amino acids (okp1Δ231-406) thus missing a part of the coiled-coil region as well. The Okp1 wild type and tested deletion construct are shown in Fig. 3.3.1.

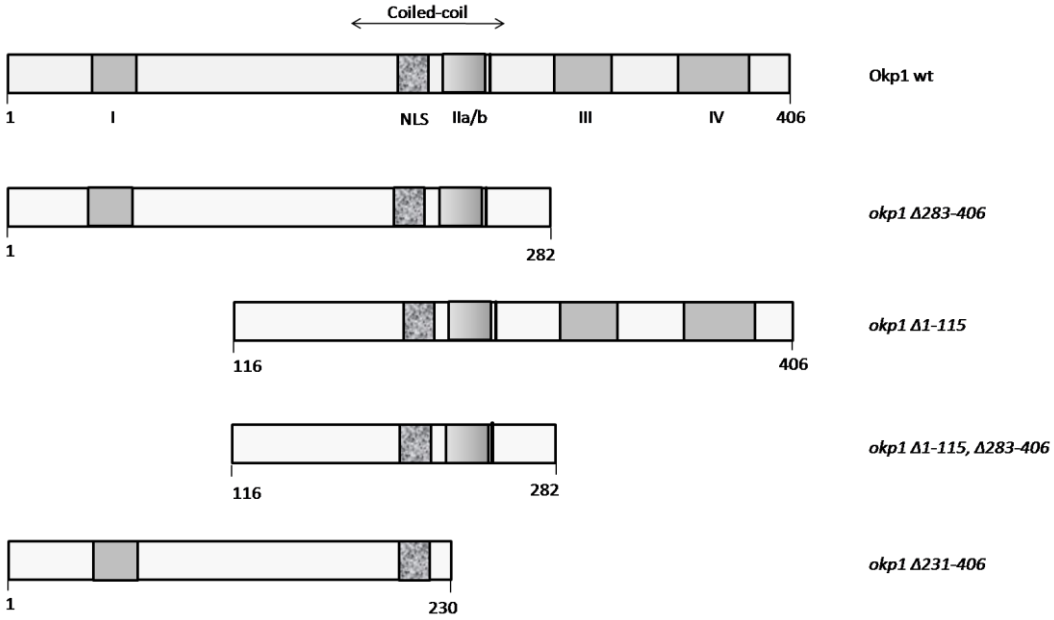

Fig. 3.3.1 Schematic representation of the Okp1 deletion mutants.

NLS denotes a putative nuclear localization signal and it is labeled as a texture box. Roman numerals and gray areas indicate possible regions of homology with CENP-F proteins that were here used only as guidance for the deletion constructs. Arabic numerals refer to the Okp1 amino acid positions.

3.3.1 The Okp1 coiled-coil region is sufficient for cell viability

To examine which region of the Okp1 protein is essential for cell growth, we used the respective Okp1 mutants and evaluated their functionality by the Plasmid Shuffle method. These constructs were integrated into the OKP1-locus in the yeast genome of the OKP1-shuffle strain (YJL132) in which the endogenous OKP1-gene was deleted. Since the OKP1 is an essential gene, this strain has a copy of the OKP1 gene on URA3-plasmid (YJL132/pJL467). The URA3 marker encodes orotidine-5'phosphate decarboxylase, an enzyme which is required for the biosynthesis of uracil. When streaked out on media containing fluoroorotic acid (5`-FOA), cells are unable to grow since 5`-FOA is harboring the plasmid. Therefore, ura3- cells can be selected on media

containing 5'-FOA whereas URA3+ cells cannot grow. If the integrated deletion mutant can complement for the wild-type OKP1 present on the URA3-plasmid, cells which lost the plasmid will survive on 5'-FOA containing plates. On the other hand, if the deletion of the Okp1 protein part cannot complement for the wild-type protein, the cells will not be able to grow.

To test the viability of the OKP1 deletion mutants, the respective strains were first grown in YPD for 2 days. Ordinarily, within this period the strain loses the OKP1-URA3 plasmid. Subsequently, serial dilutions of the respective strains were then spotted onto YPD as a growth control and on SDC + 5'-FOA plates to test for viability (Fig. 3.3.2).

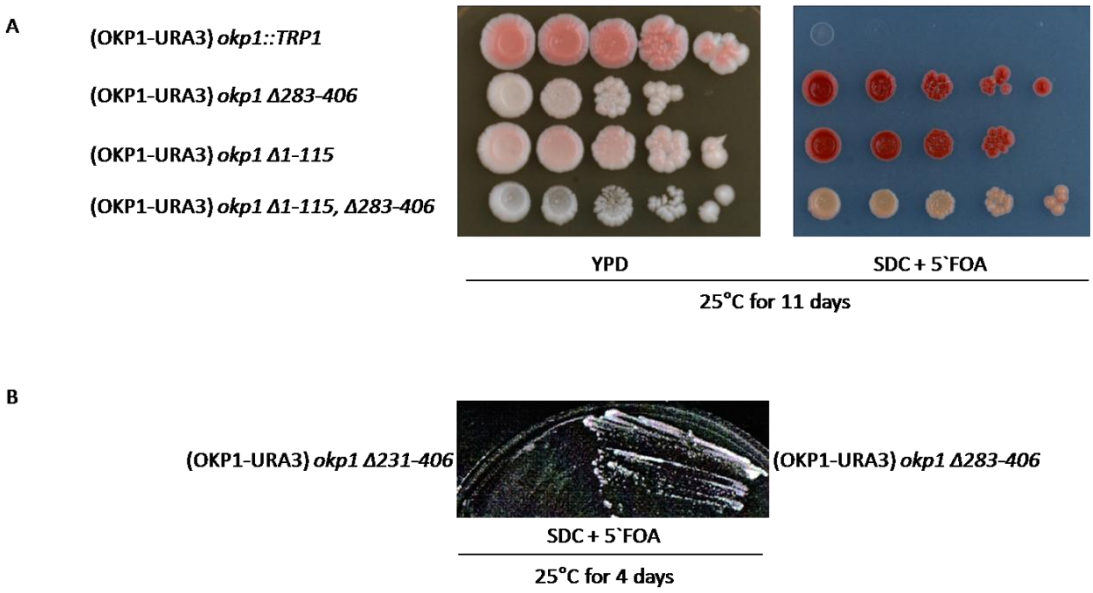

Fig. 3.3.2 Viability test of the Okp1 deletion mutants.

(A) Tested ability of the indicated deletion Okp1 strains containing preserved coiled-coil region to grow in the absence of the OKP1-URA3 plasmid. As a control, cells were plated onto YPD plate. The plates were incubated at 25°C for 11 days. The two strains containing the *okp1Δ283-406* and *okp1Δ1-115* were constructed by M. Lachner.

(B) Compared growing ability of the two Okp1 deletion strains missing the large C-terminal protein segment. The *okp1Δ283-406* can and the *okp1Δ231-406* strain cannot grow on plate containing 5`-FOA at 25°C for 4 days. Taken from M. Lachner`s diploma thesis.

Whereas the three mutants preserving the coiled-coil region of the Okp1 protein are viable on plates containing 5'-FOA, the okp1Δ231-406 mutant is lethal. Even the double mutant okp1Δ1-115, Δ283-406 with approximately 60% of the protein sequence deleted, was able to complement the full length protein. Partial disruption of the coiled-coil region or the lack of additional 50 amino acids compared to the okp1Δ282-406 mutant, result in a non-viable the okp1Δ231-406 mutant. Thus, the region between the 231. and the 282. amino acid is essential for the Okp1 protein function, and therefore for cell viability.

3.3.2 *In vitro* analysis of the CMO-complex formation

In order to analyze whether the viable Okp1 deletion mutants show a distinct impact on protein-protein interactions within the CMO-complex, we utilized the strategy previously described for the wild type Okp1 protein within the complex (refer to chapter 3.2.2). The different Okp1 deletions were expressed in *E.coli* and subsequently purified via the His_6-tag on the Ctf19. Because the truncated constructs showed significant reduction of protein amounts on the coomassie-level, the Okp1 and all its deletion constructs were N-terminally Flag-tagged. Therefore we used the Western blot analysis to reveal if there is significant difference in CMO-complex formation between the wild type and any truncated Okp1-variant (Fig. 3.3.3).

CMO-complex formation analysis scheme:

His_6-TEV-CTF19, MCM21 and OKP1-(*okp1*-) Flag *E.coli* expression ⇒ Ni-NTA purification ⇒ α-Flag Western blot analysis

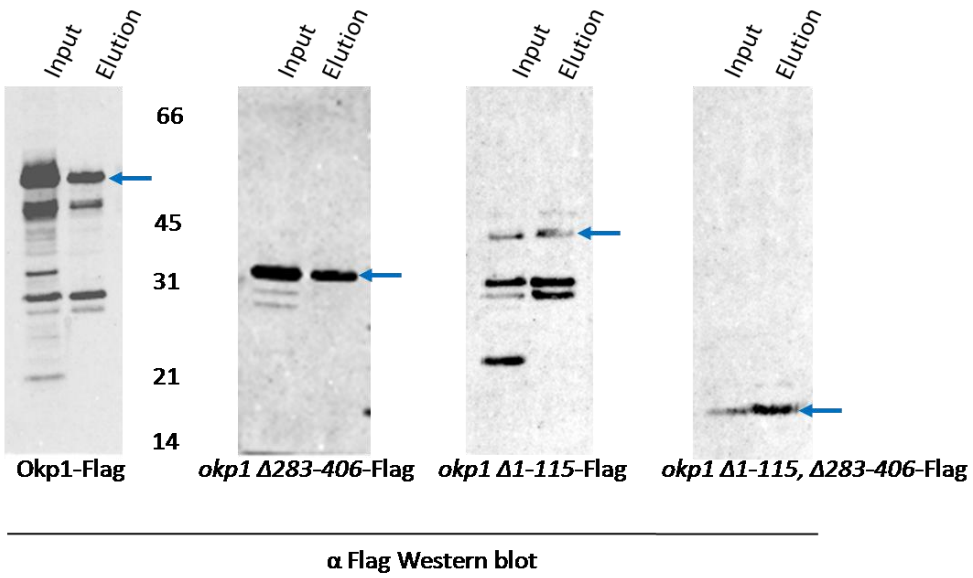

Fig. 3.3.3 Reconstitution of the various CMO-variants.

Expression and purification of the CMO-complexes containing the wild type or the truncated Okp1 subunit using α-Flag antibody. Blue arrow indicates the purified Okp1 full length and truncated products. Input = 0,02%. Elution = 0,05%.

Our analysis revealed that all mutants could be purified in the form of a complex with Ctf19 and Mcm21 proteins in amounts comparable with the wild type control. Thus, the N-terminally 116 and C-terminally 124 amino acids of the Okp1 protein seem not to be required for complex formation *in vitro*. Moreover, it is likely that the central coiled-coil region of the Okp1component interacts with the Ctf19 and Mcm21 proteins to form the CMO-complex.

In summary, we examined formation of the CMO-trimeric complex *in vivo* and *in vitro* by analyzing different domains of the essential Okp1 component of the complex. We identified a central coiled-coil region of the Okp1 protein as the region required for the complex formation *in vitro* and as essential for cell viability.

3.4 Reconstitution and organization of the budding yeast COMA-network

A variety of expression and purification conditions have been employed within this work to reconstitute the budding yeast COMA-complex (refer to Tables 3.1.1 and 3.1.2). We have described previously the outcome of the successfully reconstituted timeric CMO-complex but the outcome was never entirely satisfactory with four COMA-components. Since the COMA-complex can been isolated from the *S. cerevisiae* cell extracts, we speculate that chaperone proteins or other components of the COMA-network might be involved in the complex assembly.

3.4.1 Purification of the Okp1-associated proteins from yeast cells

Previous studies have used the essential Okp1-3FLAG and Ame1-3FLAG affinity purification to isolate the COMA-network (De Wulf, McAinsh et al. 2003). We wanted to confirm and further investigate this data by purifying the COMA-network through a tandem affinity purification (TAP) strategy (based on the method from Puig et al., 2001). We used the Okp1-TAP protein to perform affinity purification from asynchronous cell extract. The complex components were isolated by immune precipitation using human IgG agarose beads, acid eluted and analyzed on colloidal coomassie-stained gradient gels by mass spectrometry. Proteins that originated from budding yeast, and that were enriched after the purification, were labeled in Fig. 3.4.1.

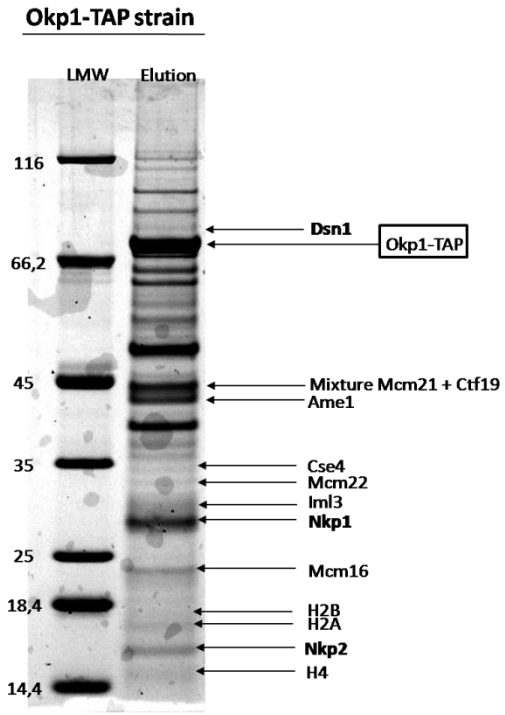

Figure 3.4.1 Purification of kinetochore proteins associated with Okp1-TAP.

75% of acid eluted proteins were analyzed on a colloidal coomasse-stained 4-12% NuPAGE gel after the TAP purification from yeast whole cell extract. Proteins were identified by mass spectrometry and labeled.

As expected, all eleven components of the COMA-network were detected. Besides these, histone proteins and a specialized histone H3, Cse4 protein, were found. Interestingly, the Dsn1 protein, a Mtw1-complex component that has not been identified in formal purification experiments, was also specifically co-purified. We further investigated this by *in vitro* binding assays using the reticulocyte lysate system (refer to chapter 3.5.1).
Predictably, the four COMA-complex proteins were enriched the most, judged by the densitometry of identified protein bands on stained gel. Additionally, our purification noted two more proteins to be more abundantly present. The Nkp2 and especially the Nkp1 proteins had been co-purified with Okp1 in great amounts. We therefore continued to explore the possibility that Nkp1 and Nkp2 might be in a strong physical interaction with the COMA-core or at least the Okp1 protein.

3.4.2 Reconstituted hexameric complex of the COMA-, Nkp1- and Nkp2-proteins

To evaluate interaction between the COMA-complex and Nkp1 and Nkp2 proteins as a direct interaction, we started to reconstitute the hexameric COMANN-complex. We employed the polycistronic expression vector containing all four COMA genes, earlier reported not to be a very good method of reconstituting the COMA-complex itself (refer to chapter 3.2.7), in combination with a compatible pCOLADuet-1 vector. This strategy was chosen because it allows testing of both *in vitro* and *in vivo* complex reconstitution. Additionally, the protein purification strategy was elevated by the GST-tagging of the Nkp1 protein, thus enabling two sequential affinity purifications if required.

- pST39, which carries the *bla* gene (ampicillin resistance), was used for co-expression of His_6-TEV-Ctf19, Mcm21, Okp1 and Ame1 (COMA-) proteins
- pCOLADuet-1, which is kanamycin resistant, was used for co-expression of Nkp2 and His_6-Thr-GST-Nkp1 proteins.

Both expression vectors were transformed in Rosetta *E.coli* strain and protein synthesis was induced by adding the IPTG as previously described for engagement of a solely polycistronic vector. After cell lyses, an IMAC purification step followed by a GST-purification was used and eluted proteins were analyzed on colloidal coomassie-stained gradient gel (Fig. 3.4.2).

Protein purification scheme:

Ni-NTA purification ⇒ GST purification ⇒ SEC

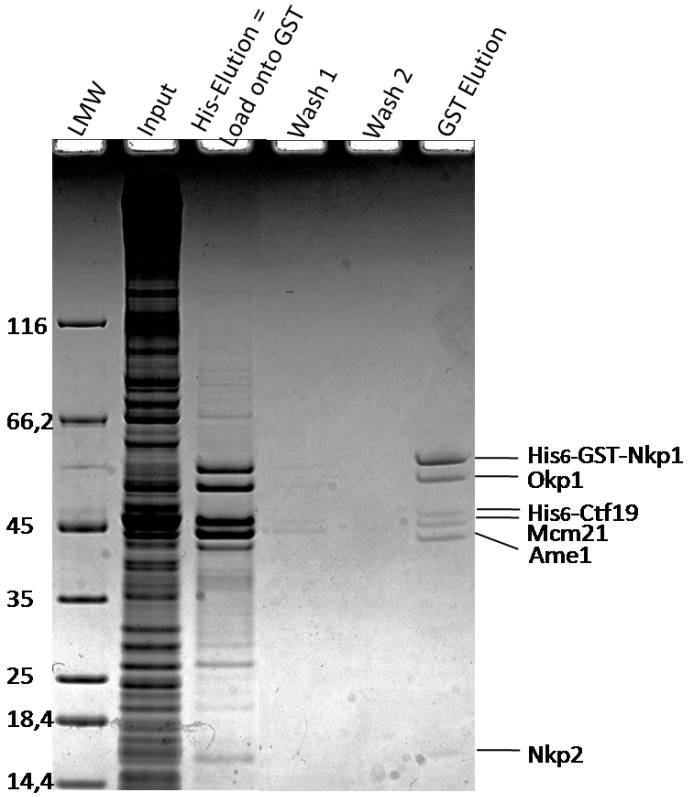

Fig. 3.4.2 Reconstitution of the hexameric COMANN-complex.

The colloidal coomassie-stained 4-12% Nu-PAGE gel shows different stages of the purification procedure; harvested cell extract (0,025%), eluate from the His-column (1%) which is also the load onto the GST agarose beads (2%), two extensive washings (0,6%) and finally GST-elution (70%). Proteins were identified by mass spectrometric analysis.

The applied purification strategy demonstrated the existence of the hexameric protein complex and proved direct protein-protein interaction between the COMA-complex and Nkp1 and Nkp2 proteins. Surprisingly, the complex contained a stable Ame1 protein. This finding implies a possible critical role of the Nkp1 and Nkp2 proteins in preserving Ame1 protein from proteolytic degradation during the complex formation or purification itself. The purified complex had almost no protein contaminants. Yet, the complex yielded a small amount of proteins, as it was a not unexpected outcome of the two subsequent affinity purification steps.

To further explore the hexameric COMANN-complex integrity and to obtain additional information about the size of the complex, we next performed a gel filtration chromatography on the Superose 6 column (Fig. 3.4.3). Despite very good complex purity, it has been difficult to analyze the small amounts that we could obtain by the two

affinity purification steps. This was the reason for attempting a purification strategy using only a His_6-tag on the Cft19 subunit.

- pST39, which carries the *bla* gene (ampicillin resistance), was used for co-expression of His_6-TEV-Ctf19, Mcm21, Okp1 and Ame1 (COMA-) proteins
- pCOLADuet-1, which is kanamycin resistant, was used for co-expression of Nkp2 and Nkp1 proteins without any tag.

Because the previous observation that protein contamination with unspecific RNA might interfere with the SEC analysis (chapter 3.2.3), we simultaneously monitored the nucleic acid content of collected fractions on the EtBr-stined agarose gel (Fig. 3.4.3 C).

Protein purification scheme:

Ni-NTA purification ⇒ SEC

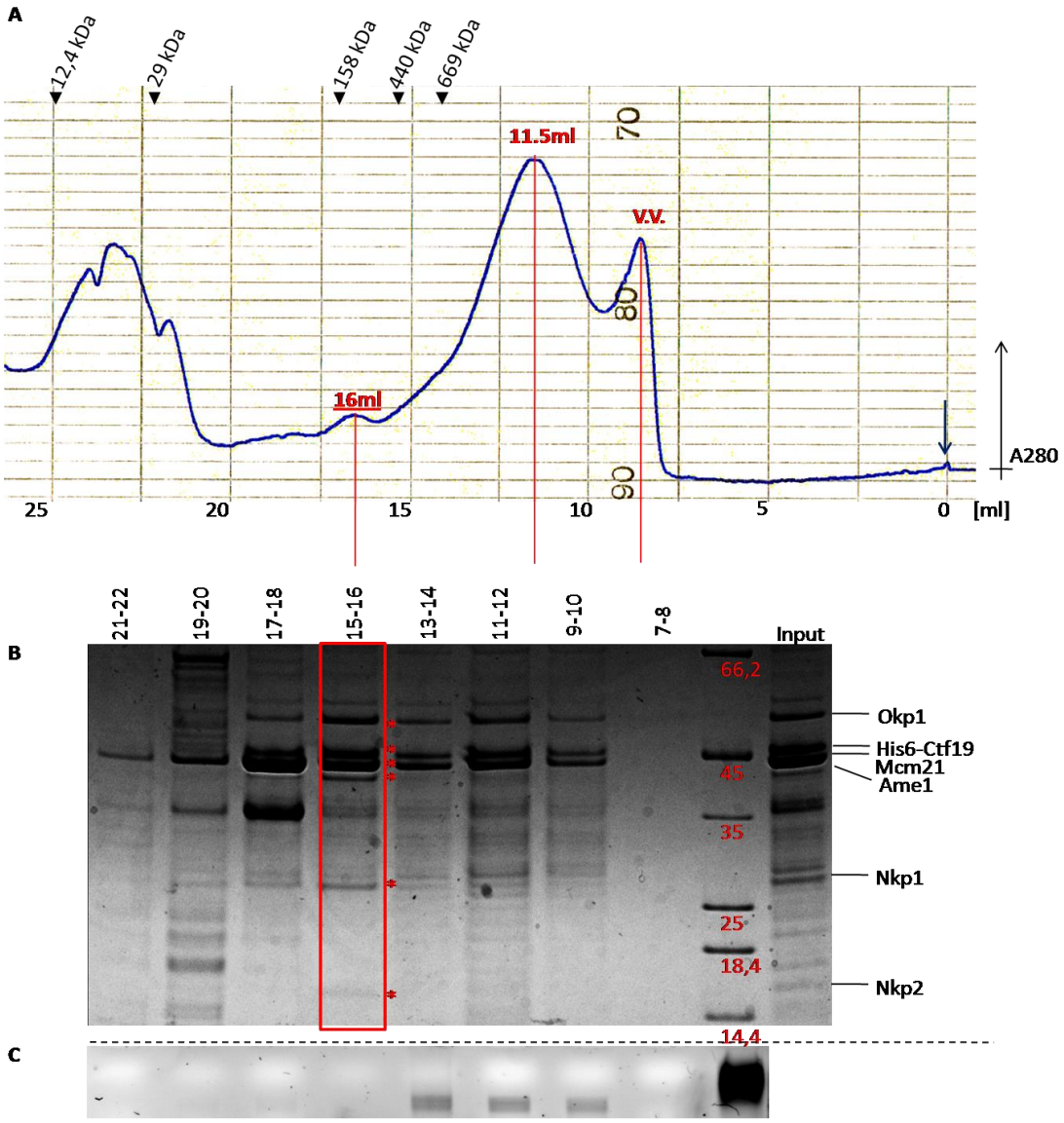

Fig. 3.4.3 SEC runs of the reconstituted COMANN-complex.

(A) SEC runs on the Superose 6 column. The chromatogram shows absorbance at 280 nm during the run. The arrow indicates injection of the sample.

(B) Coll. coomassie-stained gradient gel showing collected fractions of the reconstituted hexameric complex. Input = 1%. Fractions were TCA precipitated (35%) and analyzed. Each red asterisk within the red square represents one kinetochore protein labeled on the right side of the gel.

(C) Same collected fractions were monitored for the nucleic acid content. 10% of each fraction was precipitated and analyzed on EtBr-stained agarose gel.

The size exclusion profile of the hexameric complex directly loaded onto the Superose 6 after the IMAC, consists of a void volume peak at 8 ml, a large broad peak around 11,5 ml

(which corresponds to proteins with a molecular weight larger than the 669 kDa marker used to calibrate this column) and a small peak at 16 ml. As for the SEC runs in our previous experiments, the absorption peaks at 280 nm and the amount of proteins verified by the coomassie-staining on the SDS-PAGE after the run on the Superose 6, could not be directly correlated. Nevertheless, when taking into account the nucleic acid content of the same samples, it became clear that the major absorption at 280 nm (11,5 ml peak) originated from the oligomerized kinetochore proteins (with the exception of the Ame1 and probably the Nkp1 and Nkp2 proteins) and nucleic acids. The minor peak around 16 ml corresponds to the hexameric form of the COMANN-complex (theoretical, calculated MW=217 kDa), also determined by mass spectrometric analysis of the protein bands within the marked fraction. Obtained (experimental) MW of the COMANN-complex, based on the extrapolation from the calibration curve for the column (Fig. 3.2.9) is 218,3 kDa.

3.4.3 Analyzing the binding site within the COMA-complex for the Nkp1 and Nkp2 dimer

It has not been analyzed before whether the Nkp1 and Nkp2 proteins form a stable dimer. We tried to reconstituting the dimer from *E. coli* by constructing a plasmid that expressed the Nkp2 untagged protein and the Nkp1 with an N-terminal His_6-GST-tag. Nkp2 was purified via the His_6- or the GST-tag and purified proteins were analyzed on coomassie-stained SDS-PAGE (Fig. 3.4.4).

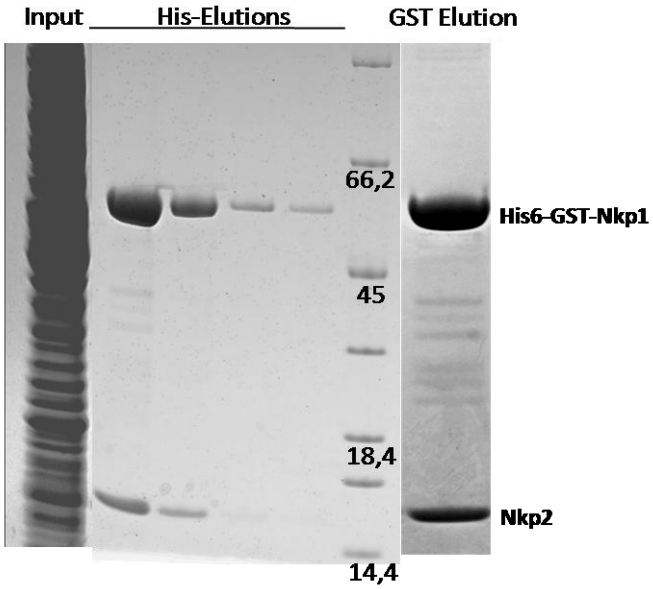

Fig. 3.4.4 *In vitro* reconstitution of dimer between the Nkp1 and Nkp2 proteins.

Coomassie-stained 4-12% Nu-PAGE revealed the dimer formation between the Nkp1 and Nkp2 proteins if purified by IMAC and if additional GST-purification was performed. Input = 0,025%, His-elutions = 1%, GST-elution = 20%.

This experiment revealed that the Nkp1 and Nkp2 proteins can be assembled to form a stable heterodimer.

Next, we asked whether the Nkp1 and Nkp2 dimer interacts with the essential Ame1 and Okp1 proteins or it also requires the Ctf19 and Mcm21 components of the COMA-complex. We co-transformed and purified separately the two essential genes Ame1 and Okp1 from the pETDuet-1 plasmid in combination with Nkp1 and Nkp2 on pCOLADuet-1 plasmid (with and without the tag) (Figure 3.4.5), as well as the two nonessential genes, Mcm21 and Ctf19 from the pST39-expression plasmid also in combination with Nkp1 and Nkp2 on pCOLADuet-1 plasmid (with and without the tag) (Figure 3.4.6). Then we performed two subsequent affinity purifications. This strategy gave us the opportunity to understand how the two separate parts of the COMA-complex interact with their binding partners, the Nkp1 and Nkp2 proteins.

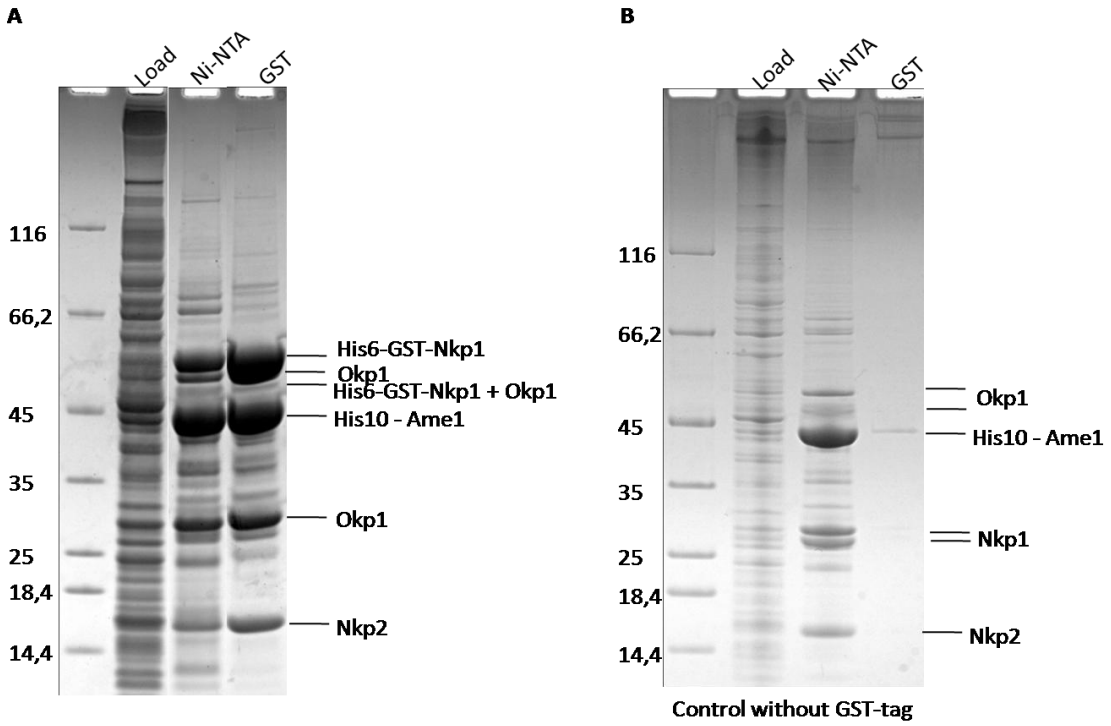

Fig. 3.4.5 The Nkp1 and Nkp2 dimer directly interacts with essential Ame1 and Okp1 proteins.

(A) The His_{10}-Ame1 and Okp1 heterodimer was expressed in combination with the Nkp2 and His_6-GST-Nkp1 heterodimer and the tetrameric complex was reconstituted firstly through the Ni-NTA and secondly through the GST-purification. Proteins were analyzed by colloidal coomassie-staining on 4-12% Nu-PAGE and identified by mass spec. Load = 0,01%, Ni-NTA Elution = 1% and GST Elution = 80%.

(B) The His_{10}-Ame1 and Okp1 heterodimer was expressed in combination with the Nkp2 and Nkp1 heterodimer without any tag. The Ni-NTA affinity purification was applied first and the GST-purification second. Proteins were analyzed by colloidal coomassie-staining on 4-12% Nu-PAGE and identified by mass spec. Load = 0,01%, Ni-NTA Elution = 1% and GST Elution = 80%.

Here we confirmed a direct protein-protein interaction between the essential Ame1 and Okp1 proteins with the Nkp1 and Nkp2 constituents of the COMA-network. Although some proteolytic degradation could be detected, it is clear that all four proteins could be preserved throughout the expression and purification procedure.

The nonessential Ctf19 and Mcm21 heterodimer did not show the same interaction with Nkp1 and Nkp2 proteins when analyzed in the same manner (Fig. 3.4.6).

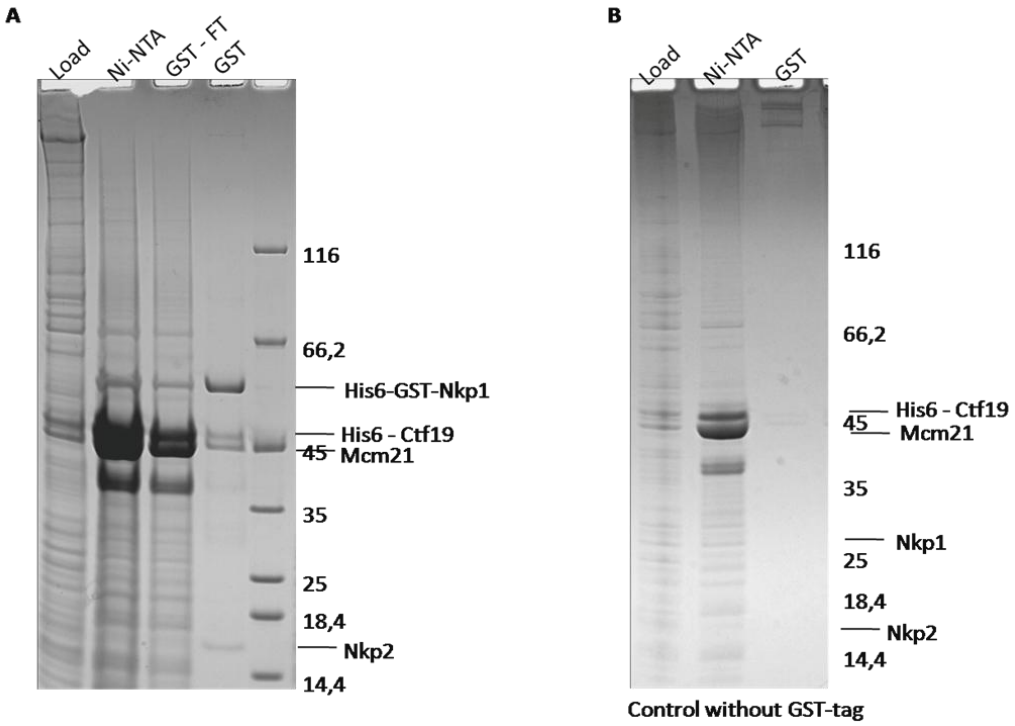

Fig. 3.4.6 The Nkp1 and Nkp2 dimer does not interact with non-essential CTF19 and Mcm21 proteins.

(A) The His_6-Ctf19 and Mcm21 heterodimer was expressed in combination with the Nkp2 and His_6-GST-Nkp1 heterodimer and then purified by the two sequential affinity steps; the Ni-NTA and secondly the GST-agarose beads. Proteins were analyzed by colloidal coomassie-staining on 4-12% Nu-PAGE and identified by mass spec. Load = 0,025%, Ni-NTA Elution = 1% and GST Flow Through = 2% and GST Elution = 40%.

(B) The His_6-Ctf19 and Mcm21 heterodimer was expressed in combination with the Nkp2 and Nkp1 heterodimer without any tag. The Ni-NTA affinity purification was applied first and the GST-purification second. Proteins were analyzed by colloidal coomassie-staining on 4-12% Nu-PAGE and identified by mass spec. Load = 0,025%, Ni-NTA Elution = 1% and GST Flow Through = 2% and GST Elution = 40%.

We could only observed a weak interaction between the four nonessential proteins from the COMA-network (Ctf19, Mcm21, Nkp1 and Nkp2 proteins) after co-expression of all subunits in *E. coli* or a contamination that was also poorly seen in a control. Thus, the local binding interface for the direct interaction revealed between the COMA-complex and Nkp1 and Nkp2 proteins, established predominantly the essential part of the COMA-complex, Ame1 and Okp1 proteins.

In summary, *in vitro* experiments demonstrated that the hexameric COMANN-complex could be reconstituted as stable. The Nkp1 and Nkp2 proteins together with the

previously used polycistronic vector containing all four COMA-genes, prove that the added dimer stabilize the Ame1 protein within the complex. Also, it has been shown that the Nkp1 and Nkp2 proteins form a dimer in solution. New directly interacting partners among the COMA-network were detected. Data provided in this work revealed a new insight into the structural organization of the budding yeast COMA-network and localized the interacting proteins within the network in more detail. Observations described in this chapter orient the Nkp1 and Nkp2 proteins in very close proximity to the two essential Ame1 and Okp1 proteins on one hand, and more distal to the Ctf19 and Mcm21 protein on the other.

3.5 Reticulocyte lysate binding assays

The *S.cerevisiae* kinetochore is composed of more than 65 different proteins. Most of them are organized into discrete protein subcomplexes which are assembled in a hierarchical order (De Wulf, McAinsh et al. 2003). Even though important progress has been made in the past years toward better understanding architecture of the budding yeast kinetochore, little is known about direct protein-protein interactions between various subcomplexes. In order to analyze local binding interfaces between the COMA core and protein complexes in its close proximity, *in vitro* binding assays were performed.

To obtain individual proteins for testing the direct interactions with recombinant COMA proteins, *in vitro* gene expression system was used. For *in vitro* protein synthesis we employed a rabbit reticulocyte lysate (TNT® Quick Coupled Transcription/ Translation System from Promega). This system combines a prokaryotic phage RNA polymerase with eukaryotic extracts and utilize an exogenous DNA template, in this case plasmid DNA with a phage SP6 promoter (Fig. 3.5.1).

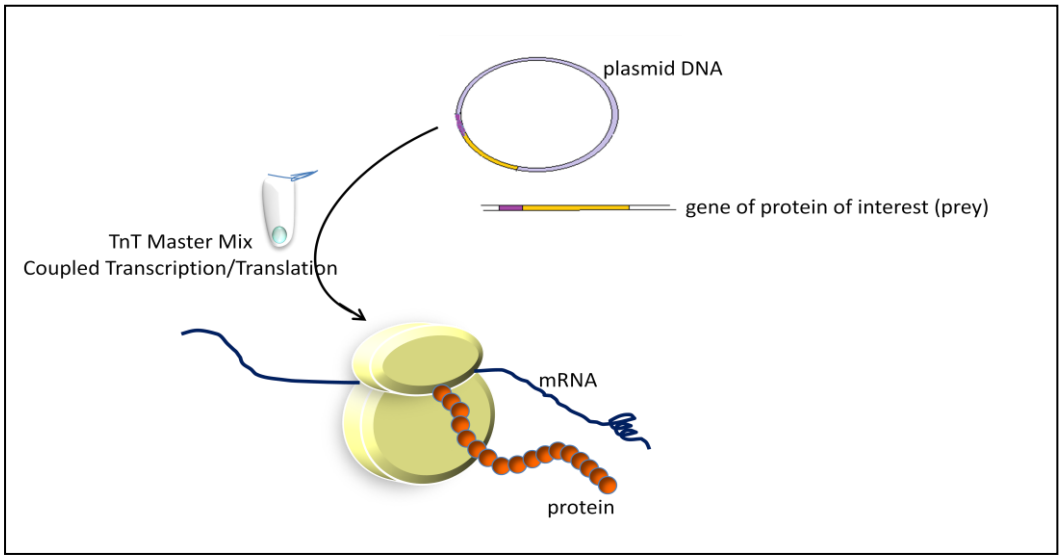

Figure 3.5.1 Cell-free transcription/translation system

After synthesis in the presence of ^{35}S- labeled methionine, each protein produced by *in vitro* translation reaction was analyzed on SDS-PAGE and used as a prey for the binding assays. As a control reaction, two types of reactions were set under the same conditions as for the protein of interest. One control contained no DNA and the other control

contained luciferase-encoding plasmid to produce functional unrelated luciferase protein (Fig. 3.5.2).

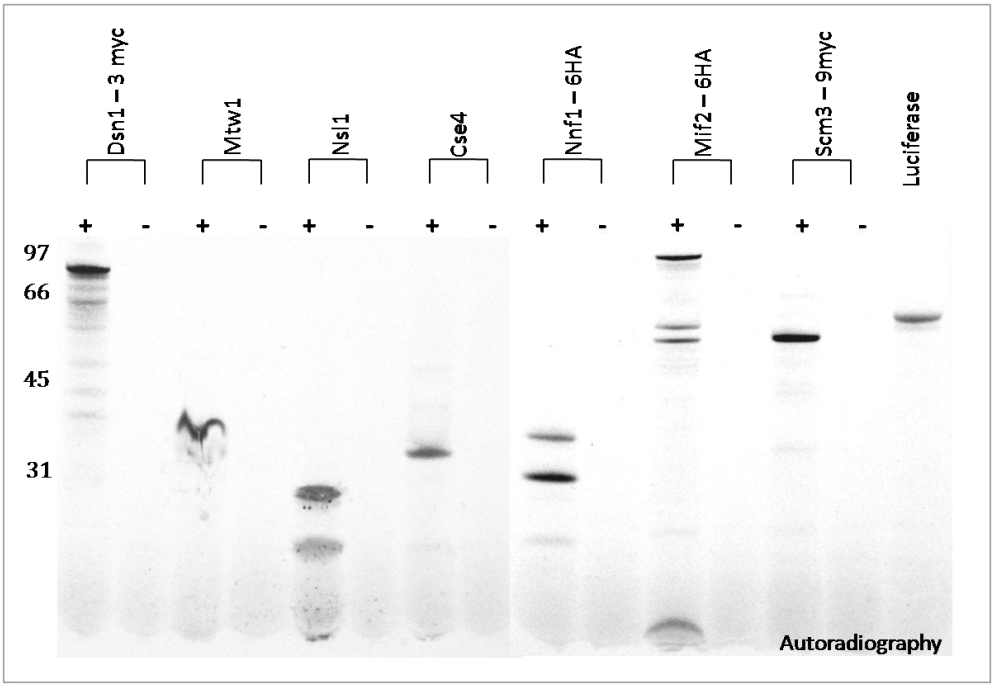

Fig. 3.5.2 Radioactively labeled proteins produced using TnT System.

Autoradiography of 4% produced prey proteins tested for binding with the COMA protein components, together with their negative controls (without plasmid DNA). Mtw1-complex components: Dsn1-3myc (70 kDa), Mtw1 (33 kDa), Nsl1 (25 kDa), Nnf1-6HA (31 kDa) as well as more inner kinetochore proteins: Cse4 (27 kDa), Scm3-9myc (37 kDa) and Mif2-6HA (70 kDa). Luciferase (61 kDa) represents a positive control for the TnT system.

We were interested in exploring the potential association with kinetochore components that were shown by *in vivo* fluorescence microscopy (Joglekar, A. P., K. Bloom, et al. 2009) and biochemical complex interaction studies (Hornung, P., M. Maier, et al. 2010) from budding yeast to localize in close proximity to the COMA protein network. The CMO-trimeric complex and His_{10}-Ame1 protein were expressed in *E.coli* and used as bait proteins for the binding studies. After the His-fusion proteins were imobilized on the Ni-NTA magnetic agarose beads (Qiagen), they were mixed with the protein produced in the TnT reaction. Folowing a short incubation period and extensive washing, bait-prey protein complexes were eluted either by boiling or by TEV-cleavage and analyzed by autoradiography. The experimental scheme is depicted in Figure 3.5.3.

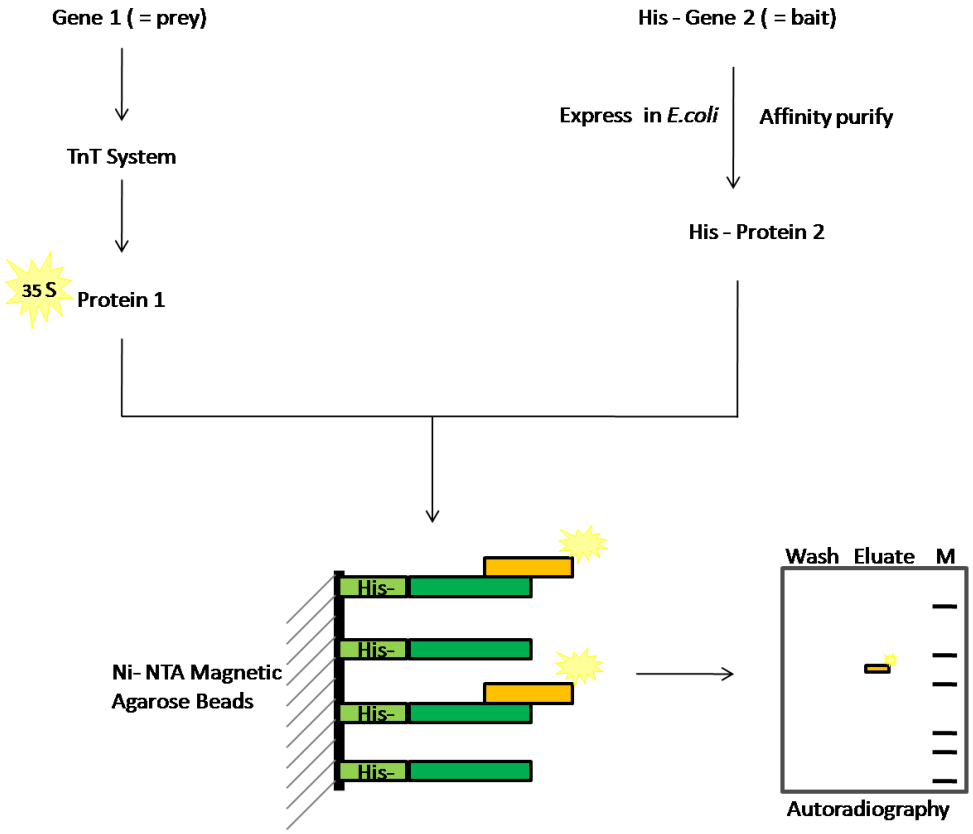

Fig. 3.5.3 The study mechanism of protein-protein interaction using the *in vitro* transcription/ translation TnT system.

We wanted to gain insight into direct and independent protein-protein interactions between the central COMA-complex and, on one side the closest proteins toward the kinetochore-microtubule interface (Mtw1 complex components), and on the other side to test protein components that could interact with the centromeric chromatin (Mif2, Cse4, Scm3 proteins).

3.5.1 The COMA complex interacts directly with the Mtw1 complex via Dsn1 protein

In order to identify direct physical interactions among separate components of the Mtw1- and the COMA-complexes, Ame1 protein and the putatively formed CMO-trimeric complex were immobilized on magnetic beads and incubated with radioactively labeled

in vitro translated Mtw1 components (Dsn1, Mtw1, Nnf1 and Nsl1 proteins) in separate tubes. Bait-prey complexes were eluted by boiling the magnetic beads and analyzed by autoradiography (Fig.3.5.4 A). To evaluate the amount and purity of the bait proteins, control samples in which no ^{35}S-labeled proteins (preys) were added, were analyzed on coomassie-stained gel after the mock binding assays were completed (Fig. 3.5.4 B).

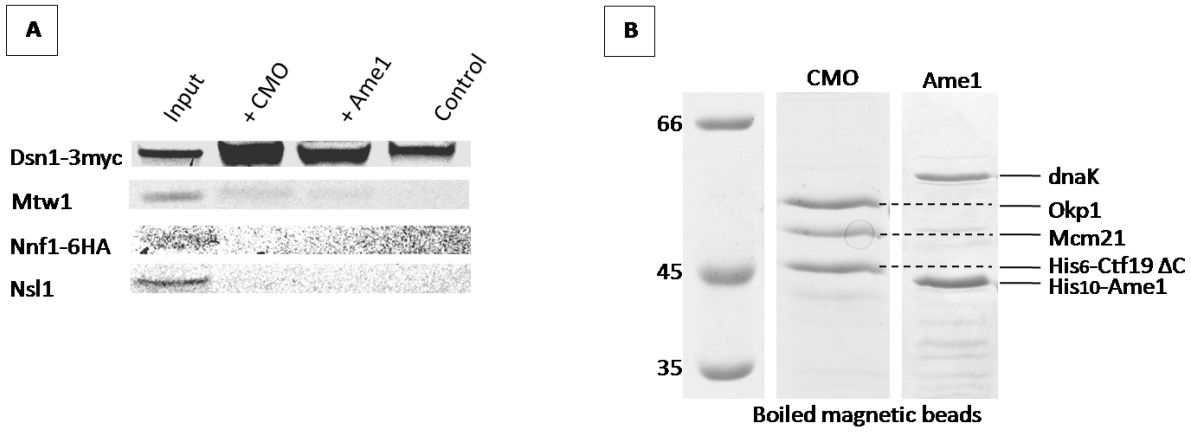

Fig. 3.5.4 Autoradiography and coomassie-stained gel images of studied interactions between *in vitro* translated Mtw1 complex components (Dsn1, Mtw1, Nnf1 and Nsl1) and purified CMO-complex and Ame1 protein separately.

(A) Interaction between the ^{35}S methionine-labeled Mtw1 complex components and the CMO-complex and Ame1-protein was studied using magnetic agarose beads. Proteins were eluted by boiling the beads and analyzed by autoradiography. In the control reaction Mtw1-complex proteins were incubated with the pre-equilibrated Ni-NTA magnetic agarose beads only, eluted by boiling the beads and analyzed.

Input lane show 5% of the assay input, Co-Immunoprecipitation (IP) lanes show 100% of the input.

(B) Coomasie-stained gel of the control sample in which no ^{35}S-labeled proteins (preys) were added. After the mock binding was performed, proteins were eluted by boiling the agarose beads and 50% of the elutions were analyzed by MS.

From the autoradiography image it was revealed that the Dsn1 component of the Mtw1-complex interacts with the tested baits, the CMO-complex and Ame1 protein. The background levels of unspecific protein binding were illustrated in the control lanes. Further, the autoradiographic densities of each protein band were quantified using the

ImageJ software. The results of each experiment were subtracted for the background binding and normalized according to the input signal (Fig. 3.5.5).

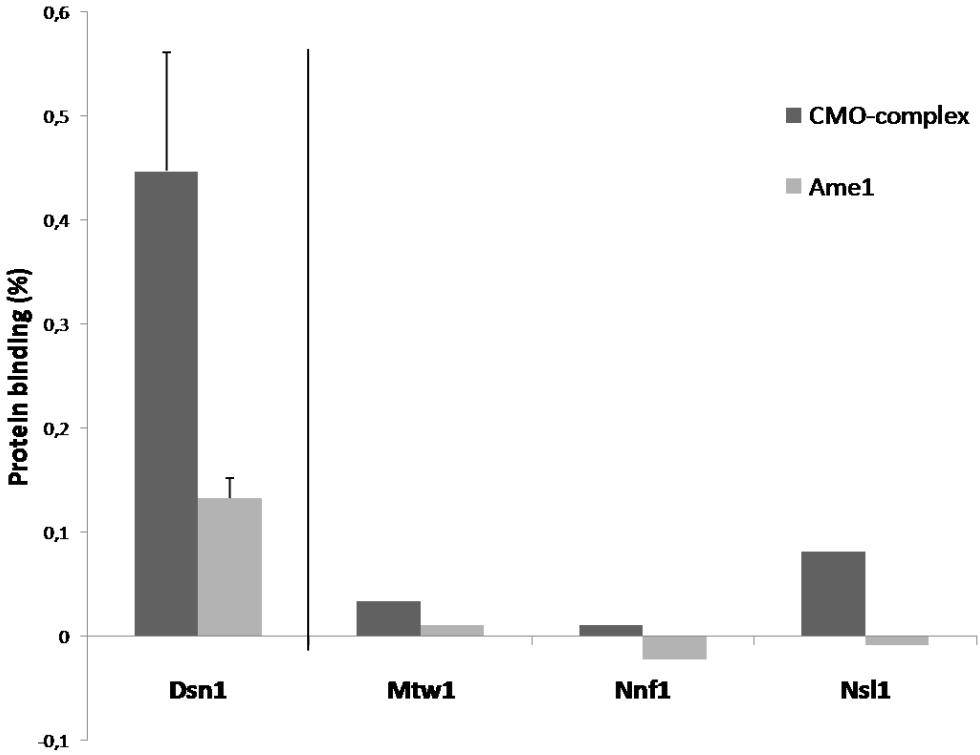

Fig. 3.5.5 Quantification of direct protein-protein interactions between the Mtw1-complex and CMO-complex and Ame1 protein separately, from the autoradiogram in Figure 3.4.4 A. The ImageJ software was used for this purpose.

The histogram shows the result of densitometric analysis of autoradiographic bands in which the protein levels were measured, subtracted for the background binding and expressed as a percentage of the input of each prey protein. For only the Dsn1 protein interactions, two separate experiments were performed. Data represents means ± s.e.m. for experiments performed n=2.

This result clearly demonstrates the direct interaction between the Dsn1 protein and proteins from the COMA-complex. It was revealed that the Dsn1 interacts with the CMO-complex and Ame1 protein independently. The interaction with the Ame1 protein solely, is more than three times weaker compare to the CMO-complex. According to the quantificational method, Nsl1 protein may weakly interact only with the CMO-complex and not with the Ame1 protein.

The analysis of the bait proteins under the assay conditions revealed that the treatment did not severely degrade proteins (Fig. 3.5.4B). Proteins were purified as full-length proteins with the exception of the Ctf19 protein. As shown before, a truncated version of the His_6-Ctf19ΔC could be observed during the IMAC and SEC. It is notable not only that

the His_6-Ctf19ΔC can form the stable complex with Mcm21 and Okp1 protein (Fig. 3.1.3 B), but that here we can conclude that C-terminus of the Ctf19 protein is not required for the Dsn1 protein interaction with the CMO-complex.

To find binding partners between a putatively assembled COMA- and the Mtw1-complex components, an additional experiment was performed. By co-expressing Ame1 His_6-Okp1 and Mcm21-TAP Ctf19 proteins, a putatively formed tetrameric COMA-complex was purified using human IgG agarose and further applied for the binding assay. The TEV-elutions were finally analyzed by autoradiography (Fig. 3.5.6 A). In parallel, the control sample after the mock binding was analyzed on coomassie-stained gel by MS (Fig. 3.5.6 B).

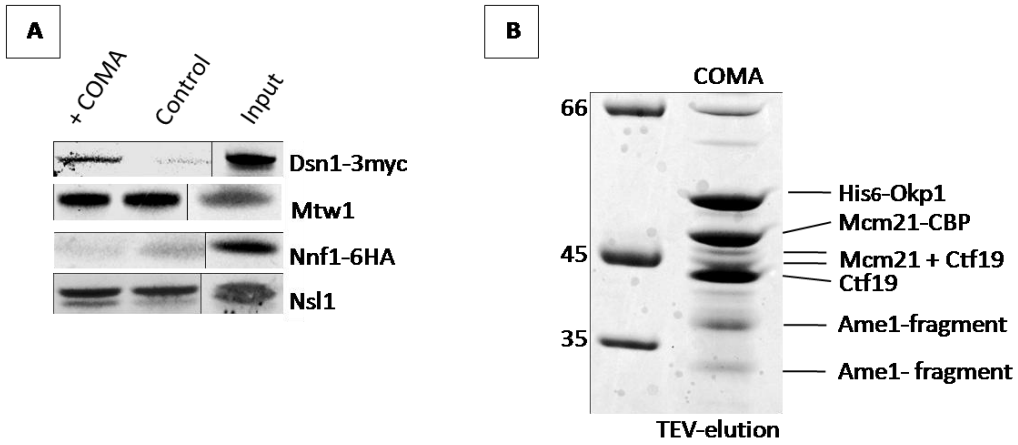

Fig. 3.5.6 Autoradiography and coomassie-stained gel images of studied interactions between *in vitro* translated Mtw1 complex components (Dsn1, Mtw1, Nnf1 and Nsl1) and a putatively formed COMA-complex.

(A) A putatively formed COMA-complex was incubated with ^{35}S methionine-labeled Mtw1 complex components while still being immobilized on the human IgG agarose beads at 4°C overnight. After extensive washing, proteins were eluted by TEV-cleavage and analyzed by autoradiography.

Input lanes show 5% of the assay input, Co-Immunoprecipitation (IP) lanes show 13,5% of the input.

(B) In the control reaction Mtw1 complex proteins were incubated with the pre-equilibrated Human IgG agarose beads. After extensive washing, proteins were eluted by TEV-cleavage and 20% was analyzed by MS on coomassie-stained gel.

Analysis of the proteins from the control sample revealed that Okp1, Mcm21 and Ctf19 were TEV-eluted as full-length proteins, and that Ame1 degraded as seen before (Fig. 3.5.6 B). From the autoradiography image direct interaction between the Dsn1 protein and the putatively formed COMA-complex was confirmed. The autoradiographic densities of each protein band were quantified using the ImageJ software as for the binding assay with the CMO-complex and Ame1 protein (Fig. 3.5.7).

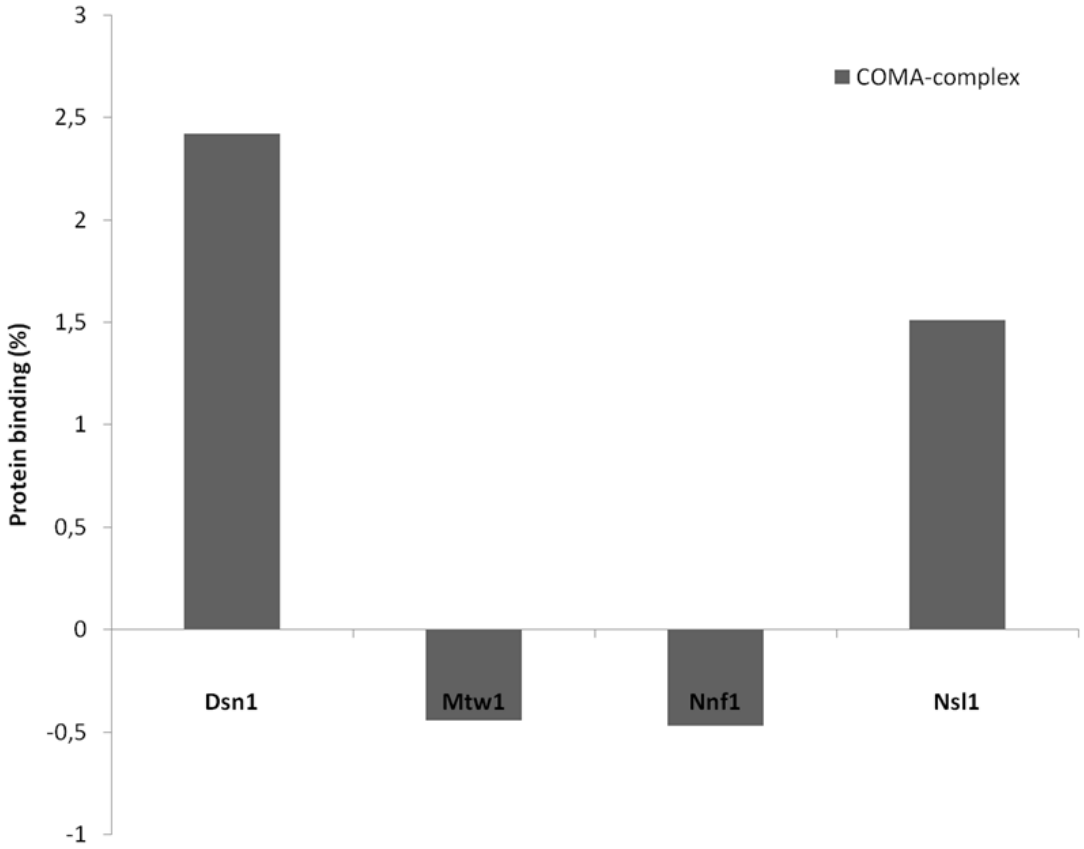

Fig.3.5.7 Quantification of direct protein-protein interactions between the Mtw1- and the putatively assembled COMA-complex components.

Histogram shows the result of densitometric analysis of autoradiographic bands in which the protein levels were measured, subtracted for the background binding and expressed as a percentage of the input of each prey protein.

It was shown before that Dsn1 protein co-purifies with the Okp1-TAP protein from cell lysates of budding yeast (Fig. 3.4.1). It thus might be a direct binding partner of the COMA-complex or one of its subunits. This was confirmed. According to the densitometric quantification, another protein from the Mtw1 complex, the Nsl1 protein, might also interact with the putatively assembled COMA-complex as it was previously shown that it interacts weakly with the CMO-complex. Direct protein-protein interaction between Nsl1 and Ame1 proteins was not registered in the assay. For the other two proteins, Mtw1 and Nnf1, no binding was observed as well. Since the reticulocyte binding assay has not been done more than once, except for the Dsn1 protein interactions, and since the intensity of the signals was quite weak, the data described represents preliminary data.

3.5.2 The COMA-complex interacts with inner kinetochore protein components Mif2 and Cse4

To investigate the binding partners of the COMA-complex with several inner kinetochore components, the same approach as for the Mtw1-complex has been applied. The selected binding partners were Mif2, Cse4 and Scm3 proteins, three essential kinetochore components that localize closely to the centromeric chromatin. The CMO-tetrameric complex and Ame1 protein were immobilized separately on magnetic beads and incubated with *in vitro* translated Mif2, Cse4 and Scm3 proteins in individual tubes. Pre-equilibrated Ni-NTA magnetic agarose beads without any COMA component were incubated with the same *in vitro* translated proteins in the control experiments (Fig. 3.5.8 A).

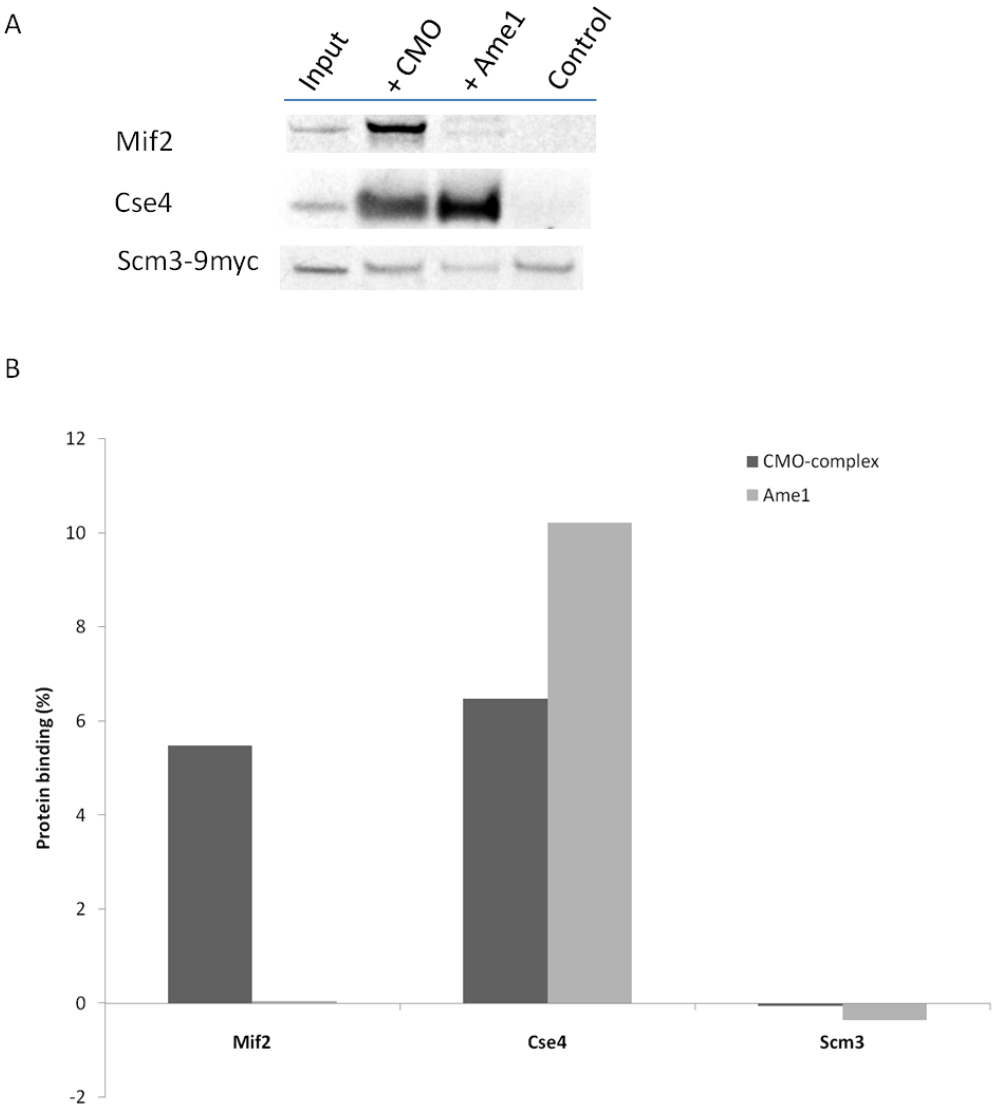

Fig. 3.5.8 Autoradiography image and quantified results of the direct interactions inspected between the COMA components and named inner kinetochore proteins.

(A) Direct protein-protein interactions between bacterially expressed and purified CMO-trimeric complex and Ame1 protein separately, and *in vitro* translated Mif2, Cse4 and Scm3 kinetochore proteins are shown. In the control reactions Mif2, Cse4 and Scm3 proteins were incubated with the pre-equilibrated Ni-NTA magnetic agarose beads.

Input lanes show 5% of the assay input, Co-Immunoprecipitation (IP) lanes show 100% of the input.

(B) Histogram shows the result of densitometric analysis of autoradiographic bands in which the protein levels were measured, subtracted for the background binding and expressed as a percentage of the input of each prey protein; Mif2, Cse4 and Scm3 respectively.

The autoradiographic densities of each protein band were quantified; the results of each experiment were subtracted for the background binding and normalized to the input signal (Fig. 3.5.8 B).

Taken together, these experiments revealed three different types of dependencies and interactions. Mif2 protein directly associates with the CMO-trimeric complex and no interaction with the Ame1 protein could be observed under the same conditions. Cse4 protein interacts with both Ame1 and the CMO-protein components independently. The Scm3 protein showed no association with the COMA proteins, as could be predicted since it behaves as a specific Cse4 histone chaperone and not as a constitutive kinetochore component (Zhou, Feng et al. 2011).

The reticulocyte binding assay has not been done more than once for the tested inner kinetohore proteins. Thus, the data described represents preliminary data. In addition to that, the fully assembled tetrameric COMA-complex remains to be tested under the same condition as the Mtw1-complex.

In summary, the data of *in vitro* binding assays demonstrate the bonding function of the COMA-complex. The *in vitro* binding assay approach suggest that the COMA-complex links centromeric chromatin via Mif2 and Cse4 proteins on one side, and interacts with the Mtw1-complex via Dsn1 protein on the microtubule-interface-side. The fact that Mif2 protein interacts only with the CMO-complex and not with the Ame1 protein on an individual basis, indicates a spatial organization of the budding yeast central kinetochore layer. Most probably, the Mif2 and CMO-complex are in closer proximity compare to the Mif2 and Ame1.

4. DISCUSSION

The COMA-network is a central kinetochore group of proteins that consists of eleven subunits (Ctf19, Okpl, Mcm21, Ame1, Ctf3, Mcm16, Mcm22, Chl4, Iml3/Mcm19, Nkp1 and Nkp2) that are found to consistently co-purify from yeast extracts when one of their members is affinity purified (Cheeseman, Anderson et al. 2002), (De Wulf, McAinsh et al. 2003). Yeast purifications of these kinetochore proteins also contained Cse4, Nsl1 and Mtw1 proteins in low amounts. From the preparations, it could be suggested that the COMA-network and the Mtw1-complex (which two subunits, Mtw1 and Nsl1 proteins, were co-purified with the COMA) assemble at the kinetochore in close proximity to each other and to the kinetochore core (since the specialized histone H3, Cse4 protein, also co-purified with the COMA). Furthermore, the Bub3 protein, a member of the spindle assembly checkpoint (SAC) mechanism, was also found to co-purify with the COMA, linking the COMA-network to the SAC.

4.1 Reconstitution of the COMA-complex

Hydrodynamic analysis (size-exclusion chromatography together with glycerol-density gradient ultracentrifugation) revealed the presence of a tetrameric COMA-complex as well as the two heterodimers Okp1-Ame1 and Ctf19-Mcm21 in crude yeast extracts (De Wulf, McAinsh et al. 2003). Here, we tried to reconstitute the COMA-complex from a heterologous system. The Ctf19-Mcm21 and Okp1-Ame1 heterodimers together with the CMO- and COMA-complexes, as obtained by reconstitution from *E. coli* expression proteins, will be compared to the COMA-complex from *S. cerevisiae* in the following.

Firstly, we reconstituted the Ctf19-Mcm21 heterodimer. The existence of a Ctf19 Mcm21 hetero was shown by three different experiments: Mcm21-TAP Ctf19 (Fig. 3.1.3A), His_{10}-Mcm21 Ctf19 (Fig. 3.1.3B) and His_6-Ctf19 Mcm21 (Fig. 3.2.2 and 3.2.3) were co-purified by IMAC or the TAP-purification method. Furthermore, the evidence for a direct physical interaction between the Ctf19 and Mcm21 proteins was acquired when a putative heterodimeric complex was isolated by subsequent gel filtration using the Superose 6 and Superdex 200 columns. The Ctf19 and Mcm21 complex, according to the gel filtration chromatography, elutes at volumes corresponding to a tetramer (if spherical shape of the dimer was anticipated) with an apparent MW of ~170 kDa. However, from the work done by De Wulf *et. al*. it is known that the dimer has a high

axial ratio (represented as the degree of elongation of the ellipse) and friction coefficient (which measures the maximum shape asymmetry from a sphere) and it appears that the molecule has an elongated, filamentous shape. With this in mind, we can conclude that the Ctf19 Mcm21 complex most likely elutes as a fibrous dimer. Additionally, when using the pET-expression vector, a small amount of complex consisted of monomeric subunits, whilst using a polycistronic expression vector a considerable amount of proteins eluted at higher volumes appearing as oligomeric. The combined hydrodynamic analysis, when the crude yeast extracts were used, estimated MW~94 kDa which corresponds to the theoretical MW~100 kDa for the heterodimer (De Wulf, McAinsh et al. 2003).

Second, the application of various expression and protein purification strategies from *E. coli* could not reconstitute a stable dimer between the Ame1 and Okp1 essential COMA-components (Fig. 3.1.4). A direct physical interaction between them was detected, but the Ame1 protein was already very prone to proteolytic degradation in the cell and also during the purification procedure. Combined hydrodynamic analysis of the COMA-complex in crude yeast cells presented a stable and elongated Ame1 Okp1 heterodimer with estimated MW~94kDa (which corresponds to the theoretical MW~105kDa) (De Wulf, McAinsh et al. 2003). This indicates that the chaperone proteins or additional component from the COMA-network may be involved in the assembly of the complex.

We next examined the trimeric CMO-protein complex. Although the CMO-complex can assembly independently from Ame1, this apparently does not reflect the situation in budding yeast cells. The co-purification of the Okp1 protein with Ctf19 Mcm21 dimer using a polycistronic expression vector through multiple purification steps had an unanticipated outcome. The trimeric CMO-complex does not require the Ame1 component for its assembly or stability maintenance *in vitro* (Fig. 3.2.5). When additional analysis of the CMO-complex by subsequent gel filtration chromatography was applied, it was shown that the trimeric complex could form a variety of oligomeric states, from dimer/tetramer formation to highly oligomerized forms (Fig. 3.2.7). The molecular weight of the CMO-complex, according to gel filtration chromatography on the Superose 6 column, was considerably higher than expected if the complex consisted of spherical monomeric subunits (Fig. 3.2.8) and it is estimated to MW~1,34 MDa. When DLS measurement was performed, the experimental MW~800 kDa was obtained.

Finally, when we attempted to *in vivo* reconstitute the four-protein COMA-complex, placing the AME1 on the fourth position of the polycistronic expression vector, all our experiments failed to detect a complex with a stable form of Ame1 protein (Fig. 3.2.16). Since the heterotetrameric COMA-complex has been shown as a stable complex in *S. cerevisiae*, we could think once more of additional proteins that may be required for its assembly and that were lacking in *E. coli*. Recently, the experiments performed by Hornung *et al*. have described the successful reconstitution of the yeast COMA-complex at a stoichiometry of 1:1:1:1. Strikingly, the only difference between the polycistronic expression construct that we made and the one from the mentioned experiment was in the C-terminal position of the His_6-tag on the most proteolytically degradable component AME1 (thus selecting for Ame1 protein with an intact C-terminus), with the same order of all genes. Since the amount of *E. coli* culture used for the COMA-complex expression was not detailed in the article, we assumed that a large-scale protein production was employed, thus enabling the successful purification of stable proteins even if present in very small amounts.

Next, we were interested in testing whether an intact COMA-complex could be reconstituted from the trimeric CMO-complex and the Ame1 protein separately. A purification procedure included two separate IMAC purifications, mixture of the purified proteins followed by a gel filtration chromatography (Fig. 3.2.18). Isolation of the tetrameric COMA-complex showed a near homogeneity of the four proteins but again as an oligomeric or very elongated form with a molecular weight much higher than the one originally obtained from the yeast cell purification (De Wulf, McAinsh et al. 2003). The apparent MW of the *in vitro* reconstituted COMA-complex was 1,8 MDa. The apparent MW of the COMA-complex purified from *S. cerevisiae* and analyzed on calibrated velocity gradient and SEC was MW~183 kDa. If only the SEC was applied, the COMA-complex from budding yeast extracts yielded the elongated, fibrous complex with apparent MW~500 kDa. When whole cell extracts were then analyzed by the glycerol-gradient density ultracentrifugation, it appeared as very fibrous molecule with axial ratio (a:b) 9±0,1 (De Wulf, McAinsh et al. 2003). Although both SEC analyses, from *E. coli* and from the crude yeast cell extracts, estimated mass of the COMA-complex to be higher than expected, they do not agree. The reason for this difference may be the exposure of hydrophobic protein regions that have been protected in budding yeast by additional COMA-components (like the Nkp1 and Nkp2 proteins; see below). Also, based on the results

acquired from the experiments using other proteins which are distributed throughout the inner, central and outer kinetochore (Dam1, Spc34, Ask1, Ndc80, Sli15, Dsn1, Mif2) and have been described as targets for the phosphorylation (e.g. by the Aurora kinase Ipl1), we speculate that additional post-translational modifications may have a role in modulating the stability and activity of the COMA-complex (Cheeseman, Anderson et al. 2002), (Westermann, Cheeseman et al. 2003). If, how and which post-translational modifications are exactly involved in the formation of a stable and unperturbed COMA-complex is still under the extensive investigation, but it could be a reason that then results obtained are distinct from those when the budding yeast extracts were used. In any case, using the Scan Prosite tool (Sigrist, Cerutti et al. 2010), 36 phosphorylation sites on the Okp1 and 17 on the Ame1 proteins were predicted (Table 4.1).

	Ctf19	**Mcm21**	**Okp1**	**Ame1**
CK2 phospho site	4	10	14	6
PKC phospho site	4	3	12	5
TYR phospho site	/	/	3	/
CAMP phospho site	2	/	2	/
Polo phospho site	/	2	3	1
CDK phospho site	/	2	1	5
Aurora (Ipl1) phospho site	1	1	1	/
Sum of phospho sites	11	18	36	17

Table 4.1 Scan Prosite predicted phosphorylation sites of the COMA proteins.
CK2 phospho site=Casein kinase II phosphorylation site; PKC phospho site=Protein kinase C phospho site; TYR phospho site=Tyrosin kinase phosphorylation site; CAMP phospho site=cAMP- and cGMP-dependent protein kinase phosphorilation site; Polo phospho site=Polo-like kinase phospho site; CDK phospho site=cyclin-dependent kinase phospho site; Aurora (Ipl1) phospho site=Aurora (Ipl1) kinases phospho site.

Beside the phosphorylation, that can regulates the kinetochore function via cyclin-dependent kinases, Polo-like kinases and Aurora (Ipl1) kinases, the sumoylation and ubiquitination processes may also be involved in the COMA-complex formation.

Through the analysis of the Ctf19, Mcm21 and Okp1 protein sequences, specific coiled-coil domains were at first predicted and then assessed as stable by the limited

proteolysis technique (Fig. 3.2.15) (Lupas, Van Dyke et al. 1991). The α-helical coiled-coil region is the simplest of all protein-protein interaction motifs and approximately 5% of the *S. cerevisiae* proteome contains a coiled-coil region. We also found for the essential Okp1 protein that the coiled-coil protein domain has to be intact in order for cells to preserve their viability (Fig. 3.3.2 B). It is likely that many of these coiled-coils mediate protein-protein interactions or protein oligomerization (Meier, Stetefeld et al. 2010). In our opinion it is realistic to assume that these long coiled-coil regions caused the oligomeric behavior of the COMA-proteins during testing by gel filtration chromatography. Moreover, the coiled-coils provide the structural framework for many elongated proteins (Molecular Biology of the Cell. 4th edition. Alberts B, Johnson A, Lewis J, et al. New York: Garland Science; 2002). Thus, the shape of the complex caused the appearance of the COMA-proteins higher than expected. To support this, it has been observed in yeast extracts that the purified COMA-complex, when analyzed by glycerol-density gradient ultracentrifugation, showed significant shape asymmetry from a sphere (De Wulf, McAinsh et al. 2003).

4.2 A possible unspecific RNA association with the COMA-proteins

The kinetochore is a very complex and dynamic structure and there was a tremendous progress of understanding the assembly pathway within the last years. Still, the exact mechanism, proteins and structural RNA molecules involved in the formation of kinetochore structure and organization are not completely known or explained.

Here, affinity purifications of the Ctf19-Mcm21 dimer and the CMO-complex contained a substantial amount of RNA. Despite much work on kinetochore assembly mechanisms and structure, the contribution of RNA to kinetochore assembly is still unclear and under consideration by scientists from the field of study. Within this work, weak unspecific RNA-COMA protein interaction has been detected during affinity purification procedure. It became clear that RNA co-purifies with the CMO-complex when the IMAC purified sample was analyzed on the EtBr-stained agarose gel (Fig. 3.2.10). Nucleic acids show altered mobility on the gel after the proteins were removed by the Proteinase K treatment (Fig. 3.2.12), which could indicate an unspecific interaction between RNA and the CMO-complex. This could, in fact, reflects the situation where one or more CMO-

proteins interact with the CEN-DNA, but since the RNA molecules were much more accessible during the protein purification from *E. coli*, the result was as described.

There is no evidence that RNA interacts with the kinetochore proteins in budding yeast so far. But it has been reported that centromeric RNA is an integral component of the kinetochore in HeLa cells and that kinetochore proteins CENP-C (yeast homologue Mif2) and INCENP (yeast homologue Sli15, one of the Aurora kinase complex members together with Ipl1/Aurora B, Bir1/Survivin and Nbl1/Borealin) accumulate in the human interphase nucleolus (Wong, Brettingham-Moore et al. 2007). The data by Wong *et. al.* suggests that centromere satellite RNA directly facilitates the accumulation and assembly of centromere-specific nucleoprotein components at the nucleolus and mitotic centromere, and that the sequestration of these components in the interphase nucleolus provides a regulatory mechanism for their timely release into the nucleoplasm for kinetochore assembly at the onset of mitosis. It has also been reported that centromere-encoded RNAs are integral components of the maize kinetochore (Topp, Zhong et al. 2004). Moreover, RNA is a known component of sex chromosome dosage compensation complexes in mammals and *Drosophila* (Amrein 2000), (Wutz 2003), of human pericentromeric heterochromatin (Maison, Bailly et al. 2002) or of the yeast telomerase complex (Zappulla and Cech 2004). So far, RNA has not been documented as part of the budding yeast kinetochore.

On the other side, there may be no CMO-RNA interaction and the RNA may just be a contaminant. In order to preserve the CMO-complex in solution, we performed the IMAC and SEC under the low salt conditions. As a consequence, it is possible that nucleic acids retained on the Ni^{2+} chelating matrix and purified from the cell lysate. This is supported by the observation that after RNA removal from the purified samples, no alternate elution profile of the CMO-complex was observed on gel filtration (Fig. 3.2.13).

4.3 Interaction of the Ame1 Okp1 dimer with Nkp1 and Nkp2 proteins

A list of eleven proteins that co-purify together and form the COMA-network was confirmed by modified TAP-purification from the budding yeast cells (Fig. 3.4.1). A diligent analysis of proteins that co-purified with Okp1-TAP protein, prompted us to focus on the two most abundantly present proteins, Nkp1 and Nkp2, as potential binding

partners for the COMA-complex. The Nkp1 and Nkp2 proteins were characterized as part of the COMA-network when co-purified in the Mcm16-purification (Cheeseman, Anderson et al. 2002) and they still await more extensive studies. A direct protein-protein interaction between Nkp1 and Nkp2 with the COMA-complex was shown by IMAC and gel filtration chromatography when the entire hexameric COMANN-complex was reconstituted (Figure 3.4.2 and 3.4.3). The Nkp1 Nkp2 heterodimer was also purified from His_6-GST-Nkp2 Nkp1 either by IMAC or the GST-purification (Fig. 3.4.4). Interestingly, the addition of Nkp1 and/or Nkp2 proteins greatly stabilizes the purified COMA-proteins, in particularly the readily degradable Ame1 protein. According to the SEC, there is again high molecular weight fraction with putatively oligomerized kinetochore proteins, with the exception of the Ame1 protein. Importantly, a complete hexameric COMANN-complex (calculated molecular weight of 217 kDa), also eluted from the Superose 6 and it has the estimated MW~218,3 kDa. The elution position and densitometry of the protein bands indicated that the hexameric complex contains one copy of each protein. One possible explanation for this behavior is that the hydrophobic residues that were exposed at the surface of the folded protein complex without the Nkp1 and Nkp2 (and that could cause the propensity of the complex to oligomerize) may became much less exposed after the Nkp1 and Nkp2 binding, which then stabilize the whole hexameric complex. On that basis, we could analyze whether the intact COMA-complex from *S. cerevisiae* cell extract also contains the small Nkp1 and Nkp2 proteins that were not tested so far. Also, it appears that the elongated shape of the COMA-complex turns into the more spherical, once the Nkp1 and Nkp2 assemble.

To test the structural organization of the complex in more detail, we analyzed the physical interaction of the Nkp1 and Nkp2 with essential and nonessential dimers of the COMA-complex and found that the four-subunit complex could be predominantly assembled with the two essential Ame1 and Okp1 proteins (Figure 3.4.5). A weak interaction between the four nonessential proteins from the COMA-network (Ctf19, Mcm21, Nkp1 and Nkp2 proteins) after co-expression of all subunits in *E. coli* might be just a contamination that might have been missed in the control experiment due to the lower input in this experiment without the GST-tag (Fig. 3.4.6). Furthermore, comparing the COMA-network purified from a wild type and a Ctf19 and Mcm21 deleted strain by quantitative mass spectrometry (SILAC) revealed that the interaction of Nkp1 and Nkp2 dimer with the COMA-complex is facilitated predominantly via the Okp1 and Ame1

proteins (unpublished data performed by Jennifer Ortiz and Maria Knapp from the Lechner group).

4.4 Direct interaction of the proteins from Mtw1-complex and centromeric chromatin with the COMA-proteins

The direct binding between the COMA-core and protein complexes in its close proximity, was analyzed by *in vitro* binding assays. The individual proteins were tested for the binding with either the Ame1 and CMO-complex or the putatively formed COMA-complex.

It has been shown before, either in *E. coli* or budding yeast cells, that the COMA- and Mtw1-complex interact to each other (De Wulf, McAinsh et al. 2003) (Hornung, Maier et al. 2010), (Maskell, Hu et al. 2010) (Westermann, Cheeseman et al. 2003). When testing more closely direct interaction between the two neighboring COMA- and Mtw1-complexes, our preliminary results suggested that the Dsn1 protein was required for the binding surface between them (Fig. 3.5.5 and Fig. 3.5.7). This result is in the agreement with the co-purification of the Dsn1 protein shown previously when the Okp1-TAP protein purification was performed from the budding yeast cell lysate (Fig. 3.4.1). Another candidate that may have a similar function is the Nsl1 component of the Mtw1-complex, particularly when the putatively formed tetrameric COMA-complex represented the bait (Fig. 3.5.7). Since the reticulocyte binding assay has not been done more than once, except for the Dsn1 protein interactions, and since the intensity of the signals was quite weak, the data described represents preliminary data and remains to be verified.

This result is distinct from the recent publication where the Mtw1 Nnf1 and the Dsn1 Nsl1 dimer subcomplexes were tested separately in *E. coli* pull down experiments with the COMA-complex (Hornung, Maier et al. 2010). They found that the dimer formed between the Mtw1 and Nnf1 proteins interacts more efficiently with the COMA-complex when compared with the Dsn1 and Nsl1 dimer. On the other hand, there are also recent data from biochemical and EM studies that suggests that the contact between the Mtw1-complex and more inner kinetochore proteins (as the COMA-complex is) is established via the Dsn1 and Nnf1 proteins (Maskell, Hu et al. 2010). Interestingly, high-resolution

co-localization data places the Nnf1 closest to the inner centromere, and thus also to the COMA-complex, in both humans and *S. cerevisiae* (Wan, O'Quinn et al. 2009). The direct interaction between the COMA-proteins and Nnf1 protein was not detected in the *in vitro* binding assays we performed. Taken together, the interface between these two middle kinetochore complexes, the Mtw1- and COMA-complex, still remains to be clarified in the future studies.

In respect to the interaction with components from the centromeric chromatin we obtained preliminary evidence that the Mif2 protein directly associates only with the CMO-trimeric complex and not with the Ame1 protein, and that the Cse4 protein interacts with both Ame1 and the CMO-protein components (Figure 3.5.8). The Cse4 inner kinetochore protein was also found when biochemical purification of the Okp1-TAP from yeast extract was performed. Since the data described represents the preliminary results, further experiments remain to confirm the protein-protein interactions. The impact of these physical interactions between the inner kinetochore proteins and the COMA-components is still an open question, but we could anticipate that, beside the molecular organization of the kinetochore and the interphase kinetochore dynamics, this linkage may have an influence on the SAC and cell cycle progression.

4.5 A refined model of the budding yeast kinetochore central domain

The data provided during this work adds new information to the current model of the *S. cerevisiae* central kinetochore domain. The proposed molecular architectures of the inner and central kinetochore proteins, examined in this thesis and deducted from direct protein-protein interactions, are schematized in Figure 4.1.

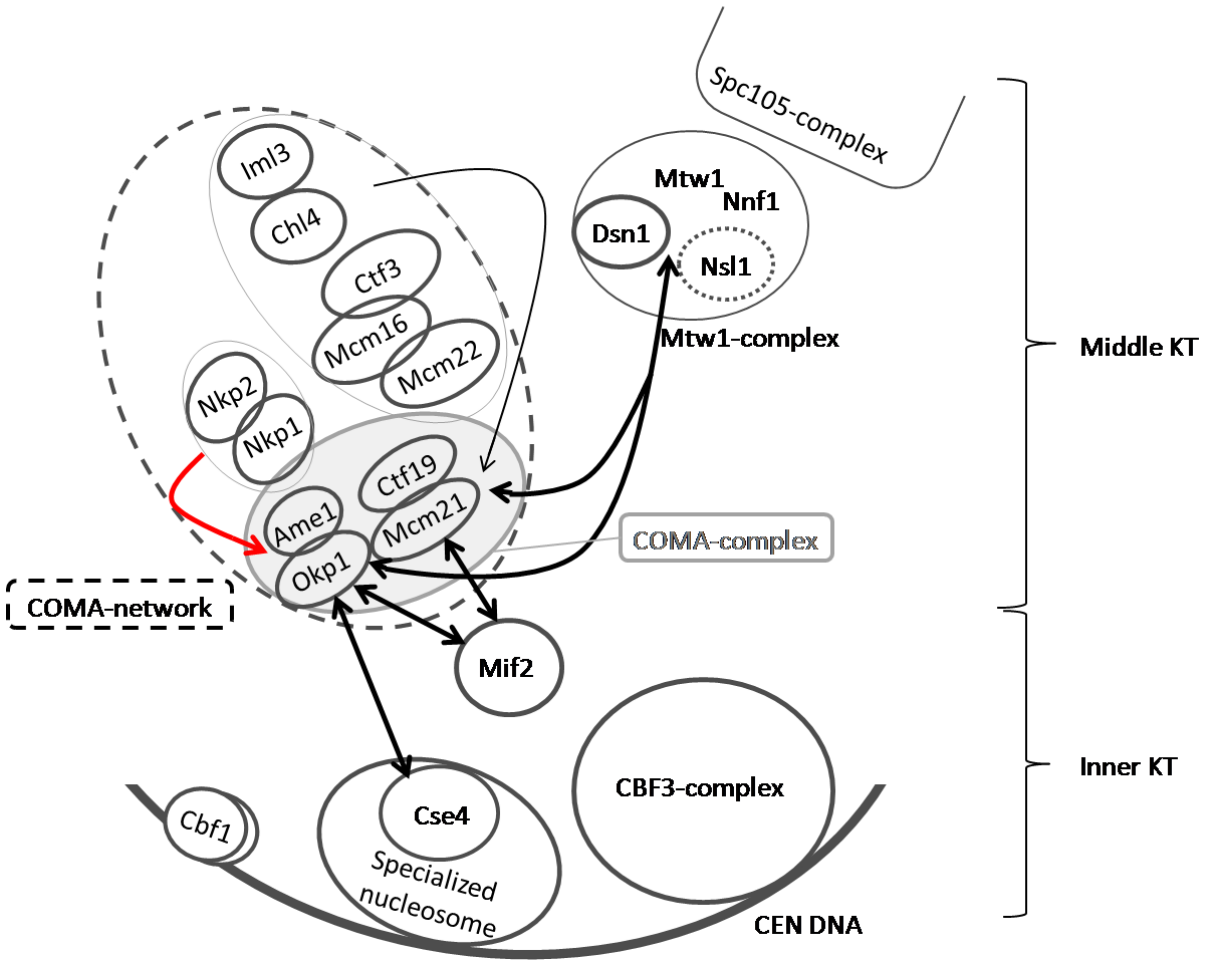

Fig. 4.1 New structural model of the *S. cerevisiae* inner and central kinetochore domains.
Newly identified direct protein-protein interactions are depicted as tick arrows. The tin black arrow between the Ctf19-Mcm21 proteins and the group of the COMA-network proteins including Iml3, Chl4, Ctf3, Mcm16 and Mcm22 indicates the previously indentified interactions that may not be direct. The red tick arrow between the Nkp1-Nkp2 and Ame1-Okp1 dimers indicates the newly discovered physical interaction that stabilizes the COMA-core.

The centrally positioned COMA-network is apparently spatially organized in two parts. The two essential Ame1 and Okp1 proteins directly interact with the Nkp1 and Nkp2 proteins on one side of the network (demonstrated in this thesis within the chapters 3.4.2 and 3.4.3). This newly identified direct interaction within the COMA-network in in line with the SILAC experiments and provides a new insight into the spatial organization within the central kinetochore layer. The other seven non-essential proteins (Ctf19, Mcm21, Ctf3, Mcm22, Mcm16, Chl4 and Iml3) are located on the distinct side. It has been

shown by the ChIP analysis that the Ctf3, Mcm16 and Mcm22 proteins interact with CEN DNA via the Ctf19 subunit of the COMA-core (Measday, Hailey et al. 2002). Also, as revealed by combination of ChIP, *in vivo* localization studies and protein immunoprecipitation, it has been established that the Iml3 and Chl4 proteins localize to the kinetochore in a Ctf19-dependent manner (Pot, Measday et al. 2003).

The closest protein toward the kinetochore-microtubule interface (the Mtw1-complex components) that directly interacts with the COMA-complex is the Dsn1 protein (Fig.3.5.5 and Fig. 3.5.7). The Nsl1 protein showed weaker interaction with the COMA-complex as well, but since the data presented here are only preliminary data and since there are no additional publications that support this finding, this interaction has to be further investigated.

Additionally, more inner protein components that could interact with the centromeric chromatin, the Cse4 and Mif2 proteins, may be located in the direct vicinity of the COMA-complex. In more detail, the Mif2 protein is located further from the Ame1 and closer to the CMO-complex side (Fig. 3.5.8). These direct interactions has been newer shown before and have to be confirmed.

5. MATERIALS AND METHODS

5.1 Plasmids, strains and oligonucleotides

5.1.1 Plasmids

Plasmid	Relevant genotype
pAS1101	AME1 in pETDuet-1
pAS1102	His_6-OKP1, AME1 in pETDuet-1
pAS1109	CTF19 in pCOLADuet-1
pAS1110	MCM21-TAP in pCOLADuet-1
pAS1111	AME1 in pETDuet-1
pAS1112	MCM21-His_{10}, CTF19 in pCOLADuet-1
pAS1113	AME1, His_6-OKP1 in pETDuet-1
pAS1117	MCM21-TAP, CTF19 in pCOLADuet-1
pAS1118	DSN1-3myc in pSP64 PolyA
pAS1119	MTW1 in pSP64 PolyA
pAS1120	NSL1 in pSP64 PolyA
pAS1121	CSE4 in pSP64 PolyA
pAS1122	NNF1-6HA in pSP64 PolyA
pAS1123	SCM3-9myc in pSP64 PolyA
pAS1129	MIF2-6HA in pSP64 PolyA
pAS1141	His_{10}-AME1 in pETDuet-1
pAS1142	His_{10}-AME1, OKP1 in pETDuet-1
pAS1143	His_6-OKP1 in pET24d
pAS1149	His_6-TEV-CTF19 in pST39
pAS1150	MCM21 in pET3aTr
pAS1151	OKP1 in pET3aTr
pAS1153	His_6-TEV-CTF19, MCM21 in pST39
pAS1164	His_6-TEV-CTF19, MCM21, OKP1 in pST39
pAS1166	His_6-TEV-CTF19, MCM21, OKP1, AME1 in pST39
pAS1172	CTF19, MCM21, OKP1 in pST39
pAS1207	Δaa 1-115, Δaa 283-406 okp1
pAS1216	His_6-TEV-CTF19, MCM21, OKP1 Δaa 1-116, Δaa 282-406 in pST39
pAS1217	His6-TEV-CTF19, OKP1 Δaa 1-116, Δaa 282-406 in pST39
pAS1225	His_6-TEV-CTF19, MCM21, OKP1 Δaa 282-406 in pST39
pAS1226	His_6-TEV-CTF19, MCM21, OKP1 Δaa 1-116 in pST39
pAS1227	His_6-TEV-CTF19, OKP1 Δaa 282-406 in pST39
pAS1228	His_6-TEV-CTF19, OKP1 Δaa 1-116 in pST39
pAS1252	His_6-TEV-CTF19, MCM21, OKP1 Δ1-116, Δ282-406-Flag in pST39

pAS1253	His6-TEV-CTF19, OKP1 Δaa 1-116, Δaa 282-406-Flag in pST39
pAS1255	His_6-TEV-CTF19, MCM21, OKP1 Δaa 282-406-Flag in pST39
pAS1256	His_6-TEV-CTF19, OKP1 Δaa 282-406-Flag in pST39
pAS1257	His_6-TEV-CTF19, MCM21, OKP1 Δaa 1-116-Flag in pST39
pAS1258	His_6-TEV-CTF19, OKP1 Δaa 1-116-Flag in pST39
pAS1267	NKP2 in pCOLADuet-1
pAS1270	NKP2, NKP1 in pCOLADuet-1
pAS1271	NKP2, His_6-Thr-GST-NKP1 in pCOLADuet-1
pBL887	AME1 (5`-ORF-3`)
pBS1479	TAP-tag (CBP-TEV-Prot.A)-TRP1-KL
pCOLADuet-1	T7-promoter, MCS1, MCS2, LacI, His_6-tag, S-tag, ColA origin ($KanMX6^R$)
pET3a	T7-promoter, T7-tag, MCS, LacI, ColE1 replicon (Amp^R)
pET3aTr	T7-promoter, T7-tag, MCS, LacI, ColE1 replicon (Amp^R)
pET16b	T7-promoter, His_{10}-tag, MCS, Factor Xa, LacI, ColE1 replicon (Amp^R)
pET24d	T7-promoter, T7-tag, MCS, LacI, His_6-tag, ColE1, f1 origins ($KanMX6^R$)
pETDuet-1	T7-promoter, MCS1, MCS2, LacI, His_6-tag, S-tag, ColE1 replicon (Amp^R)
pJL465	OKP1 (5`-ORF-3`)
pJL473	OKP1 (5`-ORF-3`) in pRS415
pJL485	MIF2 (5`-ORF-3`)
pJL494	CTF19 (5`-ORF-3`)
pJL498	MCM21 (5`-ORF-3`)
pJL537	MCM21 (5`-ORF-3`) in pET16b
pML634	Δaa 283-406 okp1
pML635	Δaa 231-406 okp1
pML659	Δaa 1-115 okp1
pRS415	CEN6 ARS LEU2
pSP64 PolyA	SP6-promoter, MCS, Poly-A, Amp^R
pST39	T7-promoter, T7-tag, MCS, LacI, ColE1 replicon (Amp^R)
pYM13	TAP-tag; kanMX6; Amp^R
pYM19	9myc; His3MX6
pYM20	9myc; hph; Amp^R

5.1.2 *E. coli* strains

DH5α E. coli strain was used for amplification of plasmid DNA. The genotype of the strain is: DH5α supE44 lacU169 (φ80lacZM15) hsdR17 recA1 endA1 gyrA96 thi1 relA1.

For the recombinant expression of the budding yeast genes, the Rosetta pLysS strain was used. The strain genotype is: F- ompT hsdSB(RB- mB-) gal dcm λ(DE3 [lacI lacUV5-T7 gene 1 ind1 sam7 nin5]) pLysSRARE (CamR).
Both strains were typically grown with shaking (180-220 rpm) at 37°C. During protein expressions, the Rosetta pLysS strain were grown at different temperatures after the protein inductions depending on the proteins stability and solubility.

5.1.3 *S. cerevisiae* strains

All strains used in this work were derived from either YPH499 or W303.

Strain	Relevant genotype
CJY15-1	*MATa DSN1-3myc::kanMX6*
YAS1311	*MATa AME1-TAP::klTRP1*
YJL132	*MATa okp1::TRP1+ pJL467*
YJL153	*MATa mcm21::TRP1, ctf19::HIS3*
YJP406	*MATa OKP1-TAP::klTRP1*
YMK1515	*MATa OKP1-TAP::klTRP1 arg4::loxP bar1::loxP*
YMK1540	*MATa mcm21::TRP1 ctf19::His3 arg4::loxP OKP1-TAP::klURA3*
YMS231	*MATa sst1::loxP*
YMS242	*MATa ndc10-1 NNF1-6HA::klTRP1*

5.1.4 Oligonucleotides

All oligonucleotide sequences are in 5`to 3`direction.

Name	Sequence
179-4	ACTCGAGCTAGTGTATATCTTCTTCGGT
179-17	ACTCGAGCTGCAGCTAGTTTGTTTTTAAATTCATGCACAAC
179-39	TCAACGACGGGGTGCGTTC
179-46	TAGTGCTAGGCGCGCCGTATGGCAGCTGA
179-47	CTGAAACAATGGCGGCCGCCTAGTGTATATC
179-48	TAGTGCTAGGTACCGCATGGCAGCTGA
179-49	TGGCAGCTGATAGAGATAATTTTTTAC
179-50	CTAGTGTATATCTTCTTCGGTCTTATC
179-51	ATTTGAGCTCTTAACTTTAAGAAGGAGATATACATATGGGAAGCGCAACAAGTGGAG
179-52	TATATTGGTACCTAGTTTGTTTTTAAATTCATGCACAAC
179-53	ATTTGAGCTCTTAACTTTAAGAAGGAGATATACATATGGCAGCTGATAGAGATAA
179-54	CAATGGAGGTACCCTAGTGTATATCTTCTTCGGTCTTATC
179-55	CTTTTGGAGGAAACTAGGAAGTTGTGCATGAATTTAAAAACAAACGAAAAGAGAAG-ATGGAAAAA
179-56	CTCTCCAAGGTTTTCTGAGGCTCGTTGGCGGAGAAGTTACGTAACTTAGAAAAACTC-

	ATCGAGCA
179-57	CGCGAATCCGGACTACTTGTCATCGTCGTCCTTGTAGTCGTTTGTTTTTAAATTCATG
179-58	GCGAATCCGGACTACTTGTCATCGTCGTCCTTGTAGTCGTGTATATCTTCTTCGG
6His-Tag-1	TGGGCAGCAGCCATCACCATCATC
AME1-10	ATAAACATATGGATAGAGACACTAAATTAGC
AME1-11	ATATCTCGAGCTAAATCGATAGACTTGGTTGTAATTCGTTAGA
AME1-41	GAAAAACCTCACCATGGATAGAGACACTAAATTAGC
AME1-42	GAGCGGATCCGGATTCCCCTCTAGAA
AME1-44	CTTGTCGAGACGCGTCTATAGACTTGGT
AME1-45	GAAAAACCTCCATATGGATAGAGACAC
AME1-46	GAAAAACGTCGACATGGATAGAGACACTAAATTAGC
AME1-47	CTTTTGAAGCGGCCGCCTATAGACTTGGTTGTAATTCGTTAGA
CSE4-3	AAACTCGAGCTAAATAAACTGTCCCCTGA
CSE4-4	TATTCTCGAGATGTCAAGTAAACAACAATG
CSE4-5	CTTTGTTTTTGGATCCTTTACTGTCT
CTF19-1	AATCATATGGATTTTACGTCTGATAC
CTF19-2	ACTCGAGTCACCTGGCGTACATGTC
CTF19-8	GAACGCAACCATGGATTTTACG
CTF19-9	GGCAAATGGATCCTCACCTGGC
CTF19-10	CCCGGACATGTACGCCAGG
CTF19-11	CTGCAGAAACACGATGAATCC
CTF19-12	CGATGTGTCGTGCGAATTCGTC
DSN1-2H-1	GAAGCGTGATCAGTATGAGTCTGGAACCCACACAAACG
GST-3	GAGCGTGCAGAGATTTCAATGC
HPH-primer	GACCGATTCCTTGCGGTCCG
KAN&HIS	TGGGCCTCCATGTCGCTGG
MCM21-7	AACTGCAGCCATGGTGCCAGGAGCGTTACTGATAGTTTG
MCM21-8	GTAACGCTCGAATTCCATGAGTAGAATCGATGATTTAC
MCM21-9	ATTTTTGTAAGCTTTCACTTGAATATTGTCGCG
MCM21-10	GTAACGCTCCCATGGATGAGTAGAATCGATGATT
MCM21-11	TTGTTACCATGGACTTGAATATTGTCGCG
MCM21-12	TGATAAACCCATGGGTAGAATCGATGATT
MIF2-3	GGAAAGCTTTTCACTCATGGATTATATGAAATTG
MIF2-4	CACATCACTGCAGCCCAAAAGTGTCAAACG
MTW1-5	CAAAACACATATGTCTGCTCCCACTATGA
MTW1-6	CCACGGATCCTTATAACACATCATCAAGTA
NKP1-1	TGTAGGAGATCTATGACAGACACATATAATAGC
NKP1-2	TAATTGAAAGGTACCTTACTTCTTTAACTC
NKP1-3	TGTAGGAGATCTTATGACAGACACATATAATAGC
NKP1-4	GGAGATATACATATGACAGACACATATAATAGC
NKP2-1	ATTACCACCATGGAGAACTCTGAACAGCTG
NKP2-2	CGGGATGTCGGATCCTAGTTTTCCTC
NNF1-2H-1	GCGGGATCCGTATGGTTAACTCACATGGAATACGG
NSL1-6	ATAAACATATGTCACAAGGTCAGTCCAAAAAA
NSL1-7	ATATGGATCCTCAATCCTCCTCCAGGAAGTCC
pBS1479-1	ATATGGTACCTCAGGTTGACTTCCC
pET-1	GGAGATATACATGTGGGCAGCAGCC
pUC-primer	TCACACAGGAAACAGCTATGAC
S1	CGTACGCTGCAGGTCGAC
S2	ATCGATGAATTCGAGCTCG
S3	CGTACGCTGCAGGTCGAC
S4	CATCGATGAATTCTCTGTCG
SCM3-1	CTACAAATTAACAGAAGG
SCM3-S2	TTCTGATGGTAATGAAATTCGAATATACGGCATTTTAGCACCTTAATCGATGAATTC-GAGCTCG
SCM3-3	TTCAAGAAGTACGAGGCCAAACTCTCGAAAAGGATATTACGAGATCGTACGCTGCAG-GTCGAC
SP6-Promoter	TATTTAGGTGACACTATAG
T7-Promoter	TAATACGACTCACTATAGGG
T7-Terminator	GCTAGTTATTGCTCAGCGG

TAP-fw	TCCATGGAAAAGAGAAG
TAP-rev	TACGACTCACTATAGGG
TAP-universal	TATCAAGCTTCAGGTTGACTTCCCCGCCTAATTCGCGTCTAC
Trp-primer	GCTATTCATCCAGCAGGCCTC

5.2 Standard media and culturing conditions

E. coli strains were grown in LB liquid medium or plates at 37°C with addition of appropriate antibiotics.

LB:
5 g/l Yeast extract
10 g/l Tryptone
10 g/l NaCl
pH 7,0

SOB:
20 g/l Tryptone
5 g/l Yeast extract
0.5 g/l NaCl
25 mM KCl
10 mM $MgCl_2$
pH 7,0

Solid media contained 2% (w/v) agar.

Final concentration of antibiotics: Ampicillin or carbencillin=100 µg/ml
Kanamycin=30 µg/ml
Chloramphenicol= 34 µg/ml

S. cerevisiae strains were grown in YPD medium at 25°C. All plates contained 2% (w/v) agar.

YPD:
10 g/l Yeast extract
20 g/l Peptone from casein
20 g/l Glucose

SD (synthetic dropout):
6.7 g/l Yeast Nitrogen Base w/o amino acids
20 g/l Glucose
0.8 g/l Complete Supplement Mixture –Ade/His/Trp/Leu/Ura
Amino acids supplement[1] final concentration:
Adenine 30 mg/l
Histidine 20 mg/l
Leucine 20 mg/l
Tryptophan 30 mg/l
Uracil 20 mg/l

[1]For SD-Ura: no addition of Uracil.

YPD plates with gentamicin: YPD plates with the addition of 200 mg/l G418.

For FOA: SD plates containing all amino acids and 0.1% 5´-FOA.

5.3 Chemicals, enzymes, antibodies and other materials

Company	Products
AppliChem	β-mercaptoethanol, Adenin sulphate, Ammonium persulfate, Bromphenol blue, DTT, EDTA, Formaldehyde, Glycin, Pepton, Potassium chloride, Saccharose, Sodium dihydrogen phosphatate, Sodium hydroxide, TCA, TEMED, Tween 20, Uracil, MeOH, NP40
Baker	Ethanol, Isopropanol, Methanol
Becton Dickinson	Bacto Yeast Extract, Tryptone, Yeast Nitrogen base aminoacids
Bio 101	Complete Supplement Mixtures
Biocat	Phusion High-Fidelity DNA Polymerase
Bio-Rad	PolyPrep Chromatography Columns, Protein standards
Boehringer	Enzymes
Braun	Glass beads (Ø 0,45-0,5 mm)
Fermentas	DNA ladders, dNTPs, Enzymes
Fluca	Diethanolamine, Lithiumacetate
GE Healthcare	HiLoad Supedex 200 16/60, HisTrap HP columns, PD-10 Desalting columns, LMW protein calibration kit, Superose 6 10/300 GL
Hartmann Analytic	^{35}S-Methionine
Invitrogen	4-12% NuPAGE gradient gels, Alexa Fluor 680 goat anti-rabbit IgG, TEV-protease
Kodak	X-OMAT AR and X-ray films
LGC-Genomics (AGOWA)	Sequencing
Merck	Ethanol, Magnesium chloride hexahydrate, Potassium hydrogen phosphate, Triton X-100
Millipore	Centricons, Chemiluminiscent HRP substrate, PVDF blotting membranes, Sterile filtering devices
Molekula	SDS
NEB	Restriction enzymes
Peqlab Biotechnologie	IPTG
Pineda	Custom-ordered antibodies: anti-Ame1, anti-Cse4, anti-Ctf19, anti-Mcm21, anti-Mtw1, anti-Nsl1, anti-Okp1
Promega	Magnetic agarose beads, Proteinase K, TNT® Quick Coupled Transcription/ Translation System
Qiagen	GST-resins, Magnetic agarose beads, NTA-agarose beads, QiaexII glass milk for DNA isolation from agarose gels, Qiagen Plasmid Mini Kit
Roche	CDP-Star, Expand PCR Kit
Roth	Agarose, Colloidal Coomassie, EDTA, Glycine, HEPES, Lactose, Phenol, Sorbitol, Tris
Schleicher and Schuell	Blotting paper
Serva	Coomassie Brilliant Blue G250 and R250, MOPS, PEG 8000, TCA, Tween 20
Sigma	Anti-FLAG, anti-HA, anti-mouse, anti-myc, anti-rabbit, Casein from bovine milk, Human IgG Agarose, Lithium acetate, Ethidium bromide
Thermo Scientific	Oligonucleotides
VWR	Acetic acid, Sodium chloride, Potassium acetate

5.4. Equipment

Company	Products
Beckman	Centrifuges, Rotors 50.2Ti and TLA-45
Binder	Incubators for plates
Biometra	Power supplies
Bio-Rad	Blotting apparatus, Gel dryer, Power supplies
Biosciences	Li-COR Odyssey system
DynaPro	DLS instrument
Branson	Sonifier B15
Eppendorf	Heating blocks, Table top centrifuges
Fritsch	Pulverissette 6
Heraeus	Incubators for plates
Infors	Incubators for liquid cultures
Labnet	Agarose gel electrophoresis system
Lauda	Waterbath
Liebherr	Freezer -20°C, Refrigerator
Merck	Ultrasound waterbath
Microfluidics	Microfluidiser for *E. coli* cell lysis
Millipore	Water deionising facility, MilliQ Plus
Pharmacia	Size exclusion chromatography system
Sorvall	Centrifuges, Rotors SS-34, SLC-4000, SLC-6000 and H-12000
Techne	PCR machines, Heating blocks
Thermo Electron	Freezer -80°C, Photometer
Zeiss	Light microscope

5.5 Molecular biology techniques

5.5.1 Polymerase chain reaction (PCR)

For genomic tagging of yeast genes or gene deletion, Expand long template Taq Polymerase or Phusion High Fidelity Polymerase were used for amplifications.

A 50 µl reaction contained:	Program:
1 x PCR buffer	initial denaturation: 94°C 3 min
1 µM primers	
0,5 mM dNTPs	denaturing: 94°C 20 sec annealing: Tm 45 sec extension: 68°C 2,5 min } x 10
500 ng plasmid DNA	
1,5U Expand Polymerase	denaturing: 94°C 20 sec annealing: Tm 45 sec extension: 68°C 2,5min +20 sec/cycle } x 20
	final extension: 68°C 7 min

A 50 µl reaction contained:	Program:
1 x Phusion HF buffer	initial denaturation: 98°C 3 min
0,5 µM primers	
200 µM dNTPs	denaturing: 98°C 20 sec annealing: Tm 30 sec extension: 72°C 30 sec/ kb } x 30-35
100 ng plasmid DNA	
1U Phusion Polymerase	final extension: 72°C 7 min

The melting temperature of primers was calculated:

Tm= (4°C x (number of G`s and C`s in the primer) + 2°C x (number of A´s and T`s)) +/- 5°C

For Colony PCR, a homemade Taq polymerase was used with the following set-up:

A 50 µl reaction contained:	Program:
1 x PCR buffer	initial denaturation: 95°C 3 min
1 µM primers	
200 µM dNTPs	denaturing: 94°C 30 sec annealing: Tm 45 sec extension: 72°C 1 min/ kb } x 30
2-3 µl DNA-template	
3U Taq Polymerase	final extension: 72°C 5 min

One *E.coli* clone was resuspended in 25 µl water and boiled at 95°C for 5 min. After cooling on ice, 5 µl were used as a template in a 50 µl PCR reaction.

Further, in order to remove dNTPs and oligonucleotides, DNA was precipitated using NH_4OAc/isopropanol prior cloning into the appropriate vector. After adding one volume

of isopropanol, the sample was incubated at room temperature for 15 min and then pelleted at 14000 rpm at room temperature for 20 min.
Since ammonium ions inhibit polynucleotide kinase (PNK), in these cases the DNA was precipitated using LiCl/EtOH (described in details in further text).

5.5.2 Treatment with restriction endonucleases

Each standard DNA digestion was performed as described in the data sheets of the respective restriction enzyme. Usually, 1-10 µg of DNA was digested using 1-10 U of enzyme in a volume of 10-50 µl and incubated for 1-2 hours at the temperature given in the respective data sheet. The resulting fragments were analyzed on 0.7-3% agarose gels.

5.5.3 Agarose gel electrophoresis

DNA fragments were separated on 0.7-3% agarose gels, depending on the size of the DNA, after the 6x loading dye and 0,5 µg/ml ethidium bromide were added to the samples. Running buffer was 1xTAE.

TAE buffer:	242 g/l Tris	6x loading dye:	0.25% Bromphenol blue
	57.1 ml/l acetic acid		0.25% Xylene cyanol
	100 ml/l 0.5 M EDTA		30% Glycerol
	pH 7,2		

The resulting bands were detected by UV light at 254nm.

5.5.4 Extraction of DNA from agarose gels

All DNA fragments were isolated from agarose gels using the QIAEX II gel extraction kit from Qiagen according to the manufacturer's protocol.

5.5.5 Klenow reaction

Klenow polymerase was used for the removal of 3´protruding ends. The reaction was performed in the presence of 200 µM dNTPs in klenow buffer with 10 U/µg DNA. After incubation at 37°C for 10 min the enzyme was heat inactivated for 10 min at 70°C.

5.5.6 PNK treatment of DNA

T4 Polynucleotide kinase (PNK) was most commonly used for 5`-phosphorilation of PCR products prior to ligation. 1 U PNK was used for 1 µg DNA. The reaction was supplemented with 1.5 mM ATP and performed at 37°C for 1 h. After heat inactivation of the PNK at 65°C for 10 min, the phosphorylated PCR-product was ligated to an alkaline phosphatase treated vector.

5.5.7 T4 DNA Polymerase reaction

T4 polymerase was used for the removal of 3´ protruding ends or 5`overhangs fill in. The reaction was performed in the presence of 0.5 mM dNTPs in T4 DNA polymerase buffer with 4 U/µg DNA. After incubation at 12°C for 15 min, the enzyme was heat inactivated for 10 min at 75°C.

5.5.8 Treatment with Calf Intestinal Alkaline Phosphatase (CIAP)

In order to prevent re-ligation, linearized vectors were treated with calf intestinal alkaline phosphatase (CIAP) for dephosphorylation of 5`-ends. 1 U of CIAP was added to 5 µg DNA in a 50 µl reaction volume. The reaction was incubated for 1 h at 37°C for 5`-overhands or at 50°C for 3`-overhangs, and subsequently heat inactivated at 85°C for 15 min. Also, to ensure complete removal of CIAP from the probe, DNA agarose gel extraction was commonly performed.

5.5.9 Phenol/Chloroform extraction

In order to remove proteins from DNA, the sample was mixed with 1 volume of pre-equilibrated phenol (phenol:chloroform:isoamylalcohol 25:24:1), vortexed for 1 min and centrifuged for 5 min at 14 krpm. The aqueous phase was removed, re-extracted with 1 volume of chloroform and EtOH precipitated.

5.5.10 DNA Precipitation

LiCl/EtOH Precipitation:

1/10 volume of 10 M LiCl and 2,5 volumes of ice cold EtOH (100%) were added to the sample, incubated for 30 min at –20°C and centrifuged for 30 min at 4°C and 14 Krpm. The pellet was washed with 70% EtOH, dried and resuspended in TE or H_2O.

NH_4Ac/Isopropanol Precipitation:

1/10 volume of 10 M NH4Ac and 1 volume of isopropanol were added to the sample, incubated for 30 min at room temperature and centrifuged for 30 min at RT and 14000 rpm. The pellet was washed with 70% EtOH, dried and resuspended in TE or H_2O. This precipitation was used for the removal of oligonucleotides from PCR reactions.

5.5.11 Plasmid isolations from *E. coli*

Plasmid DNA for restriction analysis, cloning and transformation of *S. cerevisiae* was isolated by the alkaline lysis method (Sambrook et al. 2001). 3 ml overnight culture in was centrifuged at 4°C for 5 min (at 4000 rpm). The cell pellet was resuspended in 300 µl cold solution P1 (resuspension buffer) in presence of 0,1 mg/ml RNaseA. Lysis was performed with 300 µl solution P2 (lysis buffer) at RT for 4 min. Neutralisation was achieved by adding 300 µl solution P3 (neutralisation buffer), incubation on ice for 10 min and centrifugation at 4°C for 15-20 min at 14000 rpm. The supernatant was precipitated by the addition of 0,7 volumes isopropanol for 10 min at RT and centrifuged

for 20 min (14000 rpm). The DNA-pellet was washed with 70% EtOH, air dried and resuspended in 20-30 µl TE.

P1:	50 mM Tris-HCl pH 8,0 10 mM EDTA	P2:	0,2 N NaOH 1% SDS
P3:	2,8 M Kac pH 5,1 1 mM EDTA pH 8,0	TE:	10 mM Tris-HCl pH 8,0

5.5.12 Ligation

Ligations were performed using 100 ng of vector DNA and 2 Weiss units DNA ligase in a 10 µl reaction volume. The molar ratio of vector to insert was 1:3 for sticky-end ligations and 1:1 for blunt-end ligations. Insert and vector mixtures were incubated at 42°C for 3 min and then cooled on ice prior the ligase addition. The reaction mixture was incubated at RT at least 2 hours or overnight. DNA ligase was subsequently heat inactivated at 65°C for 20 min.

5.5.13 Chemical competent cells (according to Hanahan, 1983)

DH5α cells were inoculated in 50 ml SOB/10 mM $MgCl_2$ from a 5 ml-overnight culture. The main culture was incubated at 37°C (shaking at 180 rpm) and harvested at an OD_{578} of 0,3-0,4 (10 min at 4°C; 4000 rpm). The pellet was resuspended in 15 ml ice-cold Tbf1 Buffer and incubated on ice for 10 min. If Rosetta competent cells were made, the incubation period was prolonged to 90 min. After another centrifugation step at 4°C for 10 min (2000 rpm), the pellet was carefully resuspended in 1,8 ml ice-cold Tbf2 Buffer. 60 µl-aliquots were frozen in liquid nitrogen and stored at –80°C.

Tbf1:	30 mM KAc, pH 5,8 50 mM $MgCl_2$ 100 mM KCl 15% Glycerol	Tbf2:	10 mM MOPS/NaOH, pH 7,0 75 mM $CaCl_2$ 10 mM KCl 15% Glycerol

5.5.14 Transformation of *E. coli*

3-5 µl inactivated ligation reaction (out of 10 µl) were added to 60 µl thawed competent cells and incubated on ice for 30 min. The cells were heat shocked in a water bath for 60-90 sec at 42°C and subsequently cooled on ice for 5 min. 600 µl SOC was added and the transformation reaction was incubated for 1 h at 37°C under vigorous shaking (180 rpm) to allow recovery. 50 µl and 200 µl were plated out on appropriate plates and incubated at 37°C overnight.

SOB: 5 g/l Yeast extract
20 g/l Tryptone
0.5 g/l NaCl
10 ml/l 250 mM KCl
5 ml/L $MgCl_2$
pH 7,0

SOC: SOB supplemented with 4% Glucose

5.5.15 *E. coli* glycerol stocks

850 µl of an overnight *E. coli* culture was resuspended with 150 µl 99% sterile glycerol, vortex and frozen in liquid nitrogen. Stocks were stored at -80°C.

5.6 Cellular biology techniques

5.6.1 Yeast transformation

Method used in this study was adapted from Schiestl and Gietz, 1989. 50 ng plasmid DNA or 1-2 µg of PCR fragments were used for transformation of yeast cells. 50 ml of a logarithmically growing culture were harvested at room temperature for 3 min (3200 rpm) when OD_{578}=0,4-1. The pellet was washed first with 1 volume of autoclaved water and then with 2 ml of LiSorb. The pellet was resuspended in LiSorb to achieve 10 µl/OD. Cells were competent at that time and strictly kept on ice.
In a sterile 2 ml-eppendorf were added: 100 µl of yeast competent cells, the DNA (either plasmid or PCR product), 20 µg single stranded carrier DNA and 600 µl LiPEG. After vortexing and shaking at RT for 30 min (1500 rpm) and the addition of 70 µl DMSO, the

cells were heat shocked for 15 min at 37°C in a water bath. Cells were washed with rich YPD+2 media, recovered by shaking (180 rpm) at 25°C for at least 2 hours to increase the transformation efficiency and plated on selective plates and incubated at 25°C for 2-4 days. Correct integration or tagging was verified by colony PCR or Western blotting.

LiSorb: 100 mM LiOAc
10 mM Tris/HCl pH 8,0
1 mM EDTA pH 8,0
1 M Sorbitol

LiPEG: 100 mM LiOAc
10 mM Tris/HCl pH 8,0
1 mM EDTA pH 8,0
45% PEG 4000

5.6.2 Yeast strain construction

In this work new yeast strains were made by epitope tagging of endogenous yeast genes according to Knop, Siegers et al. 1999. Integration cassettes were amplified by PCR with oligonucleotides containing an additional 50 bp adapter sequence required for genomic integration. Most of the used were introduced at the C-terminus of the respective gene. PCR reactions and yeast transformations were performed as previously described. Integrations were verified by colony PCR or Western blotting.

5.6.3 Yeast genomic DNA extraction and colony PCR

One yeast clone from a plate was resuspended in 50 µl NTES Buffer with addition of 0,1 mg/ml RNaseA. After adding 1 volume of phenol, the sample was vortexed for 1 min. Glass beads were added in order to disrupt the cell walls and samples were shacked (2000 rpm) at 4°C for 30-45 min. A phenol/chlorophorm extraction was performed; sample was centrifuged at room temperature (14000 rpm) for 20 min. Approx. 20 µl of aqueous phase was mixed with 0,7 volumes of chlorophorm in a fresh tube. After vortexing the sample for more at least 1 min, the sample was centrifuged again and 5-10 µl of aqueous phase was transferred into a new tube. 0,5 µl of aqueous phase was finally used as template for the colony PCR.

NTES buffer: 10 mM Tris/HCl pH 8,0
100 mM NaCl
1 mM EDTA pH 8,0
1% SDS

5.6.4 Yeast glycerol stocks

The respective strain was grown on a non-selective plate at the desired temperature, usually 25°C. The cells were then scraped off the plate and resuspended in 1 ml of 15% sterile glycerol, shock frozen in liquid nitrogen and finally stored at –80°C.

5.6.5 Dot spots for growth analysis

1 OD_{578} of logarithmically growing cells was harvested at room temperature (3200 rpm for 3 min) and resuspended in 1 ml of media. Four successive 1:10 dilutions were prepared and 4 µl of each dilution was spotted onto plates which were incubated at 25°C. For the growth analysis on SDC + 5'-FOA plates, strains were grown in the logarithmic phase for 2 days in uracil containing media to eliminate the selection pressure for the URA3-plasmid.

5.7 Biochemical techniques

5.7.1 Yeast protein extracts

10-20 OD_{578} were harvested at 4°C for 3 min at 3000 rpm and washed with 1 ml ESB buffer. The pellet was resuspended in ESB-buffer containing 6,5 mM DTT at a concentration of 2 µl/OD and heated at 95°C for 3 min to denature the proteins and inactivate proteases and phosphatases. In order to lyse the cells, glass beads were added to the meniscus and shaked at 4°C for approx. 1 h (2000 rpm). After cell lysis, the tube was punctured with a hot needle and placed on top of a 15 ml falcon. A centrifugation step for 5 min at 2300 rpm and 4°C followed. The lysate was transferred to a new 1.5 ml tube and the protein concentration was determined with the Bradford assay.

ESB buffer: 80 mM Tris/HCl pH6,8
2% SDS
10% Glycerol

5.7.2 Bradford assay

To determine a total protein concentration in samples, a method of Bradford (1976) was used. To 1 µl sample and 99 µl of water, 900 µl of Bradford solution was added and incubated for 5 min at RT. The absorption of the sample was measured at 595 nm. To determine the concentration of the sample a standard curve with rabbit IgG ranging from 0 – 25 mg/ml was used.

5 x Bradford solution: 500 mg/l Coomassies Brilliant Blue G250
250 ml/l ethanol
500 ml/l H_3PO_4

5.7.3 SDS-PAGE

SDS polyacrylamide gel electrophoresis (Laemmli 1970) was performed in order to separate proteins according to their molecular weight. 8-15% SDS-polyacrylamide gels were used depending on the size of the analyzed proteins. Protein samples were mixed with an equal volume of 2xSPB and denatured at 95°C for 5 min prior SDS gel loading.
A voltage of 135-200V was applied until the bromphenol band was electrophoresed out.

2xSPB: 6,2 mM Tris/HCl pH 6,8
715 mM β-mercaptoethanol
20% glycerol
0,0025% bromphenol blue

Running buffer: 3 g/l Tris Base
14,2 g/l Glycin
1 g/l SDS

5.7.4 Western blot analysis

Proteins that were separated on a SDS polyacrylamid gel were transferred onto a PVDF membrane applying the semi-dry method of Kyshe-Andersen (1984). The transfer took place at 15 V for 1 h. The membrane was blocked against a non-specific protein binding at RT for 1 h with blocking buffer and incubated 1 h with the primary antibody. After 3 washes with blocking buffer for 10 min to remove unbound primary antibody, the secondary antibody was applied for another hour. The membrane was washed again 3

times for 10 min with blocking buffer and prepared for the visualization of the formed antibody complexes.

If the chemiluminiscent system was used, 1,5 ml of HRP substrate was used to cover the membrane and after 5 min of incubation, the chemoluminescence could be detected on a X-ray film.

If the Odyssey system (Li-COR) was used, after the first antibody incubation membrane was only washed with 1xPBS buffer/0,1% Tween 20. The secondary antibody contained fluorescent dye which could be easily detected by infrared imaging system.

After the Western Blot, the PVDF-membrane was stained 3 min with PVDF-Coomassie and subsequently distained for a Western blot control.

Antibody used in this work:

Primary antibodies:	anti HA 1:1000 anti myc 1: 1000 anti FLAG 1:10000 anti ProteinA 1:40000 anti Ame1 1:4000 anti Okp1 1:5000 anti Ctf19 1:10000 anti Mcm21 1:10000 anti Mtw1 1:5000 anti Nsl1 1:10000 anti Cse4 1:4000	Secondary antibodies:	anti mouse 1:10000 anti mouse Alexia 1:10000 anti rabbit 1:10000 anti rabbit Alexia 1:10000

Blotting buffer:	5,8 g/l Tris Base 2,9 g/l Glycin 0,38 g/l SDS	PBS:	10,3 g/l Na_2HPO_4 x $2H_2O$ 2,35 g/l NaH_2PO_4 x H_2O 4 g/l NaCl pH 7,4
Blocking buffer:	0,2% Casein 0,1% Tweeen-20 in 1 x PBS	PVDF Coomassie:	0,2% Coomassie Blue R250 10% glacial acetic acid 50% Methanol
		PVDF Destain:	10% glacial acetic acid 50% Methanol

5.7.5 Coomassie-staining of SDS-PAGE gels

To visualize proteins on SDS-PAGE, gels were usually stained with Coomassie staining as described in Cooper et al (1981). Staining was typically done for 20 min and destaining for 30-40 min. If the protein amounts were expected to be less than 50 ng proteins per

band, the Colloidal Coomassie solution Roti Blue was used. In these cases, staining were performed overnight and distaining with water until the protein bands were clear and background was negligible.

Coomassie stain for SDS-PAGE:	10% acetic acid 50% methanol 0,25% Coomassie Briliant Blue R-250	Destain for SDS-PAGE:	7% acetic acid 30% methanol
Coll.-Coomassie for SDS-PAGE:	0,02% CBB G-250 (5x Roti Blue) 5% aluminum sulfate-(14-18)-hydrate 10% ethanol 2% orthophosphoric acid		

5.8 Special methods

5.8.1 Expression of tagged-proteins from *E. coli*

For the recombinant expression of His_6-, His_{10}-tagged or TAP-tagged yeast proteins, T7-promoter plasmids, containing several important elements for rapid protein production upon its activation were used.

- The T7 Promoter is highly selective for the bacteriophage T7 RNA polymerase (not bacterial RNA polymerase). The gene of interest cannot be transcribed unless the T7 RNA polymerase is present. This is why in the pET system, gene for T7 RNA polymerase is inserted into the host chromosome (in this case Rosetta *E.coli* strain), under *lacUV5* control. When lactose, or a molecule similar to lactose, is present inside of the cell, expression is induced. Using the Rosetta expression strain provides additional stability of target genes containing a compatible chloramphenicol-resistant plasmid that provides a small amount of T7 lysozyme, which is a natural inhibitor of T7 RNA polymerase.
- *lac* operator sequence downstream of the T7 promoter is also present on the plasmid.
- Natural promoter and coding sequence for the *lac* repressor (*lacI*), is oriented so that the T7*lac* and *lacI* promoters diverge (Fig.5.1).

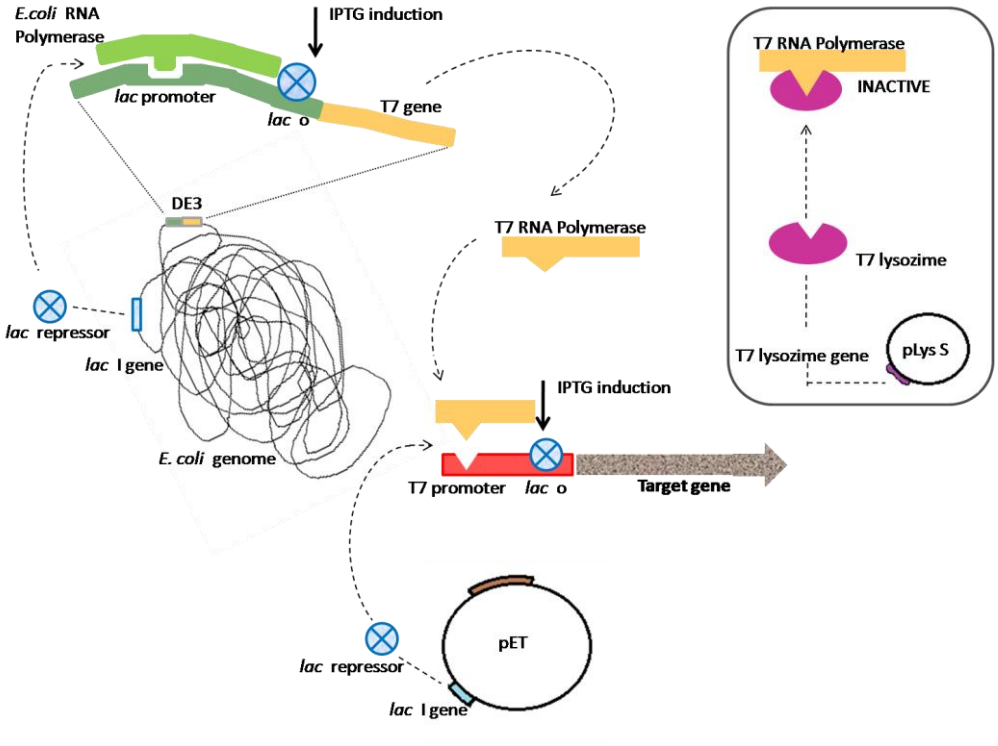

Fig.5.1 Regulation of protein expression in T7 promoter plasmids (adapted from Novagen pET System manual). See text for details.

When this type of vector is used, the *lac* repressor acts both at the lacUV5 promoter in the host chromosome (to repress transcription of the T7 RNA polymerase gene) and at the T7lac promoter in the pET vector to block transcription of the target gene by any T7 RNA polymerase that is made on the basal level. By isopropyl-β-D-thiogalactopyranoside (IPTG) the *lac* repressor is displaced from the *lac* operator since IPTG is an analogue of lactose (Blaber, 1998). Because there are *lac* operators on both the gene encoding T7 RNA polymerase and after the T7 promoter for the target gene, IPTG activates both genes. Therefore, when IPTG is added to a growing culture, the T7 RNA polymerase is first expressed, and then quickly begins to transcribe the gene of interest on the pET-plasmid.

The expression plasmids were transformed into chemically competent Rosetta pLysS *E.coli* strain. After transformation, 10 colonies were picked for each construct and grown as 50-100ml precultures at 37°C in LB medium with addition of appropriate antibiotics. Both precultures and 1-2L expression cultures were grown at 37°C under vigorous shaking until the induction.

For the Lactose induction, cells were grown to an OD_{578}/ml=0.1-0.2, cooled down to 30°C and induced with the 50mM Lactose overnight.

For the IPTG induction, cells were grown to an OD_{578}/ml=0.5-0.6, cooled down to 25°C and induced with the 0.5-1 mM IPTG for 3-6 hours or extremely overnight.
After expression cells were harvested at 4000 rpm for 25 min at 4°C, the cell pellet was resuspended in 50 ml PBS Buffer and transferred to a 50ml-falcon. Following one more round of centrifugation under the same condition, pelleted cells were flash frozen in liquid nitrogen and stored at -80°C until protein purification.

5.8.2 Purification of yeast proteins containing His-tag from *E. coli*

For His-tagged protein purifications, cell pellets were resuspended in 25 ml of either binding buffer A or B per liter of expression culture containing protease inhibitors and passed three times through an M1-10L Microfluidizer. The cell lysate was cleared of cell debris by centrifugation (11-14 000 rpm for 45 min at 4°C), passed through 0.22 µm filter and applied onto a 1ml HisTrap Chelating HP column (GE Healthcare) pre-equilibrated with lysis buffer. To remove non-specifically bounded proteins, two subsequent washing steps with 10 ml lysis buffer followed by 10 ml of washing buffer A or B were applied. Proteins were eluted from the column with the 5 x 1 ml elution buffer A or B.

Lysis buffer A:	20 mM HEPES pH 8.0 250 mM NaCl 10 mM $MgCl_2$ 40 mM imidazole 5 % (v/v) glycerol 0.1 % Triton X-100	Lysis buffer B:	50 mM Tris pH 7.5 100 mM NaCl 10 mM $MgCl_2$ 20 mM imidazole 5 % (v/v) glycerol 0.1 % Triton X-100 5 mM 2-mercaptoethanol
Washing buffer A:	20 mM HEPES pH 8.0 250 mM NaCl 10 mM $MgCl_2$ 60 mM imidazole	Washing buff. B:	50 mM Tris pH 7.5 150 mM NaCl 10 mM $MgCl_2$ 40 mM imidazole 5 % (v/v) glycerol 0.1 % Triton X-100 5 mM 2-mercaptoethanol
Elution buffer A:	20 mM HEPES pH 8.0 250 mM NaCl 10 mM $MgCl_2$ 400 mM imidazole	Elution buff. B:	50 mM Tris pH 7.5 100 mM NaCl 10 mM $MgCl_2$ 500 mM Imidazole 5 % (v/v) glycerol 0.1 % Triton X-100

5 mM 2-mercaptoethanol

Protease inhibitors: (Final conc.)
1 mM PMSF
1 mM 1,10- Phenantrolin
2 µg/ml Pepstatin A
5 µg/ml Leupeptin

Eluted proteins were analyzed on SDS-PAGE and then injected onto gel filtration columns HiLoad Supedex 200 16/60 or Superose 6 10/300 GL on FPLC (Fast Protein Liquid Chromatography, GE Healthcare) system, equilibrated with appropriate running buffers.

For subsequent GST-protein purification, His-purification eluates were used. The eluates were mixed with 1/10 volume of GST resins (50% suspension) and rotated at 4°C for 1-6 hours. After the beads were collected and spine down by short and mild centrifugation at 4°C (3 min at 2000 rpm), samples were washed three times with 3 volumes of 50mM Tris/HCl pH 8,0. Finally, the protein complexes were then eluted by short incubation (10-45 min) at 4°C with one volume of freshly made GST-elution buffer (50mM Tris/HCl pH 8,0 and 20mM Glutathione). Samples were analyzed mass spectrometry on colloidal coomassie-stained 4-12% NuPAGE gradient gels.

If TAP-purification was a second affinity purification step, imidazole-eluted proteins were used for the modified tandem affinity purification method. For this purposes, the first three imidazole-eluted fractions were combined and mixed with 1/10 volume of preequilibrated Human IgG agarose resins (50% slurry). Buffer was supplemented with 0,5 mM DTT and standard protease inhibitors (see text above). After 3-4 hours incubation at 4°C on a turning wheel, beads were collected into a chromatography column (BioRad) and washed with 10 ml of TAP-binding buffer and 0,5 ml of Washing buffer containing 5 mM NH_4OAc pH 5,0. For acid elution 5 x 1 ml 0,5 M NH_4OAc/0,5 M HAc pH 3,4 were used. The samples were vacuum-dried, resuspended in loading buffer and analyzed on colloidal coomassie-stained SDS-PAGE gel.

TAP-binding buffer:
20 mM HEPES pH 8,0
125 mM NaCl
5 mM $MgCl_2$
200 mM imidazole
0,5 mM DTT
5% (v/v) glycerol

5.8.3 Purification of TAP-tagged yeast proteins from *E. coli*

For the purification of the TAP-tagged proteins and their binding partners, the tandem affinity purification method was used. The TAP-tag contains ProteinA domain and a Calmoduline Binding Peptide (CBP) separated by a TEV cleavage site. After protein expression in *E. coli* collected cell pellets were resuspended in 25 ml of TAP-lysis buffer per liter of expression culture, containing protease inhibitors and passed three times through an M1-10L Microfluidizer. The cell lysate was cleared of cell debris by centrifugation (11-14 000 rpm for 45 min at 4°C), passed through a 0,22 µm filter and approximately 300 µl of pre-equilibrated Human IgG Agarose beads (50% slurry) were added. After 3-4 hours rotation at 4°C, beads were collected into a 10ml chromatography column (BioRad) and washed with 10 ml of TAP-lysis buffer without DTT. In order to provide efficient TEV-cleavage, beads were transferred into a 1 ml-Mobicol column (Mo Bi Tec) with 150 µl TAP-lysis buffer and TEV protease (2,5 U/ 1000 ODs) was added. The TEV cleavage reaction was performed on a turning weal at 16°C for 4 hours up to overnight.

The sample was eluted with a syringe into a new cup and analyzed on SDS-PAGE.

If a second purification step, the ion affinity purification step, was about to be completed, the eluted sample was diluted in 1 ml of final volume lysis buffer A and the purification was preceded as described.

TAP-Lysis buffer:	20 mM HEPES pH 8,0	Protease inhibitors:	1 mM PMSF
	100 mM NaCl	(Final conc.)	1 mM Phenantrolin
	10 mM $MgCl_2$		2 µg/ml Pepstatin A
	5 % (v/v) glycerol		5 µg/ml Leupeptin
	0,5 mM DTT		

5.8.4 Size exclusion chromatography (SEC)

Chromatography of different COMA subcomplexes was performed using either Superdex 200 16/60 or Superose 6 10/300 GL columns (GE Healthcare) on FPLC (Fast

Protein Liquid Chromatography, GE Healthcare) system. Protein elution was monitored with an ultraviolet absorbance detector at 280 nm, and fractions were collected throughout. All steps were carried out at 4°C. The calibration of columns with known protein standards provides the relationship between protein molecular weight and the retention volume. Protein standards included blue dextran (2,000 kDa), thyroglobulin (669 kDa), ferritin (450 kDa), β-amilase (200 kDa), aldolase (158 kDa), carbonic anhydrase (29 kDa) and cytochrome C (12, 4 kDa).

Various conditions:

S200 16/60 chromatography column:

1. TAP purified CM-complex

After TEV-elution sample was buffered to:

20 mM HEPES pH 8, 0
175 mM NaCl
10 mM $MgCl_2$
0, 2 mM DTT
5% (v/v) glycerol

The sample was filtered through 0,22 µl-filter and 500 µl was injected onto the column. Operated flow rate was 1 ml/min with a fraction size of 2 ml.

2. Ni-NTA purified AO- and CM-complexes

An eluted fraction containing most of the dimer was centrifuged at 20000 rmp for 30 min at 4°C and 1 ml was injected onto the column. Operated flow rate was 1 ml/min with a fraction size of 2 ml. In this case, composition of the running buffer was:

20 mM HEPES pH 8, 0
250 mM NaCl
10 mM $MgCl_2$
5% (v/v) glycerol

3. Ni- NTA purified CMO-trimeric complex

First 2,5 ml imidazole-eluted fraction was applied on PD-10 desalting column (GE Healthcare) and eluted in PD-10 buffer:

50 mM Tris pH 7, 5
100 mM NaCl
10 mM $MgCl_2$

5% (v/v) glycerol

The first three fractions contained almost all of the trimeric complexes and these fractions were then concentrated to around 500 µl with an Amicon Ultra Centrifugal filter device (MWCO=30 kDa, Millipore). The concentrated proteins were fist centrifuged at 20000 rmp for 30 min at 4°C and then 0, 5 ml was injected onto the column. The operated flow rate was 1 ml/min with a fraction size of 2 ml. In this case, composition of running buffer was the same as for the PD-10 chromatography.

Superose 6 10/300 chromatography column:

1. Ni-NTA purified CM-complex

Eluted fraction containing most of the dimer was centrifuged at 20000 rmp for 30 min at 4°C and 0,5 ml was injected onto the column. Operated flow rate was 0, 5 ml/min with a fraction size of 1 ml.

The running buffer contained:

50 mM Tris pH 7,5
100 mM NaCl
10 mM $MgCl_2$
5% (v/v) glycerol

2. Ni-NTA purified CMO-trimeric complex

First 2,5 ml imidazole-eluted fraction was applied on PD-10 desalting column (GE Healthcare) and eluted in PD-10 buffer:

50 mM Tris pH 7,5
100 mM NaCl
10 mM MgCl2
5% (v/v) glycerol
5 mM 2-β mercaptoethanol

The first three fractions contained almost all of the tetrameric complexes and these fractions were then concentrated to around 500 µl with an Amicon Ultra Centrifugal filter device (MWCO=30 kDa, Millipore). The concentrated proteins were fist centrifuged at 20000 rmp for 30 min at 4°C and then 200 µl was injected onto the column. Operated flow rate was 0,5 ml/min with a fraction size of 0,5 ml. In this case, composition of the running buffer was the same as for the PD-10 chromatography.

3. Ni-NTA purified COMANN-hexameric complex

Protein rich imidazole-eluted fraction was further analyzed by SEC directly after the Ni-NTA purification. 500µl of proteins were centrifuged at 4°C for 30 min (20000 rpm) prior injection onto the Superose 6 chromatography column. Operated flow rate was 0,5 ml/min with a collected fraction size of 1 ml. 35% of each collected fraction was further TCA precipitated and analyzed on colloidal coomassie-stained 4-12% Nu-PAGE gradient gel.

Chromatography running buffer composition: 50 mM Tris/HCl pH 8,0
100 mM NaCl
10 mM $MgCl_2$
5 mM 2-β mercaptoethanol

5.8.5 TCA protein precipitation

To precipitate proteins, Trichloroacetic acid (TCA) was added to the solution at a final concentration of 10-12%. Samples were firstly incubated at -20°C for 5 min, a then on ice for 30-60 min. If the protein concentration was low (< 50 ng/ml), the samples were preincubated on ice with Na-deoxycholate at a final concentration of 0.015% before TCA addition. After a centrifugation step at 4°C for 30 min (14000 rpm), the protein pellets were washed with four volumes of cold acetone and ten volumes of cold 100% ethanol by spinning them at 4°C for 15-20 min (14000 rpm). Dry sample pellets were resuspended in 1x sample buffer, neutralised with NH_3 if necessary, and analyzed on colloidal coomassie-stained gels.

5.8.6 Proteinase K treatment

Proteinase K is a serine protease that was used for general digestion of proteins in samples where the nucleic acid contamination was proved. Before protease digestion, proteins were denatured at 60°C for 15 min in presence of 5 mM DTT and 4 M Urea. After denaturation the reaction was cooled to RT and then shifted on ice where the

buffer composition was adjusted for Proteinase K digestion. The Proteinase K was added to the reaction to a final concentration of 100 µg/ml and incubated at 37°C for 1-2 hours. To terminate the reaction, 5 mM PMSF and 2 mM EGTA were added.

Proteinase K buffer:
50 mM Tris/HCl pH 7,5
10 mM $CaCl_2$
150 mM NaCl
2,5 mM $MgCl_2$
100 mM Imidazole
1,5 M Urea

5.8.7 Dynamic light scattering (DLS)

One of three methods to examine purified protein complex size and homogeneity was DSL (DynaPro, Protein Solutions). Aggregation of proteins was tested in buffer containing different salt concentrations:

20 mM HEPES pH 8.0
10 mM $MgCl_2$
5% Glycerol
150/200/300/500 mM NaCl

Prior to the measurements, sediment was removed by ultracentrifugation at 40 000 rpm for 30 min at 4°C (Rotor: TLA 45, Beckman). Measurements were performed at temperatures of 4°C and 20°C. Data processing was performed automatically by the software supplied with the instrument.

5.8.8 Limited proteolysis

Protein complex was treated with 1/20, 1/100 and 1/500 (w/w) ratio of Trypsin Gold to substrate in 50 mM Tris pH 7.5, 150mM NaCl, 10mM $MgCl_2$, 1mM $CaCl_2$ at 37°C. Aliquots were removed at the different time points within the 4 hours. Samples were boiled in the SDS-PAGE loading buffer, run on the 4-12% Nu-PAGE gradient gel and analyzed by MALDI-TOF.

5.8.9 Reticulocyte lysate binding assays

To produce ^{35}S-labeled proteins, the TNT Quick Coupled *in vitro* Transcription/ Translation System (Promega) was used. First, we cloned all yeast genes to be tested for the interactions with the COMA-proteins in plasmid containing SP6 promoter (pSP64 PolyA) using SmaI restriction site. These plasmids were purified using the Qiagen Mini Prep system and then were transcribed and translated *in vitro* for 90 minutes using the TNT SP6 Coupled Reticulocyte Lysate system (Promega, Madison, WI) in the presence of ^{35}S-labeled methionine.

One typical reaction assembled on ice in a 1,5ml-eppendorf:

TNT Quick Master Mix	40 µl
Plasmid DNA (0,5 µg/µl)	2 µl (= 1µg DNA)
^{35}S-Methionine (1,000Ci/mmol at 10mCi/ml)	2 µl
Nuclease-free H_2O	6 µl
	----------
	50 µl

2,5 µl of *in vitro* translated products were used as an input, to estimate the total amount of produced proteins. The rest of reactions were used for the pull down assays.

A) The affinity purification using the Ni-NTA magnetic agarose beads (Qiagen):

300µl binding reactions containing:	
^{35}S-labeled protein (prey); 30% of the input	22 µl
5% magnetic bead slurry coated with fusion proteins (bait)	200 µl
BSA (final conc. = 100 µg/ml)	30 µl
AEBSF (final conc. = 1mM)	3 µl
IP Buffer (20mM HEPES pH 8.0, 150mM NaCl, 10mM $MgCl_2$, 10mM Imidazole, 5% Glycerol)	45 µl
	----------
	300 µl

were set in 0,5 ml-eppendorfs and incubated for 3 h at 4°C with end-over-end tube rotation. The beads were then recovered by short centrifugation and using a magnetic separator. Samples were first washed three times with 500 µl of IP Buffer and then eluted by boiling the beads at 95°C for 5 min in SDS-SB. Finally, ^{35}S-labeled proteins were analyzed on SDS-PAGE by autoradiography.

B) The affinity purification using the human IgG agarose beads (Sigma):

The two compatible pET-vectors, pAS1113 and pAS1117, were co-transformed into *E.coli* and Ame1 His_6-Okp1 and Mcm21-TAP Ctf19 proteins were expressed (0,4mM IPTG induction at 28°C shaking 200 rpm overnight) in 2l culture. Cells were harvested by centrifugation (Rotor: H12000, Sorvall) at 4°C for 20 min. Before being resuspended in lysis/binding buffer (20mM HEPES pH 8,0, 100mM NaCl, 10mM $MgCl_2$, 5% Glycerol) with protease inhibitors (1mM PMSF, 1mM Phenanthroline, 5 µg/ml Leupeptin and 2 µg/ml Pepstatin A), cells were washed once with PBS. The cells were disrupted using a Microfluidizer. In 90ml of the crude lysate, 0,5mM DTT was added and centrifuged at 4°C for 30 min at 41 krpm (Rotor: Ti 50.2, Beckman). Clarified sample was transferred into two 50 ml falcon tubes and 300 µl (50% slurry) prepared Human IgG agarose was added to each tube. Samples were incubated on a rotor at 4°C with slow speed for 4 hours. The beads were washed with 15 ml of lysis buffer and transferred into small 1 ml Mobicol (Bio-Rad) columns. At this step, in each column the radioactively-labeled TnT-protein was added and incubated overnight at 4°C on a turning wheel. The beads were further washed extensively with lysis buffer supplemented with 0,5 mM DTT. The protein complex was cleaved of the beads by TEV cleavage at 16°C for 4 hours on a turning wheel. Samples were eluted with a syringe into a fresh tube and analyzed by autoradiography.

5.8.10 Purification of TAP-tagged yeast proteins from *S. cerevisiae* (Pull-down protocol)

For isolation of kinetochore complexes the tandem affinity purification method was adapted from Puig et al., 1999. For one TAP purification, 1-4 l of yeast culture (OD_{587} of 2) was harvested for 20 min at 4,5 krpm and 4°C. The pellet was washed with 50 ml of cold distilled water and 50 ml of lysis buffer. The pellet was resuspended in lysis buffer with protease inhibitors at an concentration of 150 OD/ml. Cells were lysed with glass beads at 4°C for 4 x 4 min (500 rpm) with 2 min pauses (in Pulverissette 6). The lysate was clarified twice at 11 krpm and 4°C for 30 min and preequilibrated Human IgG beads (10 µl of 50% slurry to 100 OD) and fresh 1 mM AEBSF were added. After a 3 h rotation at 4°C, the beads were collected in a chromatography column (Bio-Rad) and washed with 10 ml of W1 and W2 and 0,5 ml of W3 buffer respectively. Finally, the complex was acid eluted with 2 x 0,5 ml of 0,5 M NH4Ac/HAc, pH 3.4. The sample was vacuum dried,

resuspended in loading buffer and analyzed on colloidal coomassie-stained 4-12% Nu-PAGE.

Lysis buffer:
50 mM Tris/HCL pH 8,0
140 mM KCl
5 mM $MgCl_2$
10% glycerol
0,1% Triton X-100
0,05% NaDOC

Protease inhibitors:
(final concentration)
1 mM AEBSF
40 µg/ml TPCK
10 µg/ml Pepstatin
10 µg/ml Aprotinin
5 µg/ml Leupeptin
2 mM Benzamidine

W1 buffer:
Lysis buffer with 1 mM PMSF

W2 buffer:
10 mM Tris/HCl pH 8,0
250 mM LiCl
0,5% NaDOC
0,5% NP-40
1 mM EDTA
1 mM PMSF

W3 buffer:
5 mM NH_4OAc/HAc pH 5,0

Elution buffer:
0,5 M HAc
0,5 M NH_4OAc
pH 3,4

7.REFERENCES

Alushin, G. and E. Nogales (2011). "Visualizing kinetochore architecture." Curr Opin Struct Biol.

Amrein, H. (2000). "Multiple RNA-protein interactions in Drosophila dosage compensation." Genome Biol **1**(6): REVIEWS1030.

Asbury, C. L., D. R. Gestaut, et al. (2006). "The Dam1 kinetochore complex harnesses microtubule dynamics to produce force and movement." Proc Natl Acad Sci U S A **103**(26): 9873-9878.

Baker, R. E., M. Fitzgerald-Hayes, et al. (1989). "Purification of the yeast centromere binding protein CP1 and a mutational analysis of its binding site." J Biol Chem **264**(18): 10843-10850.

Barth, H. G. and B. E. Boyes (1992). "Size exclusion chromatography." Anal Chem **64**(12): 428R-442R.

Bellizzi, J. J., 3rd, P. K. Sorger, et al. (2007). "Crystal structure of the yeast inner kinetochore subunit Cep3p." Structure **15**(11): 1422-1430.

Blaber M. 1998 Spring. Web Page for Lecture 25 of Molecular Biology and Biotechnology Course: Prokaryotic Expression Vectors.

Borgstahl, G. E. O. "How to Use of Dynamic Light Scattering to Improve the Likelihood of Growing Macromolecular Crystals" Invited Chapter in Macromolecular Crystallography Protocols, **1** , 109-129, (2006).

Bouck, D. and K. Bloom (2005). "The role of centromere-binding factor 3 (CBF3) in spindle stability, cytokinesis, and kinetochore attachment." Biochem Cell Biol **83**(6): 696-702.

Brown, M. T., L. Goetsch, et al. (1993). "MIF2 is required for mitotic spindle integrity during anaphase spindle elongation in Saccharomyces cerevisiae." J Cell Biol **123**(2): 387-403.

Cai, M. J. and R. W. Davis (1989). "Purification of a yeast centromere-binding protein that is able to distinguish single base-pair mutations in its recognition site." Mol Cell Biol **9**(6): 2544-2550.

Camahort, R., B. Li, et al. (2007). "Scm3 is essential to recruit the histone h3 variant cse4 to centromeres and to maintain a functional kinetochore." Mol Cell **26**(6): 853-865.

"Centromere: structure and evolution" Editor Durdica Ugarkovic, Springer-Verlag Berlin Heidelberg (2009).

Chan, G. K., S. T. Liu, et al. (2005). "Kinetochore structure and function." Trends Cell Biol **15**(11): 589-598.

Cheeseman, I. M., S. Anderson, et al. (2002). "Phospho-regulation of kinetochore-microtubule attachments by the Aurora kinase Ipl1p." Cell **111**(2): 163-172.

Cheeseman, I. M., J. S. Chappie, et al. (2006). "The Conserved KMN Network Constitutes the Core Microtubule-Binding Site of the Kinetochore." Cell **127**(5): 983-997.

Cheeseman, I. M. and A. Desai (2008). "Molecular architecture of the kinetochore-microtubule interface." Nat Rev Mol Cell Biol **9**(1): 33-46.

Cheeseman, I. M., M. Enquist-Newman, et al. (2001). "Mitotic spindle integrity and kinetochore function linked by the Duo1p/Dam1p complex." J Cell Biol **152**(1): 197-212.

Cho, U. S., K. D. Corbett, et al. (2011). "Molecular Structures and Interactions in the Yeast Kinetochore." Cold Spring Harb Symp Quant Biol.

Ciferri, C., J. De Luca, et al. (2005). "Architecture of the human ndc80-hec1 complex, a critical constituent of the outer kinetochore." J Biol Chem **280**(32): 29088-29095.

Ciferri, C., S. Pasqualato, et al. (2008). "Implications for kinetochore-microtubule attachment from the structure of an engineered Ndc80 complex." Cell **133**(3): 427-439.
Clarke, L. and J. Carbon (1980). "Isolation of a yeast centromere and construction of functional small circular chromosomes." Nature **287**(5782): 504-509.
Cohen, R. L., C. W. Espelin, et al. (2008). "Structural and functional dissection of Mif2p, a conserved DNA-binding kinetochore protein." Mol Biol Cell **19**(10): 4480-4491.
Collins, K. A., A. R. Castillo, et al. (2005). "De novo kinetochore assembly requires the centromeric histone H3 variant." Mol Biol Cell **16**(12): 5649-5660.
Connelly, C. and P. Hieter (1996). "Budding yeast SKP1 encodes an evolutionarily conserved kinetochore protein required for cell cycle progression." Cell **86**(2): 275-285.
Cooper, T. G. (1981). "Yeast genetics and molecular biology." Nature **289**(5794): 119-120.
De Wulf, P., A. D. McAinsh, et al. (2003). "Hierarchical assembly of the budding yeast kinetochore from multiple subcomplexes." Genes Dev **17**(23): 2902-2921.
DeLuca, J. G., Y. Dong, et al. (2005). "Hec1 and nuf2 are core components of the kinetochore outer plate essential for organizing microtubule attachment sites." Mol Biol Cell **16**(2): 519-531.
DeLuca, J. G., W. E. Gall, et al. (2006). "Kinetochore microtubule dynamics and attachment stability are regulated by Hec1." Cell **127**(5): 969-982.
Doheny, K. F., P. K. Sorger, et al. (1993). "Identification of essential components of the S. cerevisiae kinetochore." Cell **73**(4): 761-774.
Espelin, C. W., K. B. Kaplan, et al. (1997). "Probing the architecture of a simple kinetochore using DNA-protein crosslinking." J Cell Biol **139**(6): 1383-1396.
Euskirchen, G. M. (2002). "Nnf1p, Dsn1p, Mtw1p, and Nsl1p: a new group of proteins important for chromosome segregation in Saccharomyces cerevisiae." Eukaryot Cell **1**(2): 229-240.
Fernius, J. and A. L. Marston (2009). "Establishment of cohesion at the pericentromere by the Ctf19 kinetochore subcomplex and the replication fork-associated factor, Csm3." PLoS Genet **5**(9): e1000629.
Fitzgerald-Hayes, M., L. Clarke, et al. (1982). "Nucleotide sequence comparisons and functional analysis of yeast centromere DNAs." Cell **29**(1): 235-244.
Fontana, A., P. P. de Laureto, et al. (2004). "Probing protein structure by limited proteolysis." Acta Biochim Pol **51**(2): 299-321.
Gardner, M. K., D. C. Bouck, et al. (2008). "Chromosome congression by Kinesin-5 motor-mediated disassembly of longer kinetochore microtubules." Cell **135**(5): 894-906.
Goh, P. Y. and J. V. Kilmartin (1993). "NDC10: a gene involved in chromosome segregation in Saccharomyces cerevisiae." J Cell Biol **121**(3): 503-512.
Goshima, G., S. Saitoh, et al. (1999). "Proper metaphase spindle length is determined by centromere proteins Mis12 and Mis6 required for faithful chromosome segregation." Genes Dev **13**(13): 1664-1677.
He, X., S. Asthana, et al. (2000). "Transient sister chromatid separation and elastic deformation of chromosomes during mitosis in budding yeast." Cell **101**(7): 763-775.
Hegemann, J. H. and U. N. Fleig (1993). "The centromere of budding yeast." Bioessays **15**(7): 451-460.
Hieter, P., D. Pridmore, et al. (1985). "Functional selection and analysis of yeast centromeric DNA." Cell **42**(3): 913-921.

Hornung, P., M. Maier, et al. (2010). "Molecular Architecture and Connectivity of the Budding Yeast Mtw1 Kinetochore Complex." J Mol Biol.
Hoyt, M. A. and J. R. Geiser (1996). "Genetic analysis of the mitotic spindle." Annu Rev Genet **30**: 7-33.
Janke, C., J. Ortiz, et al. (2001). "The budding yeast proteins Spc24p and Spc25p interact with Ndc80p and Nuf2p at the kinetochore and are important for kinetochore clustering and checkpoint control." EMBO J **20**(4): 777-791.
Janke, C., J. Ortiz, et al. (2002). "Four new subunits of the Dam1-Duo1 complex reveal novel functions in sister kinetochore biorientation." EMBO J **21**(1-2): 181-193.
Joglekar, A. P., D. C. Bouck, et al. (2006). "Molecular architecture of a kinetochore-microtubule attachment site." Nat Cell Biol **8**(6): 581-585.
Joglekar, A. P. and J. G. DeLuca (2009). "Chromosome segregation: Ndc80 can carry the load." Curr Biol **19**(10): R404-407.
Khmelinskii, A. and E. Schiebel (2008). "Assembling the spindle midzone in the right place at the right time." Cell Cycle **7**(3): 283-286.
Kiburz, B. M., D. B. Reynolds, et al. (2005). "The core centromere and Sgo1 establish a 50-kb cohesin-protected domain around centromeres during meiosis I." Genes Dev **19**(24): 3017-3030.
Kitagawa, K. and P. Hieter (2001). "Evolutionary conservation between budding yeast and human kinetochores." Nat Rev Mol Cell Biol **2**(9): 678-687.
Kitamura, E., K. Tanaka, et al. (2010). "Kinetochores generate microtubules with distal plus ends: their roles and limited lifetime in mitosis." Dev Cell **18**(2): 248-259.
Knockleby, J. and J. Vogel (2009). "The COMA complex is required for Sli15/INCENP-mediated correction of defective kinetochore attachments." Cell Cycle **8**(16): 2570-2577.
Knop, M., K. Siegers, et al. (1999). "Epitope tagging of yeast genes using a PCR-based strategy: more tags and improved practical routines." Yeast **15**(10B): 963-972.
Kotwaliwale, C. and S. Biggins (2006). "Microtubule capture: a concerted effort." Cell **127**(6): 1105-1108.
Lampert, F. and S. Westermann (2011). "A blueprint for kinetochores - new insights into the molecular mechanics of cell division." Nat Rev Mol Cell Biol **12**(7): 407-412.
Lechner, J. and J. Carbon (1991). "A 240 kd multisubunit protein complex, CBF3, is a major component of the budding yeast centromere." Cell **64**(4): 717-725.
Li, Y., J. Bachant, et al. (2002). "The mitotic spindle is required for loading of the DASH complex onto the kinetochore." Genes Dev **16**(2): 183-197.
Lin, H., P. de Carvalho, et al. (2001). "Polyploids require Bik1 for kinetochore-microtubule attachment." J Cell Biol **155**(7): 1173-1184.
Liu, D., G. Vader, et al. (2009). "Sensing chromosome bi-orientation by spatial separation of aurora B kinase from kinetochore substrates." Science **323**(5919): 1350-1353.
Lupas, A., M. Van Dyke, et al. (1991). "Predicting coiled coils from protein sequences." Science **252**(5009): 1162-1164.
Ma, L., J. McQueen, et al. (2007). "Spc24 and Stu2 promote spindle integrity when DNA replication is stalled." Mol Biol Cell **18**(8): 2805-2816.
Maison, C., D. Bailly, et al. (2002). "Higher-order structure in pericentric heterochromatin involves a distinct pattern of histone modification and an RNA component." Nat Genet **30**(3): 329-334.
Maskell, D. P., X. W. Hu, et al. (2010). "Molecular architecture and assembly of the yeast kinetochore MIND complex." J Cell Biol **190**(5): 823-834.

McEwen, B. F., A. B. Heagle, et al. (1997). "Kinetochore fiber maturation in PtK1 cells and its implications for the mechanisms of chromosome congression and anaphase onset." J Cell Biol **137**(7): 1567-1580.

McGrew, J., B. Diehl, et al. (1986). "Single base-pair mutations in centromere element III cause aberrant chromosome segregation in Saccharomyces cerevisiae." Mol Cell Biol **6**(2): 530-538.

Measday, V., D. W. Hailey, et al. (2002). "Ctf3p, the Mis6 budding yeast homolog, interacts with Mcm22p and Mcm16p at the yeast outer kinetochore." Genes Dev **16**(1): 101-113.

Meier, M., J. Stetefeld, et al. (2010). "The many types of interhelical ionic interactions in coiled coils - an overview." J Struct Biol **170**(2): 192-201.

Meluh, P. B., P. Yang, et al. (1998). "Cse4p is a component of the core centromere of Saccharomyces cerevisiae." Cell **94**(5): 607-613.

Menacho-Marquez, M. and J. R. Murguia (2007). "Yeast on drugs: Saccharomyces cerevisiae as a tool for anticancer drug research." Clin Transl Oncol **9**(4): 221-228.

Meraldi, P., A. D. McAinsh, et al. (2006). "Phylogenetic and structural analysis of centromeric DNA and kinetochore proteins." Genome Biol **7**(3): R23.

Mizuguchi, G., H. Xiao, et al. (2007). "Nonhistone Scm3 and histones CenH3-H4 assemble the core of centromere-specific nucleosomes." Cell **129**(6): 1153-1164.

Morgan, D.O. *"The cell cycle" Principles of control*; New Science Press. (2007)

Musacchio, A. and E. D. Salmon (2007). "The spindle-assembly checkpoint in space and time." Nat Rev Mol Cell Biol **8**(5): 379-393.

Nekrasov, V. S., M. A. Smith, et al. (2003). "Interactions between centromere complexes in Saccharomyces cerevisiae." Mol Biol Cell **14**(12): 4931-4946.

Ng, R. and J. Carbon (1987). "Mutational and in vitro protein-binding studies on centromere DNA from Saccharomyces cerevisiae." Mol Cell Biol **7**(12): 4522-4534.

Ohkuni, K., R. Abdulle, et al. (2008). "Ybp2 associates with the central kinetochore of Saccharomyces cerevisiae and mediates proper mitotic progression." PLoS One **3**(2): e1617.

Ortiz, J., C. Funk, et al. (2009). "Stu1 inversely regulates kinetochore capture and spindle stability." Genes Dev **23**(23): 2778-2791.

Ortiz, J., O. Stemmann, et al. (1999). "A putative protein complex consisting of Ctf19, Mcm21, and Okp1 represents a missing link in the budding yeast kinetochore." Genes Dev **13**(9): 1140-1155.

Peters, J. M., A. Tedeschi, et al. (2008). "The cohesin complex and its roles in chromosome biology." Genes Dev **22**(22): 3089-3114.

Peterson, J. B. and H. Ris (1976). "Electron-microscopic study of the spindle and chromosome movement in the yeast Saccharomyces cerevisiae." J Cell Sci **22**(2): 219-242.

Petrovic, A., S. Pasqualato, et al. (2010). "The MIS12 complex is a protein interaction hub for outer kinetochore assembly." J Cell Biol **190**(5): 835-852.

Pot, I., J. Knockleby, et al. (2005). "Spindle checkpoint maintenance requires Ame1 and Okp1." Cell Cycle **4**(10): 1448-1456.

Pot, I., V. Measday, et al. (2003). "Chl4p and iml3p are two new members of the budding yeast outer kinetochore." Mol Biol Cell **14**(2): 460-476.

Puig, O., F. Caspary, et al. (2001). "The tandem affinity purification (TAP) method: a general procedure of protein complex purification." Methods **24**(3): 218-229.

Reeves, R. and M. S. Nissen (1990). "The A.T-DNA-binding domain of mammalian high mobility group I chromosomal proteins. A novel peptide motif for recognizing DNA structure." J Biol Chem **265**(15): 8573-8582.

Ruchaud, S., M. Carmena, et al. (2007). "Chromosomal passengers: conducting cell division." Nat Rev Mol Cell Biol 8(10): 798-812.

Sambrook, J., Fritsch, E. F. and Maniatis, T. (2001). Molecular cloning - A laboratory manual (3rd edition). *Cold Spring Harbor Laboratory Press, Cold Spring Harbor, New York.*

Santaguida, S. and A. Musacchio (2009). "The life and miracles of kinetochores." EMBO J 28(17): 2511-2531.

Scharfenberger, M., J. Ortiz, et al. (2003). "Nsl1p is essential for the establishment of bipolarity and the localization of the Dam-Duo complex." EMBO J **22**(24): 6584-6597.

Schiestl, R. H. and Gietz, R. D. (1989). High efficiency transformation of intact yeast cells using single stranded nucleic acids as a carrier. *Curr Genet* 16, 339-46.

Schittenhelm, R. B., R. Chaleckis, et al. (2009). "Intrakinetochore localization and essential functional domains of Drosophila Spc105." EMBO J **28**(16): 2374-2386.

Shang, C., T. R. Hazbun, et al. (2003). "Kinetochore protein interactions and their regulation by the Aurora kinase Ipl1p." Mol Biol Cell **14**(8): 3342-3355.

Sigrist, C. J., L. Cerutti, et al. (2010). "PROSITE, a protein domain database for functional characterization and annotation." Nucleic Acids Res **38**(Database issue): D161-166.

Stemmann, O. and J. Lechner (1996). "The Saccharomyces cerevisiae kinetochore contains a cyclin-CDK complexing homologue, as identified by in vitro reconstitution." EMBO J **15**(14): 3611-3620.

Strunnikov, A. V., J. Kingsbury, et al. (1995). "CEP3 encodes a centromere protein of Saccharomyces cerevisiae." J Cell Biol **128**(5): 749-760.

Tan, S. (2001). "A modular polycistronic expression system for overexpressing protein complexes in Escherichia coli." Protein Expr Purif **21**(1): 224-234.

Tanaka, K., N. Mukae, et al. (2005). "Molecular mechanisms of kinetochore capture by spindle microtubules." Nature **434**(7036): 987-994.

Tanaka, T. U. (2005). "Chromosome bi-orientation on the mitotic spindle." Philos Trans R Soc Lond B Biol Sci **360**(1455): 581-589.

"The Kinetochore: from Molecular Discoveries to Cancer Therapy". Eds. De Wulf P., and Earnshaw W.C. Springer Publ., New York, (2008).

Tomkiel, J., C. A. Cooke, et al. (1994). "CENP-C is required for maintaining proper kinetochore size and for a timely transition to anaphase." J Cell Biol **125**(3): 531-545.

Topp, C. N., C. X. Zhong, et al. (2004). "Centromere-encoded RNAs are integral components of the maize kinetochore." Proc Natl Acad Sci U S A **101**(45): 15986-15991.

Wan, X., R. P. O'Quinn, et al. (2009). "Protein architecture of the human kinetochore microtubule attachment site." Cell **137**(4): 672-684.

Wei, R. R., P. K. Sorger, et al. (2005). "Molecular organization of the Ndc80 complex, an essential kinetochore component." Proc Natl Acad Sci U S A **102**(15): 5363-5367.

Welburn, J. P., E. L. Grishchuk, et al. (2009). "The human kinetochore Ska1 complex facilitates microtubule depolymerization-coupled motility." Dev Cell **16**(3): 374-385.

Westermann, S., I. M. Cheeseman, et al. (2003). "Architecture of the budding yeast kinetochore reveals a conserved molecular core." J Cell Biol **163**(2): 215-222.

Westermann, S., D. G. Drubin, et al. (2007). "Structures and functions of yeast kinetochore complexes." Annu Rev Biochem **76**: 563-591.

Wigge, P. A. and J. V. Kilmartin (2001). "The Ndc80p complex from Saccharomyces cerevisiae contains conserved centromere components and has a function in chromosome segregation." J Cell Biol **152**(2): 349-360.

Winey, M., C. L. Mamay, et al. (1995). "Three-dimensional ultrastructural analysis of the Saccharomyces cerevisiae mitotic spindle." J Cell Biol **129**(6): 1601-1615.

Wong, L. H., K. H. Brettingham-Moore, et al. (2007). "Centromere RNA is a key component for the assembly of nucleoproteins at the nucleolus and centromere." Genome Res **17**(8): 1146-1160.

Wutz, A. (2003). "RNAs templating chromatin structure for dosage compensation in animals." Bioessays **25**(5): 434-442.

Zappulla, D. C. and T. R. Cech (2004). "Yeast telomerase RNA: a flexible scaffold for protein subunits." Proc Natl Acad Sci U S A **101**(27): 10024-10029.

Zhou, Z., H. Feng, et al. (2011). "Structural basis for recognition of centromere histone variant CenH3 by the chaperone Scm3." Nature **472**(7342): 234-237.